To the Graduate Council:

I am submitting herewith a dissertation written by Marco Antonio De Jesús entitled “Development of Novel Substrates and Sampling Techniques for the Analysis of Drugs and Model Environmental Pollutants via Surface Enhanced Raman Spectroscopy (SERS)”. I have examined the final electronic copy of this dissertation form and content and recommend that it be accepted in partial fulfillment for the requirements for the degree of Doctor of Philosophy, with major in Chemistry.

Michael J. Sepaniak
Major Professor

We have read this dissertation
and recommend its acceptance:

Robert J. Hinde

S. Douglass Gilman

Kevin Robinson

Accepted for the Council:

Anne Mayhew
Vice Chancellor and Dean
of Graduate Students

(Original signatures are on file with official student records.)

Development of Novel Substrates and Sampling Techniques for the Analysis of Drugs and Model Environmental Pollutants via Surface Enhanced Raman Spectroscopy (SERS)

A Dissertation
Presented for the
Doctor of Philosophy Degree
The University of Tennessee, Knoxville

Marco Antonio De Jesús
May, 2004

DEDICATION

This dissertation is dedicated to my wife Ideliz and my daughters Kiara and Cindy, since without their support, love, patience and sacrifices this work would have not been possible.

This dissertation is also dedicated to my parents whose sacrifices and love allowed the completion of this work.

ACKNOWLEDGEMENTS

I want to take this opportunity to express my most sincere respect and gratitude to all the people who helped to make this work possible. First I want to thank God by whom all things are made possible. His guidance, encouragement and grace have been the light that illuminated my way during all these years.

I would also want to express my gratitude to my wife Ideliz and my daughters Kiara and Cindy for their patience, love and encouragement through all these time. It is finished! I also want to give a very special “Thank you” to my parents, for their faith in me, their support, encouragement, patience and to help me be the professional that I am now.

I also wish to thank all my friends who were always there in the good and more challenging times. Thanks to Dr. Christopher A. Tipple, the first friend that I made upon my arrival to Knoxville and who helped me to make the transition process a more enjoyable experience. Thanks to Majed Albokari, for his true friendship and encouragement during the difficult times. I also want to express my gratitude to Kathleen S. Giesfeldt for her trust, friendship and support over the past two years. It was very pleasant to collaborate with you and I wish you the best in your career. A special thanks to past group members Shannon Fox, Gerald Devault, Dr. Nickolay Lavrik, Mustafa Culha, Jim Shaeper, and Jeremy Headrick for all their assistance and advice. In addition, I whish to express my most sincere gratitude to current group members Maggie Connatser, Pampa Dutta, Nahla Abuhatab, Jenny Oran, Lance Riddle, James Patton, and Dr. Jack

Steehler for their friendship, suggestions and for making this experience a more enjoyable one.

Thanks to the Chemistry Department's staff for their support and unconditional help during these years of study. I also want to express my appreciation and respect to Tim Free and Bill Gurley for their guidance and assistance in the machine, and electronic shop respectively.

I also want to thank my committee members: Dr. Gilman, Dr. Hinde and Dr. Robinson for your suggestions, and collaboration in this research. In addition I want to express my gratitude to Dr. Sepaniak, for his dedication, patience, wisdom, and support during all these years. It has been an honor to part of your research group.

Finally I want to express my gratitude to the University of Tennessee, Knoxville and the University of Puerto Rico, Mayagüez (UPRM), for the economical support and funding to this work.

ABSTRACT

Surface Enhanced Raman Spectroscopy (SERS) has shown promise for the analysis of environmental and pharmaceutically relevant compounds due to its tremendous enhancement of Raman signals and the large amount of structural information provided by the technique. Despite these advantages, SERS has not been established as a routine analytical tool due to limitations in the analytical figures of merit such as reproducibility and linear dynamic range. This is due in part to the fact that the continuous irradiation of the laser beam over the SERS substrate can promote the rapid decomposition of sample analytes which significantly broaden and diminish the intensities of observed spectral bands. Further irradiation can promote thermal or photolytic fragmentation of analytes, thereby altering the observable bands and possibly leading to a misinterpretation of analytical data. The primary goals in this project are to develop new substrates and sampling techniques to overcome the above mentioned problems.

The initial part of this work presents the use of a Sample Translation Technique (STT) as a means to minimize the thermal and photolytic effects commonly seen in SERS. By spinning the sample rapidly, the effective residence time of analytes and substrate within the irradiated zone is dramatically decreased without reduction of spectral acquisition time or the density of analyte in the zone. The technique is first studied by acquiring SERS spectra of various environmental and pharmaceutically relevant compounds such as Naproxen

USP, riboflavin, folic acid, Rhodamine 6G, and 4-aminothiophenol using silver islands on glass and silver-polydimethylsiloxane composites as SERS substrates. In all cases, the collected spectra show improvements upon spinning at laser powers as low as 4.2(±0.1) mW. Specific differences in the appearance of the spectra and the potential use of STT for improved SERS qualitative and quantitative determinations are presented. Although the combined use of STT-SERS and silver-polydimethylsiloxane nanocomposites (Ag-PDMS) showed promise in the analysis of aromatic compounds, the results demonstrated that new methods and protocols were needed to effectively implement SERS as a routine analytical technique.

Consequently, further studies were performed to optimize the technique for the analysis of a series of naphthalene, phenol, and benzoic acid derivatives as model environmental pollutants. The presence of these chemicals in water constitutes a serious public health issue due to the toxicity, persistence and chemical activity of these chemicals in the environment. The STT technique showed a considerable improvement in the reproducibility and the sensitivity of SERS. The experimental results showed a linear dynamic range of at least two orders of magnitude with detection limits as low as 2.9×10^{-8} M and precision of less than ten percent relative standard deviation. These experiments allowed the identification and optimization of different experimental variables such as irradiation time, translation rate, and pH. The pH studies also revealed that the composition of the sample matrix can promote the selective sorption of the analyte to the SERS active substrate.

The above mentioned results indicate that the composition of the sample matrix is an important variable in SERS. Therefore, the final part of this work was devoted to studying how different variables such as pH and matrix composition can affect the sorption and SERS activity of model pollutants. The results show that the conjugate bases of weak acids can interact more efficiently with the substrate, leading to an increased signal at higher pH, while amino-aromatic compounds interact more efficiently at a lower pH. The sorption of these chemicals is an essential step in the process and has been attributed to the absorption of the analyte into the PDMS followed by its adsorption to the metallic surface. In addition, the presence of moderate concentrations ($1x10^{-4}$ M) of a supporting electrolyte such as nitrate or fluoride can improve the sorption of 4-hydroxybenzoic acid to the Ag-PDMS nanoparticles. Other ions such as phosphate and chloride cause rapid oxidation of the substrates even at concentrations as low as $1x10^{-5}$ M. The effect of these variables in the analysis of real samples is presented. The potential use of liquid chromatography for isolating the model pollutants from detrimental matrix components in natural waters is also shown.

TABLE OF CONTENTS

Chapter Page

1. Introduction to surface enhanced Raman spectroscopy (SERS): Principles, substrates and detection methods…….. 1

1.1 The Raman effect (an overview) …….. 1

1.2. Raman detection systems…… 12

1.2.1 Radiation sources…… 14

1.2.2 Sample systems…….. 15

1.2.3 Holographic optics…….. 15

1.2.4 Charged coupled devices (CCDs)…… 16

1.2.5 Modern Raman spectrophotometers…… 18

1.2.5.1 Multichannel instruments…… 18

1.2.5.2 Fourier-transform devices…… 21

1.2.5.3 Raman microscopes…… 23

1.3 The SERS effect……. 26

1.3.1 SERS enhancement mechanisms…… 27

1.3.1.1 Electromagnetic enhancement…….. 27

1.3.1.2 Chemical enhancement…….. 31

1.3.2 Substrates used for SERS detection…… 35

1.3.2.1 Metal electrodes…… 36

1.3.2.2 Colloidal particles…….. 36

1.3.2.3 Metal-nanopariticle films……. 37

1.3.2.4 Sol-gel substrates…… 39

1.4 Statement of the problem…… 41

2. Development of a sample translation technique to minimize the adverse effects of laser irradiation to the SERS signal of drugs and model pollutants…… 48

2.1 Introduction…… 48

2.2 Experimental…….. 51

2.2.1 Instrumentation…….. 51

2.2.2 Preparation of the SERS active substrates…….. 53

2.2.3 Sample preparation and data analysis……. 54

2.3 Results and discussion …… 55

3. Improving the analytical figures of merit of SERS for the analysis of model environmental pollutants……. 80

3.1 Introduction…… 80

3.2 Experimental……. 85

3.2.1 Instrumentation…… 85

3.2.2: Preparation of the SERS-active substrates…… 89

3.2.3 Sample preparation and data analysis……..... 89

3.3 Results and discussion …… 91

4. Factors affecting the sorption of model environmental pollutants onto silver polydimethylsiloxane nanocomposite Raman substrates…… 115

4.1 Introduction…… 115

4.2 Experimental…… 119

4.2.1 Instrumentation…… 119

4.2.2 Preparation of the SERS-active substrates…… 120

4.2.3 Sample preparation…… 121

4.2.3.1 pH Studies…… 121

4.2.3.2 Inorganic anion studies…….. 121

4.2.3.3 HPLC-extraction conditions…….. 122

4.2.4 Data acquisition and analysis……. 122

4.3 Results and Discussion……. 124

4.3.1 The effects of pH on analyte sorption and SERS activity…… 126

4.3.2 The effects of sample matrix composition on analyte sorption and SERS activity…… 133

4.3.2.1 Halide effects…… 135

4.3.2.2 Other naturally occurring anions……... 139

4.3.3 Structural effects on the sorption to Ag-PDMS…….. 140

4.3.4 Analysis of amino aromatic compounds via HPLC SERS…… 143

5. Concluding remarks…… 149

References..... 154

Vita…….. 167

LIST OF TABLES

Table		Page
2.1	Characterization of the SERS and conventional Raman spectra of naproxen USP……	65
2.2	Characterization of the SERS spectra of 4-aminothiophenol…….	73
3.1	Regression results for the working curves of 4-ABA, 4-OHBA, 4-ClBA, and phenolphthalein using Ag-PDMS nanocomposites.…	109
4.1	Chromatographic data for the separation of 4-ABA, 1,4-PDA, and 1,2-PDA in a 1.0×10^{-4} M mixture..……..	148

LIST OF FIGURES

Figure		Page
1.1	Energy level diagram describing the Rayleigh (A), Stokes Raman scattering (B), and anti-Stokes Raman scattering (C) processes……....	5
1.2	Rayleigh and Raman bands of solid naphthalene excited with the 632.8 line of a helium-neon laser of a JY-LabRam system……	7
1.3	Common Raman scattering processes:……..	9
1.4	Spectral differences in the fluorescence (A), and Raman signals (B), of Rhodamine 6G……	11
1.5	Schematic representation of the multichannel Raman instrument:……	19
1.6	Basic components of an FT-Raman instrument……	22
1.7	Schematic representation of a Raman microscopy apparatus:……	24
1.8	Schematic representation of the SERS effect on a silver-polydimethylsiloxane nanocomposite (A); a scanning electron microscopy (SEM) image is included for clarity (B)……..	28
1.9	Schematic representation of the electromagnetic enhancement mechanism at the surface of a silver cluster…	32
1.10	Energy-level diagram depicting the types of metal-adsorbate interactions that could be observed under SERS…….....	34
1.11	Graphical representation of a thermal-evaporation chamber…….	38
1.12	Changes in the 1135 cm^{-1} SERS signal of 4-ABA ($1x10^{-4}$ M) as a function of the laser irradiation time……	43
1.13	Damage to the Ag-PDMS substrate surface after being irradiated with 8.9 ±(0.1) mW (632.8 nm He-Ne laser):……	44
1.14	Literature survey of modern analytical techniques employed in “trace analysis”……	45
2.1	Lab-Ram setup with the prototype sample translation accessory...	52
2.2	Signal degradation profile for a $1.0x10^{-4}$M solution of naproxen USP under stationary conditions on Ag-PDMS……..	57
2.3	Differences in the 4-ATP signals under (A) STT and (B) traditional SERS mapping conditions……	59
2.4	Laser irradiation effects under spinning (bold line), and stationary (light line) conditions:……	60
2.5	Spinning (light line), and stationary (bold line), SERS spectra of a series of $1.0x10^{-4}$M solutions of tetracaine, ketoprofen, 4-chlorobenzoic acid, and 8-hydroxyquinoline on PDMS (all 1.0 s acquisition)……	61
2.6	Damage to the substrate surface after being irradiated with 8.9 ±(0.1) mW (632.8 nm He-Ne laser):…….	62

2.7	Raman spectrum of solid naproxen in a glass capillary (1.0 s acquisition).	64
2.8	One-second snapshot of the SERS spectra of a 1.0x10-4 M solution of naproxen in 1%DMSO/Water over 18.0 nm Ag-PDMS after 115 s of irradiation;……	67
2.9	Changes in the spectral features of naproxen under spinning conditions:……	68
2.10	Changes in the spectral features of naproxen under stationary conditions:……	69
2.11	Changes in the 1391 cm^{-1} bandwidth of naproxen ($1x10^{-4}$ M) under spinning and stationary conditions……	70
2.12	Changes in the spectral features of 4-ATP under stationary conditions:……	75
2.13	Changes in the spectral features of R6G under stationary conditions:……	77
2.14	Working curve of R6G (N=5) under spinning conditions……...	79
3.1	Schematic representation of the Raman instrument:…….	86
3.2	Graphical representation of the Lab-Ram setup with a Stanford SR-540 chopper……..	88
3.3	Characterization of the Ag-PDMS nanocomposites:	94
3.4	Enhancement of the SERS signal of a $1.0x10^{-5}$ M solutions of 4-aminobenzoic acid (4-ABA) during the irradiation with 2.2±(0.1) mW of the 632.81 nm radiation from a He-Ne laser onto Ag-PDMS, and conventional silver islands films……	95
3.5	Changes in the 1066 cm^{-1} SERS signal of 4-ATP ($1.0x10^{-5}$ M) as a function of the effective Ag film thickness……	96
3.6	Spectral profiles of a $1.0x10^{-4}$ M solution of 4-ABA and 1,5-DAN as a function of the irradiation time:…….	98
3.7	Changes in the analytical response of the 1443 cm^{-1} band of 4-ABA ($1.0x10^{-4}$ M) as a function of the incident laser power:…….	100
3.8	Influence of the translation rate on spectra of 4-ATP (1.0×10^{-5} M) with 2.2 mW laser power:……..	102
3.9	Differences in spectral features for a series of benzoic acid derivatives:……	104
3.10	Reproducibility of the SERS-STT signal of PHT ($1.0x10^{-5}$ M) in Ag-PDMS microtiter wells:…….	105
3.11	Working curve for 4-ABA using the Ag-PDMS nanocomposites….	107
3.12	Influence of pH on the adsorption of:……	110
3.13	pH effects on the photodecomposition of 4-ABA after the continuous irradiation of the sample with 2.2 mW of the 632.8 line of a He-Ne laser……..	113
4.1	Differences in the SERS intensity of (A) 4-ABA (pKa1 2.48, and pKa2 4.90), and (b) 1,5-DAN (pKa1 3.90), as a function of pH…..	127
4.2	Influence of pH on the adsorption of:……...	130

4.3 Changes in the SERS areas of (A) BA (pK_a 4.20), (B) PHT (pK_a 9.23), (C) 1,7-DHN (pK_a 9.28), and (D) 4-NP (pK_a 7.23) with pH… 131
4.4 Changes in the 1190-1103 cm^{-1} band area of 4-OHBA ($1.0x10^{-5}$ M) with the increased concentration of different inorganic anions:. 134
4.5 Changes in the SERS signal of 4-OHBA on Ag-PDMS upon the increased anion concentration…….. 137
4.6 Changes in the SERS signal of 4-ABA on Ag-PDMS upon the increased concentration of NaCl……... 138
4.7 Positional isomer effects in the SERS signal of a series of aminobenzoic acid derivatives (ABA), cresols, phthalic acid (PA) and nitrophenol (NP)…….. 142
4.8 SERS spectra of 4-ABA ($1.0x10^{-6}$ M) in deionized water (A) and creek water (B). The creek and DI-water background are shown in gray for clarity. 144
4.9 Baseline and background corrected SERS spectra of the fractions that eluted after injecting 20 μL of 4-ABA ($1.0x10^{-4}$ M): 146
4.10 HPLC-SERS spectra of the separation of 4-ABA (A, B), 1,4-PDA (D), and 1,2-PDA (E) in a $1.0x10^{-4}$ M mixture, using the fraction collection approach. 147

ABREVIATIONS AND SYMBOLS

EMF	Electromagnetic field
ν	frequency
ΔE_v	difference in energy for the vibration
E_s	Energy of a scattered photon
E	magnitude of the electromagnetic field
E_0	peak amplitude of the electromagnetic wave
ν_l	frequency of the incident beam
t	time
μ	dipole moment
α	polarizability of the bond
r	the bond length at any distance
α_0	polarizability
r_{eq}	equilibrium bond length
UV	ultraviolet
VIS	visible
NIR	near infrared
IR	infrared
ϕ_1	virtual energy state
Ψ	ground electronic state of the molecule

Ψ^*	lowest exited electronic
N_1	number of molecules in the lower energy state
N_2	number of molecules in the excited state
E_1	energy of the first state
E_2	energy of the second state
K	Boltzman´s constant
T	Temperature (kelvins)
σ_{sc}	scattering cross section
I_{sc}	scattered intensity
ν_l	frequency of the incident beam
h	Plank's constant
η_p	number of photons
dA	area
CCD	charged couple devices
SERS	surface enhanced Raman spectroscopy
Nd/Yag	neodymium/yttrium aluminum garnet
He-Ne	Helium-Neon
M1, M2	external mirrors
NDF	neutral density filter wheel
M3-M4	internal mirrors and optics

L1	focusing lens
NF	notch filter
S1, S2	mechanical shutter
SG	spectrograph
PC	computer
FT-RAMAN	Fourier-Transform Raman
SERRS	surface enhanced resonance Raman spectroscopy
PVD	physical vapor deposition
E_i	induced electromagnetic field
$E(\nu)$	incident electromagnetic field
ε_m	dielectric function of the metal
ε_l	dielectric function of the media
E_M	field induced by the metal
r	radii of the metal nanoparticles
d	distance
$A(\nu)$	field enhancement factor
A(SERS)	SERS enhancement factor
$A_{(L)}$	LASER enhancement factor
$A_{(R)}$	Raman enhancement factor
LUMO	lowest unoccupied molecular orbital

HOMO	highest occupied molecular orbital
QCM	quartz crystal microbalance
MTEOS	Methyltetraethoxysilane
STT	Sample Translation Technique
USP	United States Pharmacopeia
R6G	rhodamine 6G
FA	Folic Acid
4-ATP	4-aminothiophenol
Ag-PDMS	silver-polydimethylsiloxane
mW	mili Watt
cm^{-1}	wavenumber
rpm	revolutions per minute
PDMS	polydimethylsiloxane (PDMS)
FIA	flow injection analysis
KOH	potassium hydroxide
N_2	nitrogen
Ω	ohms
DI	deionized
DMSO	dimethylsulfoxide

Sym. ν	symmetric stretching
δ	asymmetric stretching
δ	in plane bending
γ	out of plane bending
π	wagging
τ	torsion
PAH´s	poly-aromatic hydrocarbons
MCL	maximum concentration limit
LOD	limit of detection
EPA	Environmental Protection Agency
GC	gas chromatography
LC	liquid chromatography
NMR	nuclear magnetic resonance
HPLC	high performance liquid chromatography
SPE	solid phase extraction
SMPE	solid phase microextraction
4-ABA	4-aminobenzoic acid
4-OHBA	4-hydroxybenzoic acid
4-CLBA	4-chlorobenzoic acid

4-ATP	4-aminothiophenol
PHT	phenolphthalein
1,5-DAN	1,5-diaminonaphthalene
1,5-DHN	1,5-dihydroxynaphthalene
1,7-DHN	1,7-dihydroxynaphthalene
∞	infinity
μm	micrometer
nm	nanometer
mm	millimeter
Ag	silver
Å/s	Angstroms per second
BA	benzoic acid
A.C.S.	American Chemical Society
4-NP	4-nitrophenol

CHAPTER 1

Introduction to surface enhanced Raman spectroscopy (SERS): Principles, substrates and detection methods

1.1 The Raman effect (an overview)

When a beam of electromagnetic radiation interacts with a molecule, most of its incident photons are elastically scattered across space at the same wavelength of the excitation source. This phenomenon is known as Rayleigh scattering and is by far the strongest component of the scattered radiation.[1] In 1928, the Indian physicist C. V. Raman and his co-workers discovered that when a molecule is exposed to an electromagnetic field (EMF), a small fraction of the incident radiation is also inelastically scattered.[2] These inelastic collisions induce an energy-transfer between the incident photons and the molecules of the analyte. The energy of the photons after these events can be can be expressed as:

$$E_s = h\nu \pm \Delta E_v \qquad \text{(Eq. 1.1)}$$

where:

h = Plank's Constant

ν = frequency

ΔE_v = difference in energy for the vibration

From the classical physics perspective, the intensity of the electromagnetic field that surrounds the analyte under normal Raman conditions can be described as:

$$E = E_0 \cos(2\pi\upsilon_i t) \qquad \text{(Eq. 1.2)}$$

where:

E = magnitude of the electromagnetic field

E_0= peak amplitude of the electromagnetic wave

ν_i = frequency of the incident beam

t =time

The interaction between this oscillating field and the electron distribution of the analyte generates a dipole moment **μ** whose frequency is directly proportional to the incident electromagnetic field as described by:

$$\mu = \alpha E = \alpha E_0 \cos(2\pi\upsilon_i t) \qquad \text{(Eq. 1.3)}$$

where:

α = polarizability of the bond

Equation 1.3 provides only an estimate of the overall deformability of the molecule upon its interaction with the electromagnetic field. In real systems, the polarizability does not have a constant value due to anharmonic changes in the vibronic modes of the analyte. Although both Raman and infrared spectroscopy provide information on the rotational and vibrational modes of a molecule, the mechanisms by which they occur are quite different. For infrared spectroscopy (IR), this process involves the absorption of the electromagnetic radiation emitted by a black-body radiator, such as an incandescent wire or a globar source. This process requires an energy match or resonance between the incident photons and those vibrational energy levels of the analyte that exhibit a net change in

their dipole moments.[2] Alternatively, Raman spectroscopy is a light scattering phenomenon that involves the inelastic energy transfer between the incident photons and the vibronic energy levels of the molecule that result in a net change in its polarizability. The polarizability (μ) can be represented by a Taylor series. For small harmonic displacements, the higher order terms of the series become negligible, thus allowing the use of a more simplified form of the polarizability which can be expressed as:

$$\alpha = \alpha_0 + (r - r_{eq})\left(\frac{\partial \alpha}{\partial r}\right) \qquad \text{(Eq. 1.4)}$$

where:

r = the bond length

α_0 = polarizability

r_{eq} = equilibrium bond length

The difference between the bond radius and its equilibrium position is a function of the vibration frequency $\nu_{f,}$ and can be represented as:

$$r - r_{eq} = r_{max}\cos(2\pi\upsilon_f) \qquad \text{(Eq. 1.5)}$$

where: r_{max} is the maximum separation atoms relative to the their equilibrium position.

Substituting equation 1.4 into equation 1.5 we obtain:

$$\alpha = \alpha_0 + r_{max}\cos(2\pi\upsilon_f t)\left(\frac{\partial \alpha}{\partial r}\right) \qquad \text{(Eq. 1.6)}$$

Replacing this equation into equation 1.3 results in:

$$\mu = \alpha_0 E_0 \cos(2\pi\upsilon_i t) + E_0 r_m \left(\frac{\partial\alpha}{\partial r}\right)\cos(2\pi\upsilon_i t)\cos(2\pi\upsilon_f t) \qquad \text{(Eq. 1.7)}$$

By replacing the corresponding half-angle identity Eq. 1.7, we can obtain a more descriptive expression for the polarizability:

$$\mu = \alpha_0 E_0 \cos(2\pi\upsilon_i t) + \frac{E_0}{2} r_m \left(\frac{\partial\alpha}{\partial r}\right)\cos[2\pi(\upsilon_i - \upsilon_f)t] + \frac{E_0}{2} r_m \left(\frac{\partial\alpha}{\partial r}\right)\cos[2\pi(\upsilon_i + \upsilon_f)t]$$

(Rayleigh) (Stokes) (Anti-Stokes)

(Eq. 1.8)

The first term of this equation corresponds to the Rayleigh scattering, while the second and third terms corresponds to the Stokes and anti-Stokes scattering of the incident photons. Figure 1.1 provides a schematic representation of these terms.

Raman scattering is a two-photon process that involves the irradiation of the sample with either an ultraviolet (UV), visible (VIS) or a near infrared (NIR) source. The incident beam creates a "virtual energy state" (ϕ_1) that is a function of the frequency of the laser source (Figure 1.1). Normally, the power of the incident laser beam is selected so its energy level is less than that required to populate the electronic states of the analyte.[3] The exposure of the sample to this electromagnetic field results in the transition of a fraction of the irradiated molecules from their ground state to ϕ_1. Once at this "virtual state", molecules

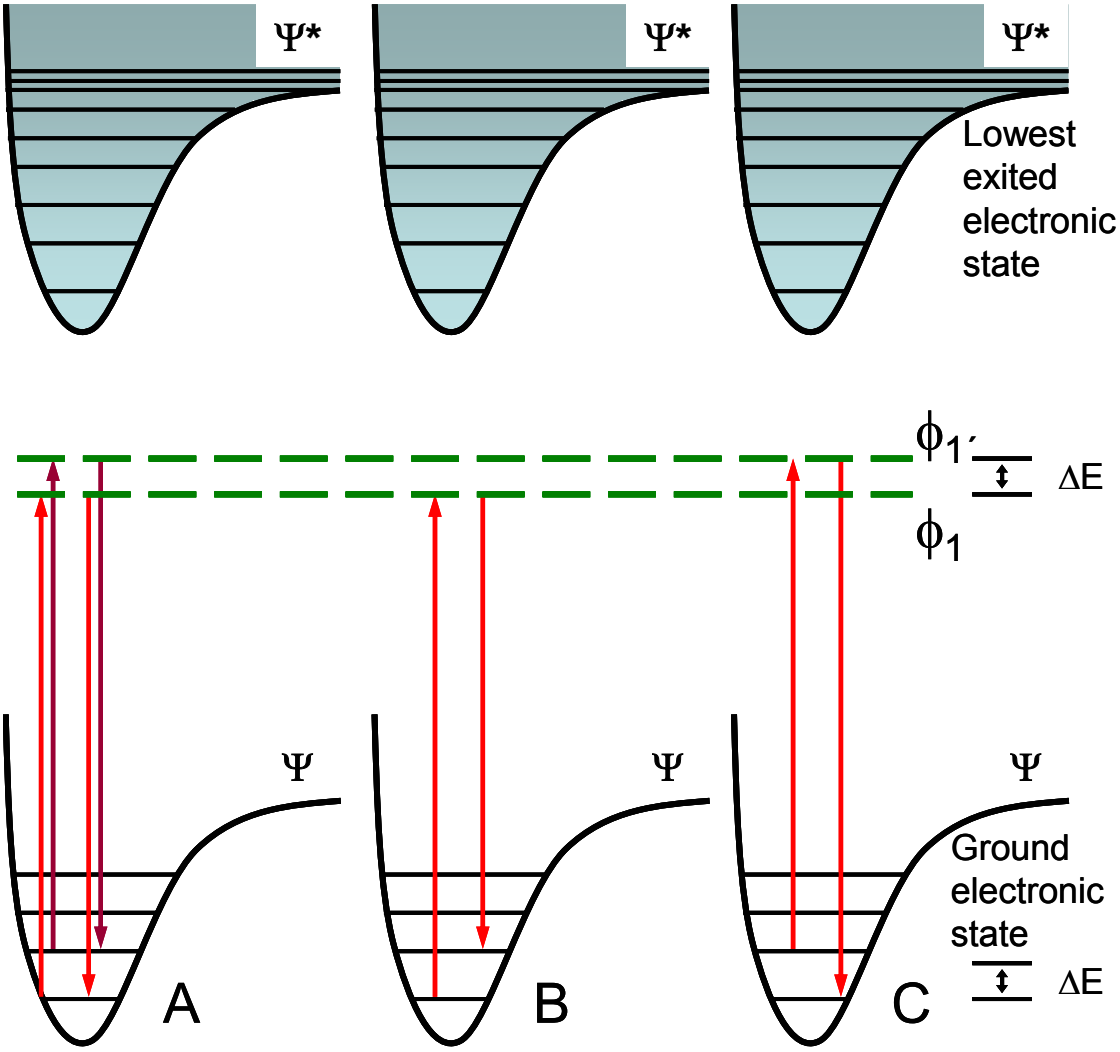

Figure 1.1 Energy level diagram describing the Rayleigh (A), Stokes Raman scattering (B), and anti-Stokes Raman scattering (C) processes.

Note: ϕ_1, and ϕ_2 are virtual states induced by the laser beam, Ψ is the ground electronic state of the molecule, Ψ^* is the lowest exited electronic state of the molecule, and ΔE corresponds to the difference in energy between states.

participate in a series of energy-transfer interactions with the incident photons. In some cases a portion of the energy of the photon is absorbed by the analyte allowing the molecule to return to its first vibrational level. As a result, the scattered photon has less energy than the incident beam resulting in what is known as a Stokes band (Figure 1.1B).

According to the Boltzman´s distribution (Eq. 1.9), a small fraction of the molecules are at the first vibrational state during the irradiation.

$$\frac{N_1}{N_2} = e^{-\frac{(E_2 - E_1)}{kT}} = e^{-\frac{h\upsilon}{kT}} \qquad \text{(Eq. 1.9)}$$

were:

N_1 = number of molecules in the lower energy state

N_2 = number of molecules in the excited state

E_1 = energy of the first state

E_2 = energy of the second state

k = Boltzman´s constant

T = Temperature (kelvins)

Under these conditions, the scattered photons absorb part of the energy of the molecule, allowing the molecule to return to its ground state. Consequently, the scattered photons are more energetic than the incoming ones, which result in an anti-Stokes band (Figure 1.1 C). From equation 1.9 we can also infer that most of the molecules exist in the ground sate under normal Raman conditions. This also accounts for the difference in intensity between the Stokes and the anti-Stokes lines as depicted in the Raman spectrum of naphthalene (Figure 1.2).

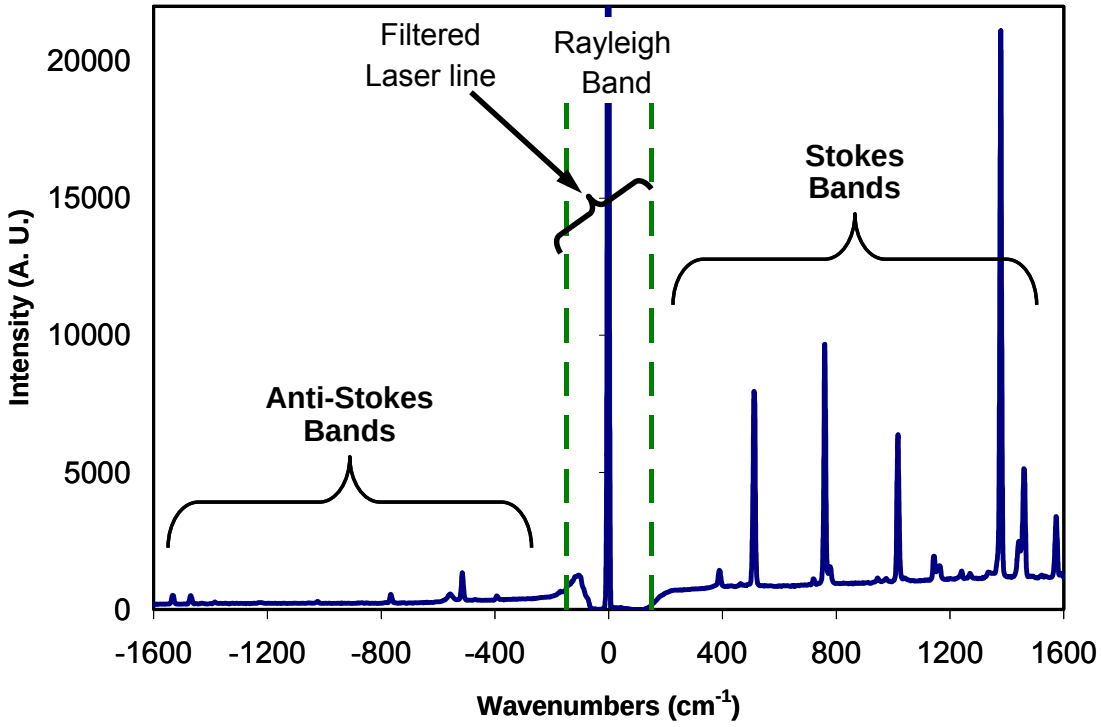

Figure 1.2 Rayleigh and Raman bands of solid naphthalene excited with the 632.8 line of a helium-neon laser of a JY-LabRam system.

Note: The acquisition parameters are set to assign a positive value to the Stokes (default) Raman shifts.

A limitation in equation 1.8 is that it predicts the same intensities for the Stokes and the anti-Stokes bands, not accounting for the quantum nature of the Raman process. A quantum mechanical analysis of the Raman effect shows that the intensity-ratio of these bands is a function of the Boltzman´s distribution:

$$\frac{I_{anti-Stokes}}{I_{Stokes}} = \frac{(\upsilon + \upsilon_f)^4}{(\upsilon - \upsilon_f)^4} e^{-(h\upsilon_f / kT)} \qquad \text{(Eq. 1.10)}$$

This equation also indicates that the Stokes bands should exhibit a higher intensity than the anti-Stokes bands under normal Raman conditions.

As previously mentioned, the energy of the virtual state normally resides below the electronic transitions of the analyte (Figure 1.3 A). However, in some cases the energy of the laser source brings ϕ_1 energetically close to an electronic state of the analyte. This phenomenon is known as pre-resonance Raman scattering (Figure 1.3 B). In other cases, the energy of the virtual state matches that of an electronic transition of the analyte resulting in what is known as discrete resonance Raman (Figure 1.3 C). When the energy of ϕ_1 is greater or equal than the dissociative continuum of the analyte, the Raman process that takes place is known as continuum Raman scattering. These processes can result in a significant enhancement of the Raman signals. In some instances, as in the case of continuum Raman scattering this also results in the rapid photodecomposition of the analyte.

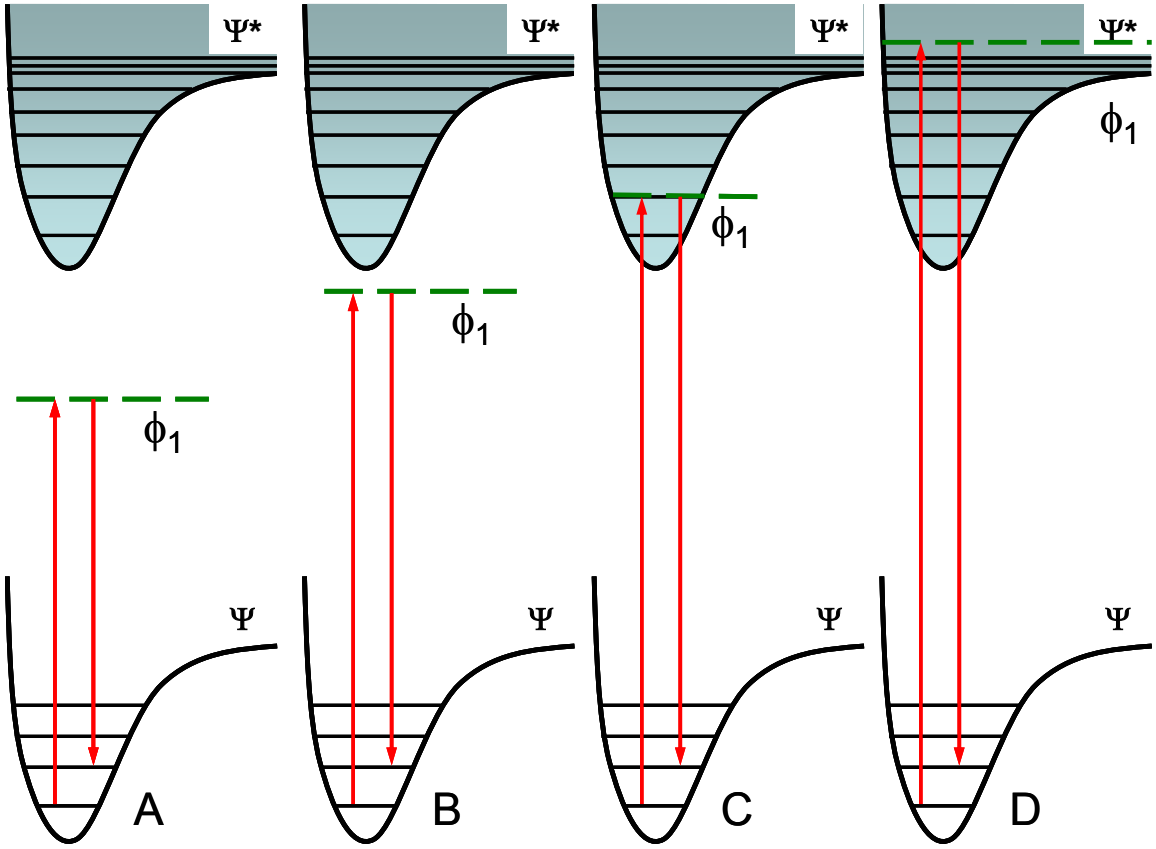

Figure 1.3 Common Raman scattering processes: (A) conventional Raman; (B) pre-resonance Raman; (C) discrete-resonance Raman; (D) continuum-resonance Raman

Unfortunately, the Raman scattering process is highly inefficient, thus limiting the effective sensitivity of the technique. The efficiency of a Raman processes can be determined with the scattering cross section (σ_{sc}):

$$\sigma_{sc} = \frac{2\pi I_s}{h\nu_i \eta_p} dA \qquad \text{(Eq. 1.11)}$$

where:

σ_{sc} = scattering cross section

I_{sc} = scattered intensity

ν_l = frequency of the incident beam

h = Plank's constant

η_p= number of photons

dA = area

The scattering cross section provides an estimate of the rate at which energy is removed from the incident beam.[3] The cross section in a conventional Raman process is in the order of 10^{-31}-10^{-29} cm^2/molecule, which is 12-14 orders of magnitude smaller than typical fluorescence cross sections (10^{-16} cm^2/molecule).[4] Despite this limitation, Raman spectroscopy offers more detailed and structurally rich information than fluorescence (Figure 1.4). This in combination with the low background Raman signal of water makes the technique an attractive tool for environmental, bioanalytical, and pharmaceutical applications.[5,6] Therefore, considerable efforts have been devoted to improve the quality of Raman instruments and to provide means to improve its apparent cross section.

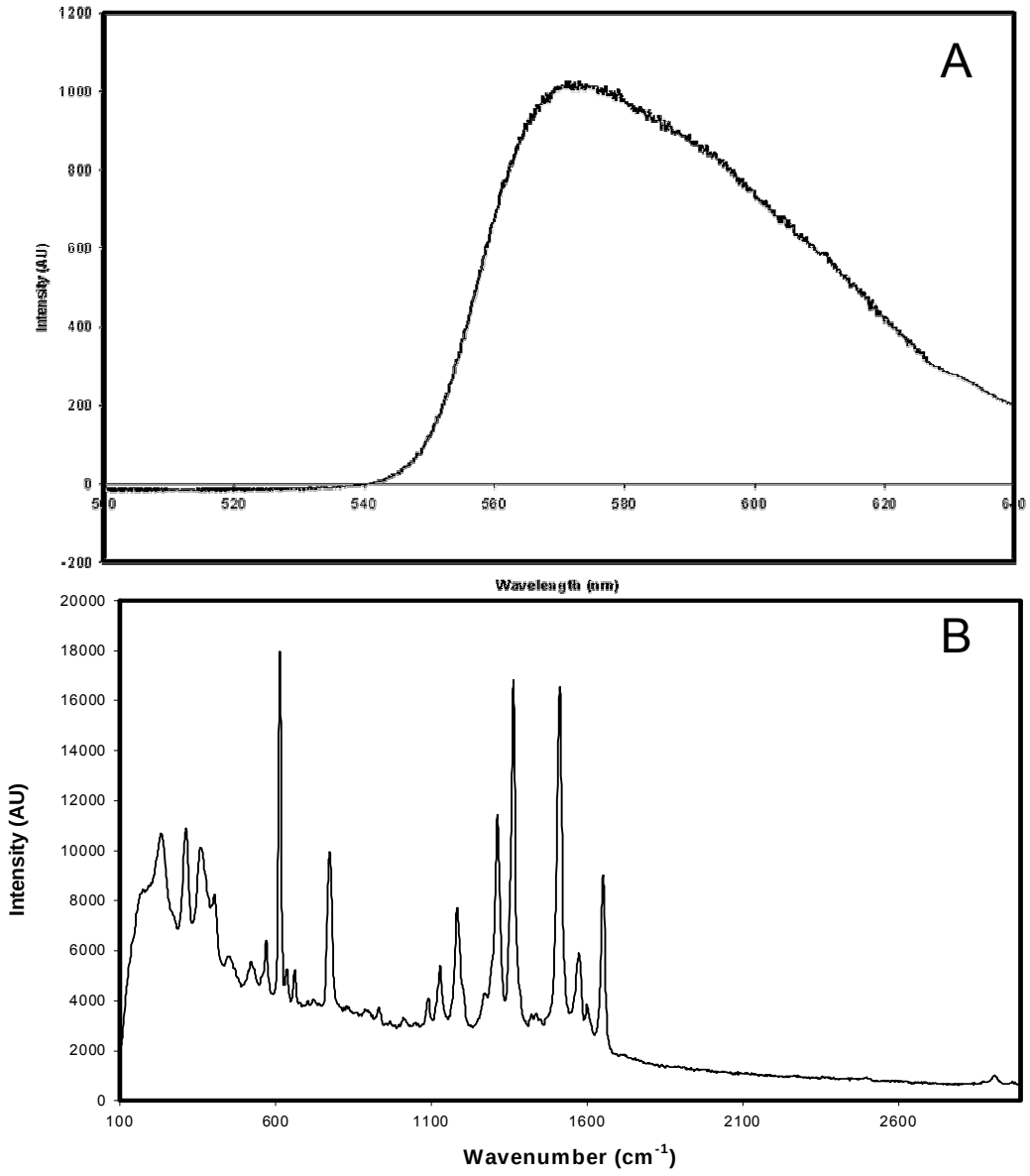

Figure 1.4 Spectral differences in the fluorescence (A), and Raman signals (B), of Rhodamine 6G.

The development of new and more efficient laser sources, as well as the production of high quality charged couple devices (CCD) and notch filters has provided a considerable improvement in the sensitivity and reliability of modern Raman instrumentation. A major breakthrough in addressing the sensitivity issue was the discovery of the surface enhanced Raman scattering effect (SERS).[7] Since then, new methods have been developed to maximize the efficiency of this phenomenon, resulting in a considerable improvement of the Raman cross section (10^{-16} cm^2/molecule) under SERS (see section 1.3).[4,8-11]

1.2 Raman detection systems

Despite its attractive features, the inherent low sensitivity of Raman spectroscopy limited the development of the technique during its early years. It was not until the 1960's that advancements in laser technology considerably facilitated the collection of Raman spectrum.[2] Since then, substantial progress has been made in the design of compact, simple, more stable and efficient laser sources. In addition, longer wavelength lasers such as the 1064 nm Nd/YAG, as well as the 785 and 840 nm diode lasers have become available. These lasers allow the use of higher laser power without causing the photodecomposition of the analyte. The use of longer wavelengths also locates the virtual state far below that of electronic transitions of the analyte. This prevents the excitation of the fluorescence-producing states in the molecule. As a result, the fluorescence background is significantly reduced (often negligible) with these sources. In addition, diode lasers offer the advantage of tunability over a 20-50 nm range

from the primary laser line, which allows a considerable reduction of the interferences from fluorescent compounds.

Progress in holographic optics also played an important role in this process. The fabrication of notch filters capable of removing over 99.5% of the laser background provided a major improvement in the collection efficiency of the technique. These laser rejection filters eliminated the need for the triple monochromator that rejected the laser line, minimizing the number of optical components (throughput advantage). This considerably lowers the price of modern Raman instruments since it allows a more economic and compact (benchtop-type) design of the instrument. The reduction in the number of optical components also permits the use of less powerful and expensive lasers without compromising the instrument performance. Another factor that contributed to the increased popularity of Raman based techniques was the recent availability of highly efficient charged coupled devices (CCDs). The low noise, high quantum-efficiency, and ruggedness of modern CCDs makes them the detector of choice in most modern Raman instruments.[12]

Modern Raman instruments can be classified as multi-channel, Fourier-Transform, and Raman microscopes. The main components of these instruments are an intense radiation source, sample irradiation system, holographic optics, and a suitable spectrophotometer. This section provides a general description of these components and the performance characteristics of each instrument with special emphasis on Raman microscopes.

1.2.1 Radiation sources

Laser sources have become the standard excitation system in Raman spectroscopy. The most commonly used lasers for Raman applications are the Argon ion (488.0-514.5 nm), Krypton ion (530.9, 647.0 nm), Helium/Neon (632.8 nm), Diode lasers (782 and 830 nm), and Nd/Yag (1064 nm). Since the intensity of the Raman signals depends on the fourth power of the laser frequency (Eq. 1.10), lower wavelength sources such as the Argon or Krypton ion, should exhibit better responses than their remaining counterparts. In theory, these sources can generate Raman signals that are up to three times more intense than those obtained with the corresponding Helium/Neon (He/Ne) source.[2] However, the high energy of these laser outputs often results in a significant increase in the fluorescence emission of the analyte, which overlap and often swamp the Raman signals. The laser-induced fluorescence of the analyte acts as background interference in Raman, thus compromising the sensitivity of the technique at lower wavelengths. The increased power density of these sources also promotes the fast thermal and photolytic decomposition of the analyte. As a result, most of the new Raman systems are shipped with a Helium/Neon source. This type of lasers offers the advantage of minimizing the above mentioned effects while keeping a reasonable sensitivity for Raman applications. He/Ne lasers also serve as a source for the excitation of the surface plasmon resonance of silver under SERS conditions.[13,14]

The recent advances in technology also allowed the use of near infrared (NIR) lasers such as Nd/YAG and diode lasers as sources for Raman

applications. The major advantages of these lasers are the dramatic reduction of the fluorescence and photodecomposition of the analyte upon irradiation. These lasers also allow the excitation of the surface plasmons of gold under SERS conditions.[15,16]

1.2.2 Sample systems

Techniques to obtain the Raman spectra of solid and liquid samples are considerably simpler than those for infrared spectroscopy (IR). Most of the traditional cell-window materials such as glass and quartz are transparent in Raman spectroscopy. This allows the use of a wide variety of cells such as ultraviolet and visible cells (e.g. fiber optics, capillary tubes, quartz and glass cells), and IR transmitting materials (e.g. KBr disks, and mulls) as sample reservoirs for Raman applications.

The low polarizability of water allows the direct analysis of aqueous samples via Raman spectroscopy with minimal background interferences. This advantage makes Raman spectroscopy a more attractive technique than infrared spectroscopy for biochemical, pharmaceutical and environmental analysis.

1.2.3 Holographic optics

Advances in holographic filtering technology have considerably simplified rejection of the Rayleigh scattering of the incoming laser beam, thus improving the costs and performance characteristics of modern Raman instruments. A first step in this process is the rejection of the secondary plasma lines of the laser.

This can be achieved by using a narrow band-pass filter (also known as an absorption or interference filter), appropriate to the line of interest. Absorption filters often consist of a dielectric material that absorbs over ninety percent of the incoming plasma lines with the exception of the laser line of interest.[2,17] The transmitted radiation then passes through a series of spatial filters (e.g. slits, and pinholes) that further reject any scattered light, which optimizes the spatial distribution of the excitation beam.

At last, the incident laser beam reaches a holographic notch filter. This type of filter is fabricated by recording the interference patterns from two mutually coherent laser beams onto the surface of a photoresist-type gelatin.[18] The created pattern produces a sinusoidal profile in the refractive index of the photoresit that reflects over 99.5 % of the incoming radiation directly onto the sample. The notch filter provides a sharp, narrow rejection of the laser line (less than 150 cm^{-1} from the central wavelength), that allows the transmission of less than 0.5% of the laser backscatter, while it transmits over 90% of the remaining frequencies to the detector. Holographic notch filters offers superior rejection of the laser line than most of the traditional dielectric filters or triple monochromators. This permits the fabrication of smaller, more economic and considerably more efficient Raman instruments.

1.2.4 Charged coupled devices (CCDs)

Charged coupled devices are by far the most commonly used detectors in Raman spectroscopy. These transducers consist of a series of silicone

photoactive elements assembled in a two dimensional array known as a chip.[19] Each element or pixel contains three electrodes sandwiched in a p,n-silicon substrate. The Raman scatter is normally dispersed over the longest dimension of the array by a suitable spectrograph. The incident photons induce a charge build-up that at the surface of the irradiated pixels, which is stored in a capacitor (well) located below the electrodes. Once the analytical signals are being collected, a microprocessor within the CCD applies a series of voltages that promote the systematic displacement of the accumulated charges to a shift register located at the end of the array. The data is then digitized and sent to a computer which converts it into the acquired spectrum. The performance characteristics of these devices are comparable to those obtained with the traditional phototubes, with the additional ability to simultaneously interrogate a considerable portion of the Raman spectrum (multichannel advantage).

CCDs are also over two orders of magnitude more sensitive than photo diode array detectors, which make them an ideal detector for sensing small electromagnetic signals such as those observed in Raman spectroscopy. Characterized by a high quantum efficiency (greater than 20% at the 500-900 nm range), low dark noise, adjustable detection area, and ruggedness these devices are almost ideal detectors for Raman spectroscopy. [20]

1.2.5 Modern Raman spectrophotometers

1.2.5.1 Multichannel instruments

Multichannel Raman systems allow the simultaneous acquisition of a Raman spectrum over a given wavelength interval (Figure 1.5). These instruments normally employ a VIS-NIR laser as the excitation source. A narrow band pass filter (<10 nm) is employed to minimize the interferences from the secondary plasma lines of the laser. As mentioned above, the power of the incident laser is regulated either by adjusting the current of the laser source or by placing a neutral density filter in front of the beam. Once the incident power is adjusted, the beam is reflected to a notch filter, which re-directs it to the sample. A fraction of the radiation is backscattered onto the surface of the notch filter which rejects the incoming Rayleigh radiation, while transmitting the Raman scatter to a spectrograph. The spectrograph in a multichannel system often consists in a single stage spectrograph assembled in a Czerney-Turner configuration. Under these conditions the Raman scatter is linearly dispersed by the grating across the longest axis of the CCD. As a result the resolution of the dispersed bands is a function of the quality of the dispersive element, and the CCD.

The performance of a grating depends upon its ability to reject stray light, f/number, resolving power, and effective bandwidth.[2] Stray light can be

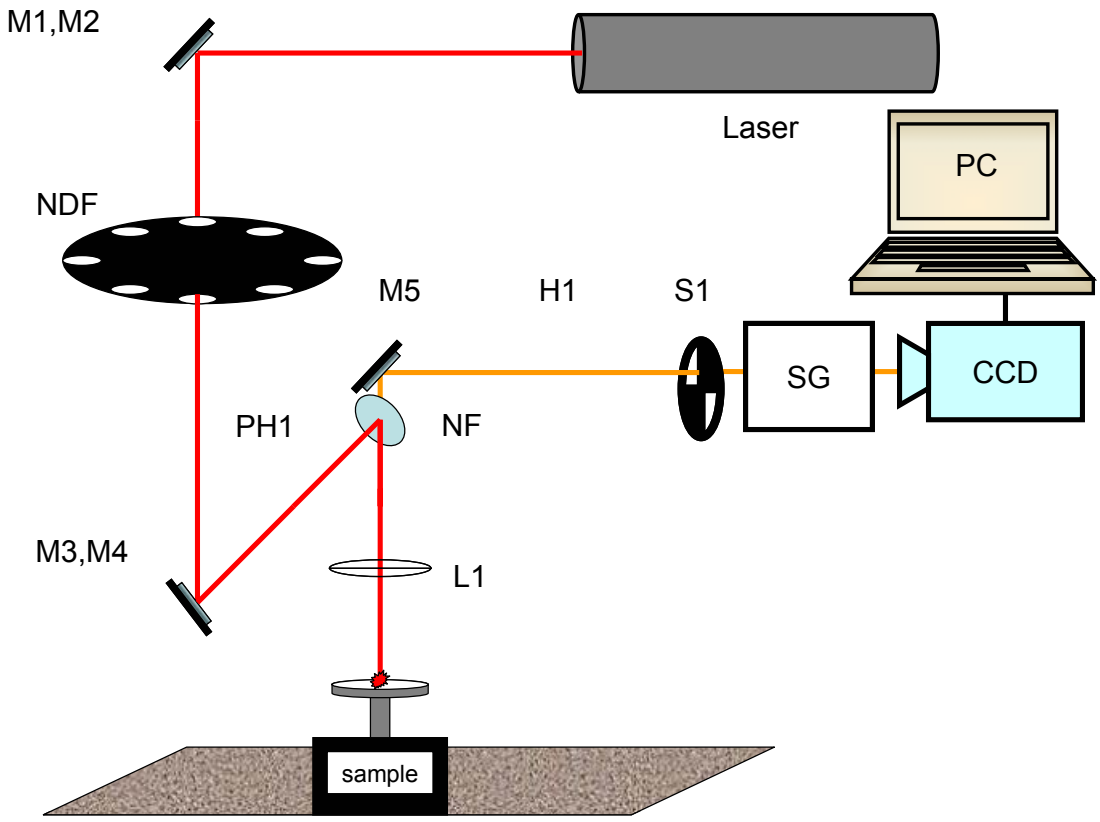

Figure 1.5 Schematic representation of the multichannel Raman instrument: VIS-NIR laser, external mirrors (M1, M2), neutral density filter wheel (NDF), internal mirrors and optics (M3-M4), focusing lens (L1), notch filter (NF), mechanical shutter (S1), spectrograph (SG), CCD camera, and computer (PC).

effectively decreased by coating the walls of the spectrograph with non-glossy black paint, and by sealing its entrance slits with optically transparent windows. The f/number is a parameter that estimates the ability of the grating to collect the incoming radiation. The light gathering power of a grating has an inverse square dependence with the f/number. Therefore, most of the commercially available Raman spectrographs have f/numbers in the range from 1-4. The effective bandwidth and resolving power depends on the number of blazing elements (grooves) in the grating. Raman spectrometers are typically manufactured with two set of gratings, one for low resolution (600 grooves/mm) and another for high resolution (1800 grooves/mm). Most of the commercially available gratings are holographically built. These gratings offer several advantages over traditional ruled gratings such as: lower cost, superior groove patterning, and better rejection of the stray light. Spectrographs use a fixed grating geometry to linearly disperse the incident radiation over the longest axis of the CCD. The spectral resolution is also affected by the physical dimensions of the CCD. Most of the currently available Raman spectrometers employ CCDs arrays of 1024 x 256 elements that are of 26 x 26 μm in size. These devices exhibit a spectral resolution of 15 cm^{-1} and less than 2 cm^{-1}, when used with the respective low and high-resolution gratings.

The main advantage of a multichannel system lies in its ability to simultaneously interrogate a considerable portion of the Raman spectrum. Sometimes the size of the CCD array is not sufficient to collect all the dispersed radiation. Under these circumstances, the user can program a multi-window

acquisition to cover the spectral region of interest. These features allow the collection of a full-spectrum more rapidly than with the traditional scanning instruments.

1.2.5.2 Fourier-transform devices

Fourier-Transform Raman (FT-Raman) spectrometers emerged as an attempt to overcome the fluorescence interferences observed in multichannel systems.[21] The main components of an FT-Raman instrument include a near infrared (NIR) laser (source) and a He/Ne laser (for internal calibration), a series of lenses to align the lasers, a sample probe, dispersive element (Michelson´s Interferometer), a laser line filter and a signal transducer shown in block form in Figure 1.6.

The Michelson interferometer is used to generate an interference pattern (interferogram) that contains the combined frequencies of all the scattered signals.[2] This pattern is detected by using a pyroelectric transducer such as indium gallium arsenide or lithium tantalate. The fast response rate of these transducers permits the efficient monitoring of interference pattern created by the interferometer. The measured signals are then deconvoluted by the computer via the Fourier Transform, resulting in the corresponding Raman spectrum.

The major advantages of FT-Raman over the multichannel systems are its superior wavelength accuracy due to the internal calibration and the effective removal of the fluorescence background by using a NIR source. However, FT-Raman systems are considerably less sensitive than the multichannel

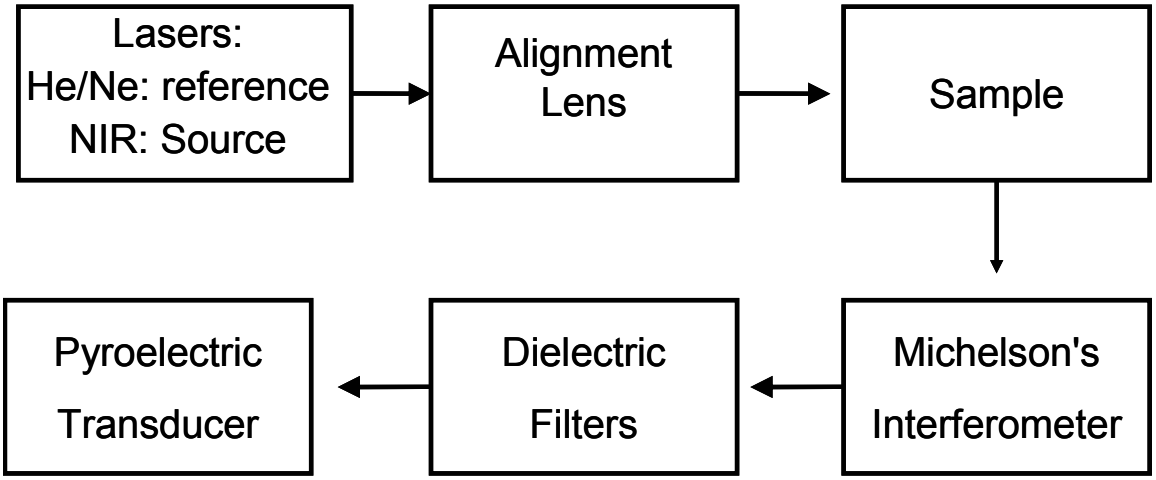

Figure 1.6 Basic components of an FT-Raman instrument.

counterparts due to the dependence of the Raman signal to the excitation wavelength, and the low sensitivity of the NIR pyroelectric detectors in comparison to the CCDs.

1.2.5.3 Raman microscopes

One of the most successful combinations in optical spectroscopy has been the coupling of the optical microscope to multichannel Raman systems. Raman microscopes offer several advantages over traditional instruments such as: low sample requirements, high throughput, good collection efficiency, and its ability to interrogate micron sized samples with good lateral resolution.[12] The confocal systems that are employed also provide a more efficient rejection of the straight light and fluorescence, thus improving the sensitivity of the technique. As a result a considerable portion of the commercially available Raman microscopes employ confocal optics as part of their detection scheme.

The basic components of a confocal Raman microscope are presented in Figure 1.7. The most common laser sources for these instruments are the argon ion (514.5 nm) and the He/Ne (632.8 nm) lasers with typical power less than or equal to 25 mW.[12] As in a multichannel system, a laser line filter is used to reject the secondary plasma lines of the laser. The power of the laser beam is regulated by adjusting the current to charge power of the laser or by using a neutral density filter. Once filtered, the incoming radiation passes through a pinhole that rejects most of the specular reflections of the laser thus increasing the spatial homogeneity of the beam. The fraction of the radiation that passes

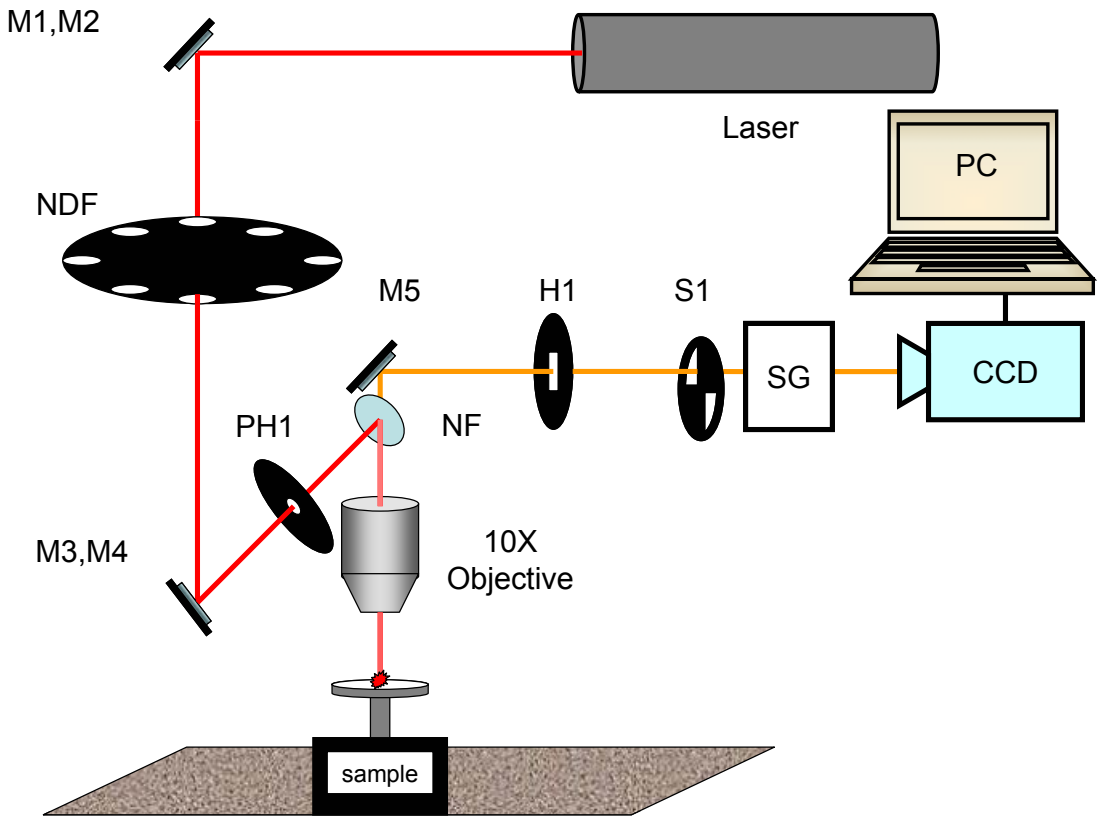

Figure 1.7 Schematic representation of a Raman microscopy apparatus: VIS-NIR Laser, external mirrors (M1, M2), neutral density filter wheel (NDF), internal mirrors and optics (M3-M4), pinhole(PH1), notch filter (NF), internal mirror (M5), confocal hole (H1), mechanical shutter (S1), spectrograph (SG), CCD camera, and computer (PC).

through the pinhole reaches the holographic notch filter which redirects it to the microscope objective. The microscope objective increases the power density of the beam by focusing the incoming radiation into a small area within the sample. The increased power density at this region results in a considerable increase of the Raman signals per unit sample area.

The Rayleigh and Raman scattering signals are then recollected by the objective in a 180° backscattering geometry. This technique normally employs microscope objectives with large numerical apertures which permits a more efficient collection of the Raman signals. These objectives also use compound lenses to compensate for their optical aberrations and to maximize its collection efficiency. The radiation collected by the microscope objective is redirected to the holographic notch filter that filters the Rayleigh scattering, and transmits the Raman scattered photons. The residual laser radiation and other interferences (e.g. room light, and fluorescence) are further decreased by the confocal hole. As in a multichannel system, the incident Raman photons are dispersed by a single stage spectrograph that redirects the Raman signals to a specific region within the CCD chip. At the end of the experiment, the digitized data is processed by the computer of the instrument forming the corresponding Raman spectrum.

Raman microscopy has proven to be an excellent tool in the analysis of electronic devices such as hard drives and integrated circuits. Its low sample requirements in combination with the confocal advantage makes Raman microscopy an attractive technique for biophysical, biomedical and environmental analysis.

1.3 The SERS effect

Surface Enhanced Raman spectroscopy was discovered about 30 years ago when Fleischmann et. al. observed a tremendous enhancement in the Raman signal of pyridine when adsorbed at the surface of a roughened silver electrode.[7] Additional studies performed by various researchers such as Jeanmaire, et. al.[22], and Albrecht, et. al.[23] proved that this was the result of a true enhancement of the Raman signal rather than increased sorption of the analyte onto the surface of the roughened silver electrode.[7] The technique proved to be effective for the study of a wide variety of analytes such as chelating agents, thiols, and different aromatic compounds.[24-26] Since the phenomenon occurs at the surface of a noble metal such as silver or gold, the technique was named Surface Enhanced Raman Spectroscopy (SERS).

The greatest advantage of SERS is the considerable enhancement of the apparent Raman cross-section that under certain conditions can be over 13 orders of magnitude greater than in conventional Raman.[27] Further enhancements in the Raman cross-section (10^{-18} cm^2/molecule) have been observed on the SERS spectra of highly adsorptive laser dyes such as Rhodamine 6G when collected under surface enhanced resonance Raman conditions (SERRS).[28] For the past 30 years, considerable effort has been made to decipher the mechanisms responsible for this phenomenon.[8,29-31] Despite these efforts, a full understanding of the mechanisms responsible for SERS has not been reached.[32] The next section is intended to provide a brief description of the currently accepted theories regarding SERS.

1.3.1 SERS enhancement mechanisms

Numerous mechanisms have been proposed to rationalize the enhancement of the Raman signals on noble metal surfaces. Such theories demonstrated that SERS is not merely a "surface effect" but more of a "nanostructure" phenomenon.[8] Until now, the mechanisms responsible for SERS are roughly divided in two main categories: electromagnetic and chemical enhancements. The former focuses on the influence of the nanostructure´s shapes, and sizes to the enhancement of the induced electromagnetic field while the latter points toward the metal-ligand interactions that can occur upon adsorption of the analyte onto the surface of the metal.

1.3.1.1 Electromagnetic enhancement

In SERS the molecules of the analyte interacts with a cluster of noble metal particles that forms a nanostructure of approximately 10 to 100 nm in dimension.[8] A schematic representation of these interactions is shown in Figure 1.8 A. This figure represents an aggregate of silver nanoparticles embedded into a Polydimethylsiloxane film via physical vapor deposition (PVD, see section 1.3.2.3). The aggregates consist of a series of polyhedral silver particles similar to those described by Balleto, et. al., for a PVD silver film.[33] The SEM picture (Figure 1.5 B), indicates that the shape of these nanoparticles can be roughly approximated as spherical. The exposure of the metal nanoparticles to the incident electromagnetic field promotes the excitation

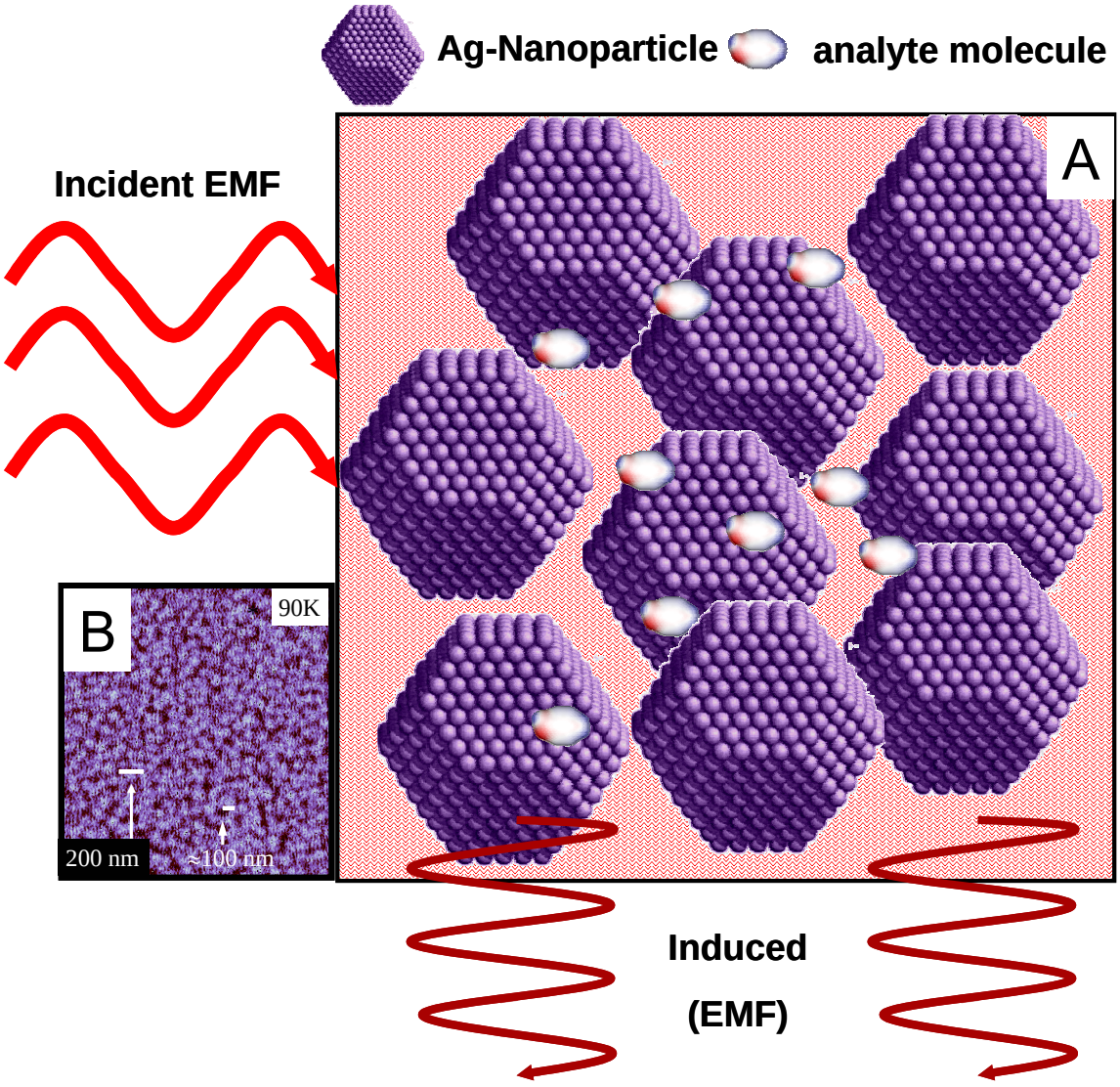

Figure 1.8 Schematic representation of the SERS effect on a silver-polydimethylsiloxane nanocomposite (A); a scanning electron microscopy (SEM) image is included for clarity (B).

of the surface plasmons of the metal inducing a new electromagnetic field at the surface of the metal.

By approximating the shape of the metal nanoparticles to that of a sphere and assuming that its size is considerably smaller than the wavelength of the electromagnetic field (Rayleigh approximation), the induced EMF can be expressed as:

$$E_i = \left[\frac{(\varepsilon_M - \varepsilon_i)}{(\varepsilon_M + 2\varepsilon_i)} \right] \times E(\nu) \qquad \text{(Eq. 1.12)}$$

were:

E_i = induced electromagnetic field

$E(\nu)$ = incident electromagnetic field

ε_m = dielectric function of the metal

ε_i = dielectric function of the media

Provided that the imaginary part of the dielectric constant of the metal is negligible, the fields are at resonance when $\varepsilon_m = -2\varepsilon_i$.

When a molecule is brought close to the surface of the metal nanoparticles, it experiences a field E_M which corresponds to the superposition of the incident EMF of the laser and the EMF induced by the excitation of the surface plasmons of the metal (Eq. 1.13).

$$E_M = r^3\left[\frac{(\varepsilon_M - \varepsilon_i)}{(\varepsilon_M + 2\varepsilon_i)}\right] + \left[\frac{1}{r + d^3}\right] \qquad \text{(Eq. 1.13)}$$

where:

E_M= field induced by the metal

r = radii of the metal nanoparticles

d = distance from the molecule to the surface of the metal particle

The effective EMF experienced by the molecule at a given distance can be correlated to the field enhancement factor A(ν) (Eq. 1.14).

$$A(\nu) = \frac{E_M}{E(\nu)} \approx \left[\frac{(\varepsilon_M - \varepsilon_i)}{(\varepsilon_M + 2\varepsilon_i)}\right] \times \left[\frac{r}{r + d}\right]^3 \qquad \text{(Eq. 1.14)}$$

By accounting for the enhancement of the laser and the Raman fields under these conditions we can express the electromagnetic enhancement of the SERS signal as:

$$A(SERS) = \left|A_{(L)}\right|^2 \left|A_{(R)}\right|^2 = \left[\frac{(\varepsilon_M - \varepsilon_i)}{(\varepsilon_M + 2\varepsilon_i)}\right]_L^2 \times \left[\frac{(\varepsilon_M - \varepsilon_i)}{(\varepsilon_M + 2\varepsilon_i)}\right]_R^2 \left[\frac{r}{r + d}\right]^{12} \qquad \text{(Eq.1.15)}$$

where:

$A_{(L)}$ = LASER enhancement factor

$A_{(R)}$= Raman enhancement factor

This relatively simple model shows that the electromagnetic enhancement scales to the fourth power of the effective electromagnetic field. The electromagnetic model also demonstrates that the strength of the induced EMF increases when the incident field is at resonance with the localized surface plasmons. The

electromagnetic enhancement of the SERS signal does not require a direct contact between the molecules of the analyte and the metal nanoparticles. However, the effective EMF experienced by the molecules of the analyte decays considerably with its increased distance from the metal surface (see equation 1.14). Therefore, a significant enhancement in the SERS signals is expected when the molecules of the analyte are at close proximity to the metal particles. The dependence of the SERS signals with the inter-particle distance suggests a dramatic increase in the induced EMF at the interstices of the metal nanoparticles. This inhomogeneous enhancement of the induced EMF may be one of the promoters of the so called "hot-spots" (Figure 1.9).[34,35]

1.3.1.2 Chemical enhancement

Over the years the experimental observations of the surface enhanced Raman phenomenon provided compelling evidence to suggest that electromagnetic enhancement is not the only mechanism involved in SERS. If the enhancement of the Raman signal were strictly dependent upon the enhancement of the metal-induced field, any molecule brought to close proximity to the substrate should exhibit an enhancement of its Raman signals. However, the experimental results show a strong dependence of the SERS signal upon the chemical and structural properties of the analytes indicating the existence of an additional enhancement mechanism in SERS.[14] Due to its strong dependence upon the chemical nature of the analyte, this mechanism is often referred to as a

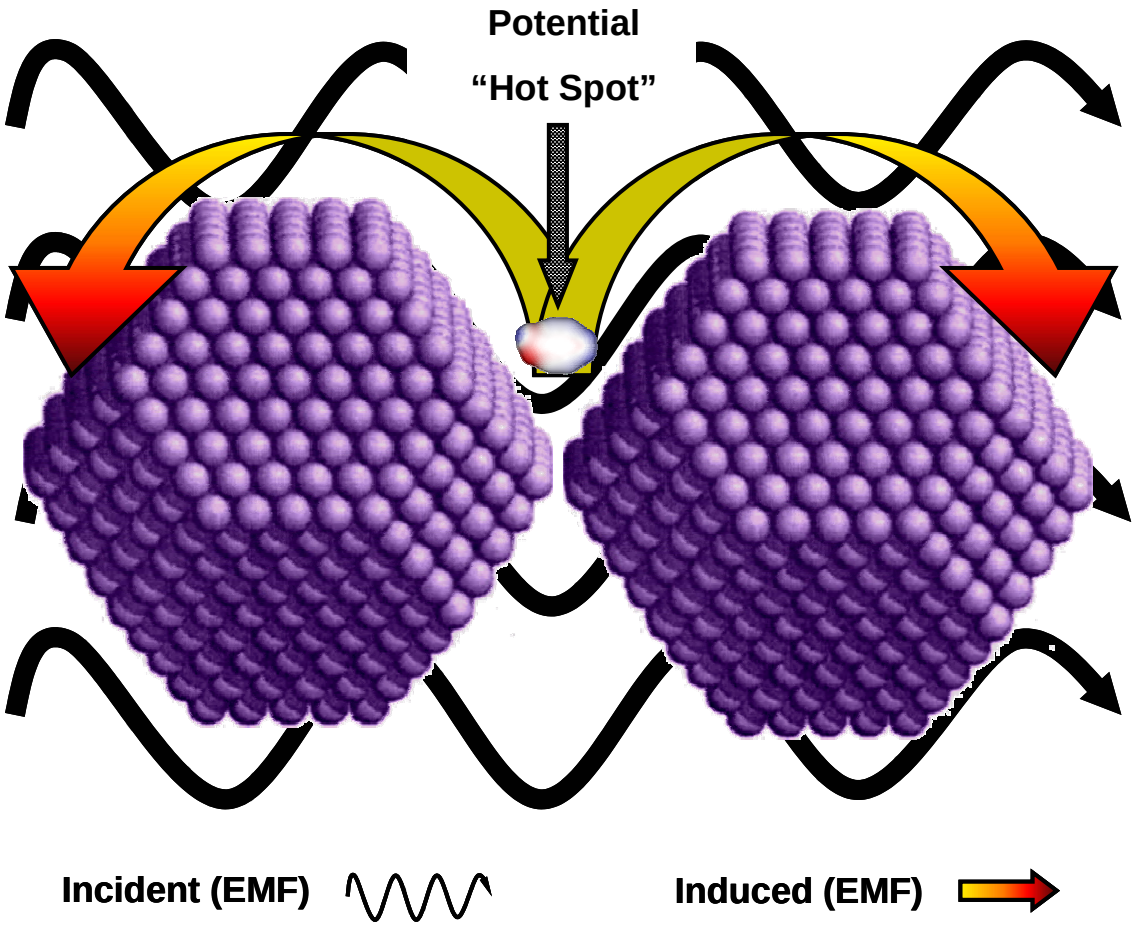

Figure 1.9 Schematic representation of the electromagnetic enhancement mechanism at the surface of a silver cluster.

"chemical enhancement". This mechanism is also known as the "first-layer effect", since it requires the adsorption of the analyte to the surface of the noble metal nanoparticles.[36,37]

The adsorption of the analyte to the metal often results in the formation of stable metal-adsorbate complexes at the surface of the substrate. Such complexes can promote a charge transfer interaction from the Fermi-level of the metal to the lowest unoccupied molecular orbital of the analyte (LUMO). Another process that can occur is the transference of an electron from the highest occupied molecular orbital (HOMO) of the analyte to the Fermi level of the metal (retro-donation). Under special circumstances the adsorption of the analyte can also promote the resonant excitation of the electronic states of the analyte upon its interaction with the metal. These processes are summarized in Figure 1.10.

Another process that often contributes to the chemical enhancement of the Raman signal is the so called "dynamic charge transfer effect". In this process, the incident photons promote the excitation of an electron of the analyte from its HOMO to its LUMO. The excited electron is subsequently transferred to the metal (via retro-donation), inducing the relaxation of the analyte and the emission of a scattered photon.

Although the enhancement factor under these conditions is in the range of $10\text{-}10^3$ cm^2/molecule, the process always operates in combination with the electromagnetic enhancement of the Raman signal.

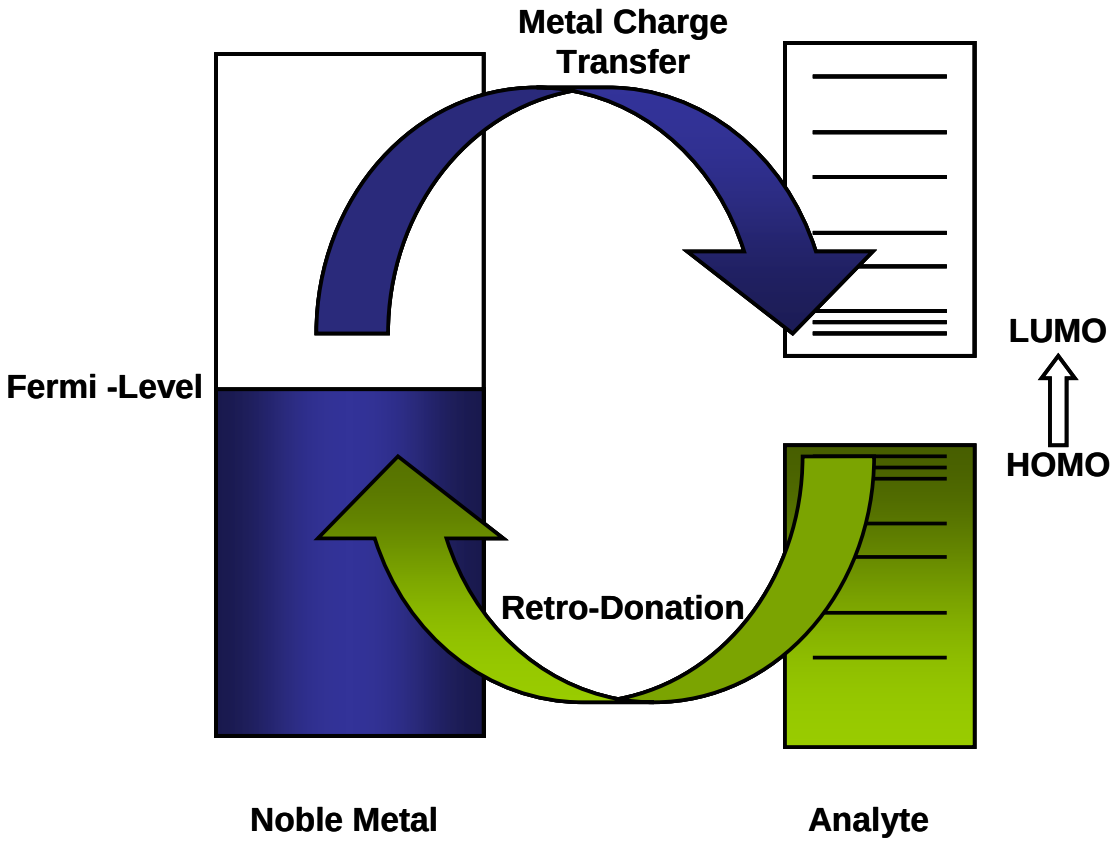

Figure 1.10 Energy-level diagram depicting the types of metal-adsorbate interactions that could be observed under SERS.

1.3.2 Substrates used for SERS detection

The surface enhanced Raman effect was first observed at the surface of a roughened silver electrode.[7] Since then, a wide variety of SERS active substrates has been employed with different degrees of success. Ideally, a good SERS substrate should be capable of maximizing the Raman cross-section, relatively inexpensive, simple to prepare, highly homogeneous, stable, robust, and reproducible. The most commonly used substrates for SERS applications are noble metal particles, such as copper, silver and gold since their surface plasmon resonances reside within the UV-NIR region.

Among these, silver-based substrates often exhibit the strongest SERS signals. However, silver particles are prone to oxidation upon contact to air, water and other oxidizing agents, thus limiting its applications for the direct analysis of real samples. Gold nanoparticles are often more stable and robust than silver, but they often exhibit a considerably lower enhancement of the Raman signals. Silver and gold nanoparticles exhibit maximum SERS activity when the dimensions of the particles are within the 10-100 nm range. These particle aggregates (clusters), typically exhibit fractal-like properties, which result in an inhomogeneous distribution of the induced electromagnetic fields over the substrate surface.[38-39] As a result, the maximum enhancement of the SERS signal often occurs in highly localized areas (hot-spots), which are randomly distributed through the entire surface.[8] A considerable amount of research has been devoted to increasing the homogeneity of these surfaces, as well as, to maximize the strength of the induced electromagnetic field. This section briefly

discusses the advantages and limitations of some of the substrates that have been developed for SERS applications.

1.3.2.1 Metal electrodes

Roughened silver electrodes were the first type of substrate employed in SERS.[7,40,41] Other types of electrodes such as gold, copper and platinum have also been used.[7] The SERS active surface is prepared by the initial oxidation of the electrode surface, followed by the etching (roughening) of the surface with a series of oxidation-reduction cycles.[42] This process results in the formation of a series of protrusions in the range from 25-500 nm.[43] The spatial orientation of the electrode is adjusted so it facilitates the focusing of the laser beam onto the surface of the metal.

Gold and silver electrodes do not provide a considerably large enhancement of the Raman signal when compared to physical vapor deposited films.[4] This has been attributed to the inhomogeneity of the electrode surface, the conductivity of the electrode, and the rapid oxidation of the surface upon contact to the sample matrix. The main advantage of this approach is that it permits the study of charge-transfer interactions by allowing the cycling of the electrode potential.

1.3.2.2 Colloidal particles

Colloidal nanoparticles are one of the most common SERS active substrates. These substrates are simple to prepare, cost effective and relatively

easy to characterize. The solutions are prepared by mixing an aqueous solution of the metal (e.g. 1% silver nitrate), with a good reducing agent such as sodium citrate or sodium borohydride.[44-45] The aggregated particles are typically 10-100 nm in diameter, and can be used either as an aqueous suspension or as a dried solid.[4] Some of the disadvantages of colloidal nanoparticles include their tendency to coagulate, low stability, inhomogeneous size distribution, light sensitivity, and low reproducibility. In addition, the reducing agents employed for the preparation of the colloid often exhibit a considerable background signal which limits their potential use for quantitative applications. In some cases the addition of inorganic salts such as sodium chloride can promote the enhancement of the Raman signal by promoting the coagulation of the colloidal particles around the analyte, thus enhancing its proximity to the metal nanoparticles. The aggregation of the silver nanoparticles around the good laser dyes such as Rhodamine 6G create areas that exhibit an unusual enhancement of their Raman cross section ("hot-spots"). The tremendous enhancement of the Raman signal in these areas has proven the potential use of SERS as a tool for single molecule detection.[46,47].

1.3.2.3 Metal-nanopariticle films

A wide variety of SERS active substrates can be prepared via the physical vapor deposition of thin-metal films onto solid surfaces such as glass, and silica.[48,49] A basic representation of a thermal-evaporation chamber is presented in (Figure 1.11). The PVD process involves the electro-thermal evaporation of a

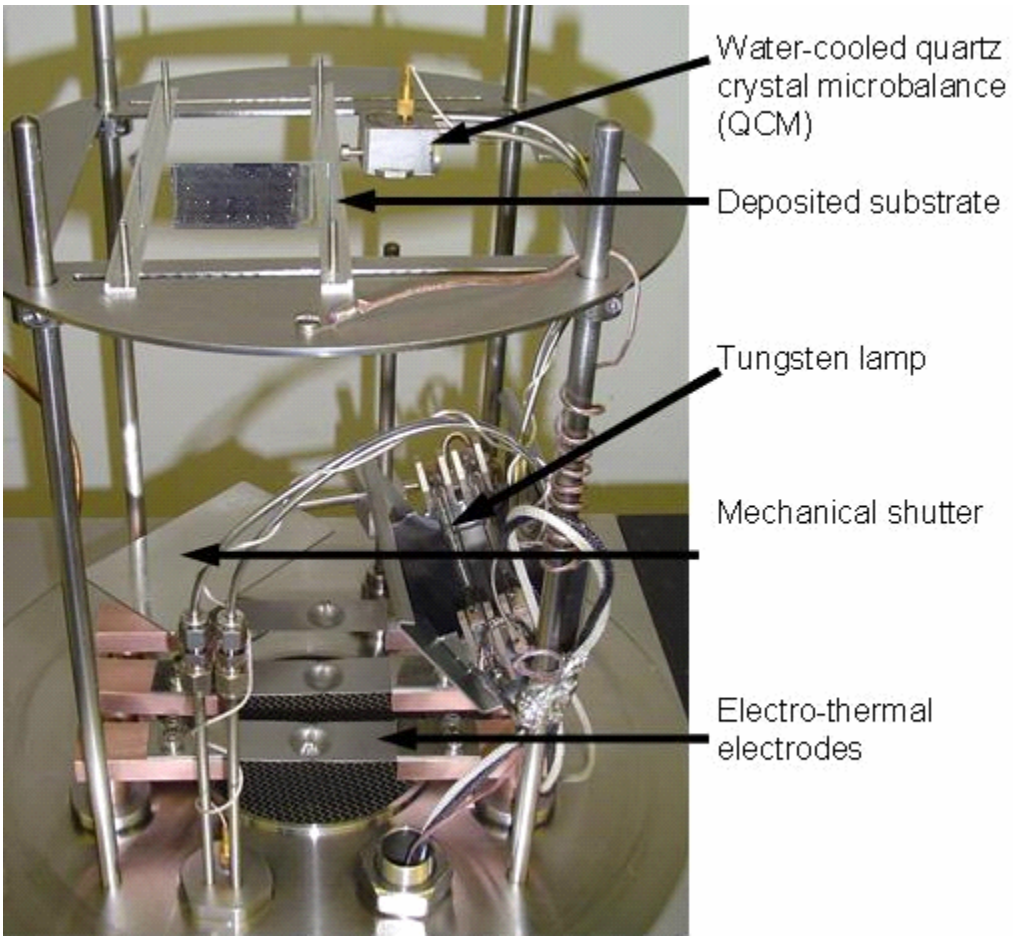

Figure 1.11 Graphical representation of a thermal-evaporation chamber.

metal under high vacuum conditions. The evaporated particles travel through the interior of the evaporation chamber reaching the surface of the solid support. Under these conditions, the adsorbed particles aggregate at the surface of the solid support forming isolated clusters also known as island films.[50,51].

The shape and size of these metal nanoparticles can be regulated by controlling the effective film thickness and deposition rate as monitored by a quartz crystal microbalance (QCM). By increasing the effective film thickness, the metal nanoparticles will start to agglomerate until coalescing at the film percolation threshold. Studies performed with silver-island films indicate that the maximum enhancement of the SERS signal occurs when the effective film thickness is below the percolation point.[52] Metal islands films also exhibit superior enhancement factors than those observed with roughened electrodes. In addition, these substrates are more reproducible and show lower background interferences than colloidal particles.[48]

Noble metal nanoparticles have also been used as coatings for a wide variety of modified surfaces such as silver coated nanospheres[53], Alumina[54], and TiO_2 surfaces[55]. This process has also been used in the coating of uniformly etched nanostructures on silica. [56]

1.3.2.4 Sol-gel substrates

A different type of SERS active substrate can be created by embedding the metal nanoparticles in a transparent polymer matrix. [57,58] This technique is commonly employed by suspending metal colloids into a sol-gel matrix.[59] The

chemical and mechanical stability of these materials provides a unique environment for the stabilization of the metal particles.[60] The substrates are often prepared by the hydrolysis and subsequent polycondensation of an silica based precursor thus forming a sol-gel.[61] Methyltetraethoxysilane (MTEOS), has been one of the most extensively used precursors in the generation of these surfaces.[57,61,62] The chemical environment of these substrates serves as a selective barrier that prevents the rapid oxidation of the substrates upon contact with water, and other oxidizing agents commonly present in aqueous samples. The porosity and the inherent selectivity of these polymers can be regulated by the careful selection of the precursors (e.g. alkoxysilane, and methyltriethoxysilane).[63,64]

A major problem in the use of sol-gels as SERS active substrates lies in preparation of homogeneous and highly reproducible films. This could be attributed in part to the random nature of the polymerization process that can induce significant changes in the porosity of the gel, thus affecting its characteristics among batches.[57] The reproducibility of the SERS signals are also affected by the inhomogeneous distribution of the colloidal particles through the substrate, which considerably limits the potential use of the technique for quantitative applications.[57] Therefore, considerable improvements are required in order to fully exploit the potential uses of this technique.

1.4 Statement of the problem

The unequivocal identification aromatic compounds in water plays an important role in pharmaceutical and environmental sciences. As a result, a significant number of the analytical techniques employed by regulatory agencies such as the Environmental Protection Agency (EPA) and the United States Pharmacopeia (USP) for this type of analysis rely in the use of chromatographic methods such as high performance liquid chromatography (HPLC) or gas chromatography (GC) for the separation of the individual components of the sample. The separated components are often detected by information-limited techniques such as UV-VIS, and fluorescence spectroscopy, or flame-ionization detection. The lack of detailed structural information obtained by these detection techniques limits their use for the unequivocal identification of the chemical constituents in complex samples. Consequently, there is a need for the development of new methods for the rapid and efficient detection/identification of these chemicals. The use of vibrational spectroscopic techniques such as SERS has gained particular interest over the past few years due to its potential for extremely low detection limits and its capability to provide more structural information than other optical spectroscopic methods, e.g. fluorescence (see Figure 1.4). Other advantages of SERS include its simplicity, relatively low cost, and low sample requirements. These features have made SERS an attractive tool for the analysis of drugs, polycyclic aromatic hydrocarbons, and other compounds of pharmaceutical and environmental interest.[4,22, 26]

Despite these advantages, SERS has not become a routine technique in these areas due to limitations in analytical figures of merit, i.e. reproducibility and linear dynamic range. The inhomogeneous adsorption of the analyte onto traditional SERS substrates (e.g. colloidal silver and silver-islands films), in combination with their susceptibility to oxidation upon contact with water and other oxidizing agents, are among the many variables that contribute to the above mentioned limitations. Another limiting factor is that relevant analytes are often sensitive to thermal and photolytic decomposition under SERS conditions.[65-67] Continuous irradiation of the laser beam over the SERS substrate can promote the rapid decomposition or fragmentation of the sample analytes, which significantly alters the observed signals (Figure 1.12). The continuous irradiation of the sample also results in permanent damage to the surface of the substrate (Figure 1.13). These variables considerably reduce the robustness, detection limits, precision, and accuracy of SERS and impose a serious limitation for its implementation as a routine analytical tool. As a result, a recent survey in SciFinder scholar under the topic “trace analysis” shows that less than 0.3 percent of the publications were based on SERS methods (Figure 1.14).

A considerable number of these effects could be overcome effectively by developing novel substrates and sampling techniques to surmount the above mentioned problems. Thus, new strategies and methods are required to

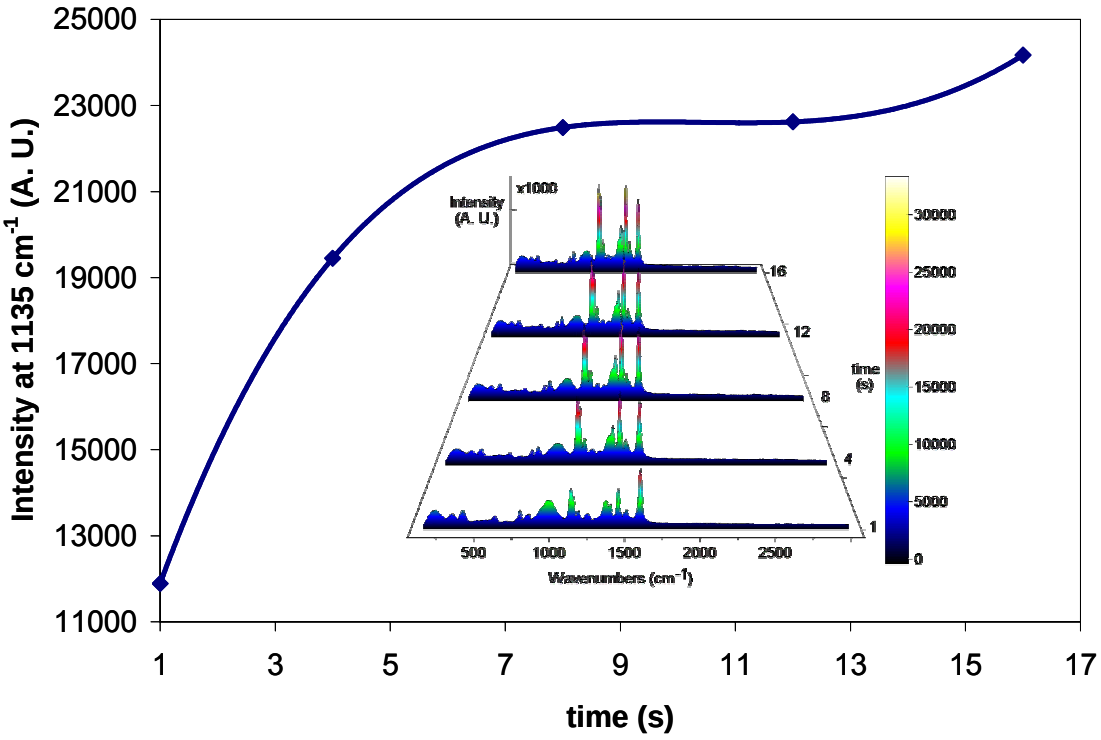

Figure 1.12 Changes in the 1135 cm^{-1} SERS signal of 4-ABA ($1x10^{-4}$ M) as a function of the laser irradiation time. The sample was irradiated with 8.9 ±(0.1) mW of the 632.8 nm line of a He-Ne laser.

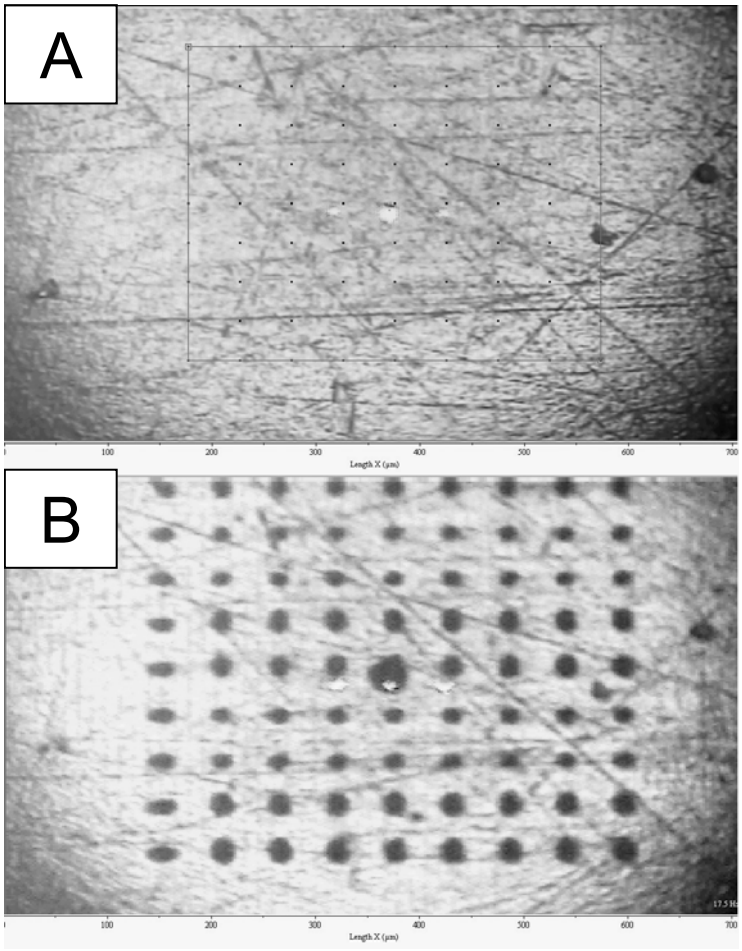

Figure 1.13 Damage to the Ag-PDMS substrate surface after being irradiated with 8.9 ±(0.1) mW (632.8 nm He-Ne laser): A. surface prior to irradiation; B. surface after irradiation.

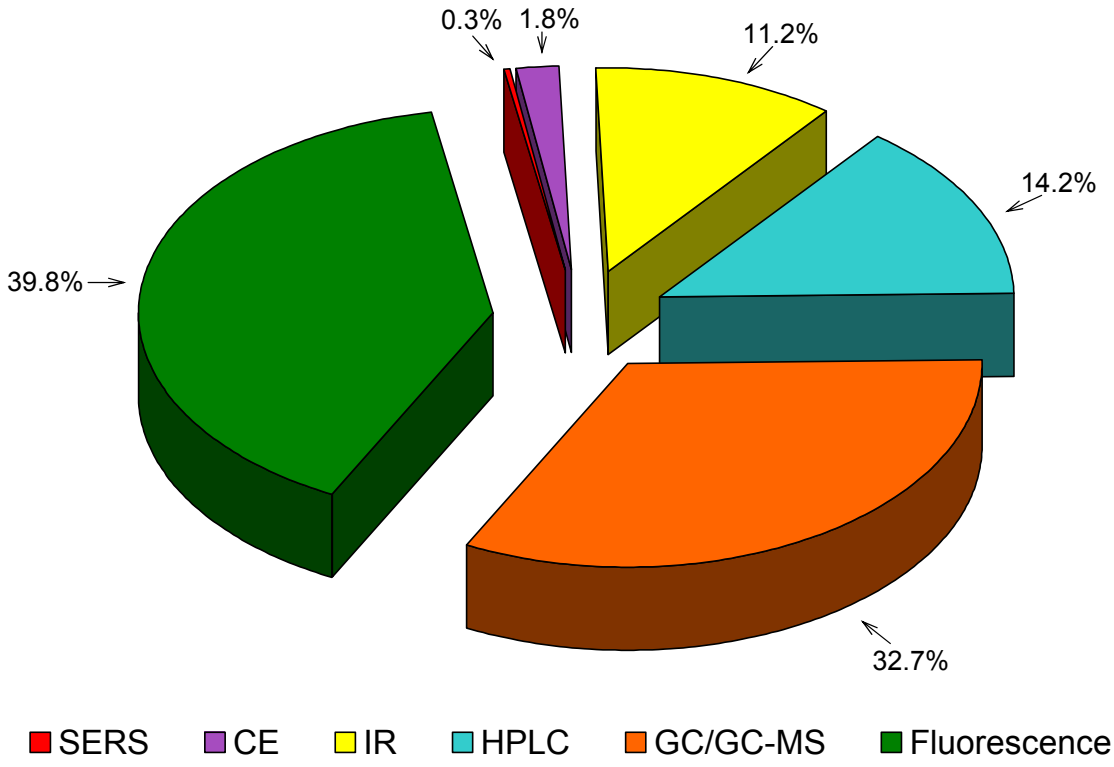

Figure 1.14 Literature survey of modern analytical techniques employed in "trace analysis".

Source: SciFinder scholar 1904-2003 (N=10991)

minimize the thermal and photolytic effects often observed in Raman. The development of more robust and homogeneous substrates that also improve the reproducibility and performance characteristics of SERS active substrates is required. The rational optimization of these variables may result in a considerable improvement in the analytical figures of merit in the technique, and facilitate its implementation as a routine tool for environmental and pharmaceutical applications.

This work seeks novel approaches to minimize the sample decomposition effects and to improve the analytical figures of merit of SERS for the analysis of pharmaceutically and environmentally relevant compounds. A dramatic reduction of the laser irradiation effects have been achieved by the judicious choice of irradiation time, incident laser power, and by the implementation of a novel sample translation technique. In addition, considerable improvements to the sensitivity, linear dynamic range, and signal reproducibility have been achieved by the use of silver-polydimethylsiloxane nanocomposites as substrates SERS applications. These novel substrates have proven to be effective for the detection of ionizable aromatic compounds, an area of considerable interest for the environmental and pharmaceutical sciences. The high structural information content in SERS provides a means for the unequivocal identification and structural characterization of the analyte, which is crucial for environmental and pharmaceutical applications. The selectivity and performance characteristics of these SERS active materials have been studied through the course of this work.

The practical considerations and protocols required for the implementation of SERS as a tool for the analysis of real samples are also studied.

CHAPTER 2

Development of a sample translation technique to minimize the adverse effects of laser irradiation to the SERS signal of drugs and model pollutants

This chapter is a revised version of an article under the same name published in Applied Spectroscopy by Marco A. De Jesús, Kathleen S. Giesfeldt, and Michael J. Sepaniak:

De Jesús, M. A.; Giesfeldt, K. S.; Sepaniak, M. J.; **"Use of a sample translation technique to minimize adverse effects of laser irradiation in surface-enhanced Raman spectrometry."**; Applied Spectroscopy (**2003**), 57(4), 428-438.

My use of "we" in this chapter refers to my co-authors and myself. My primary contributions to this article included: (A) design of the project and development of the experimental protocols to employ SERS in the qualitative and quantitative analysis of drugs and environmentally relevant compounds, (B) design and fabrication of a series of metalized-PDMS microtiter well plates, (C) design and adaptation of a sample translation apparatus for SERS applications, (D) collection and interpretation of the most of the analytical data (E) collection and interpretation of the cited literature, (F) most of the writing.

2.1 Introduction

Since Fleischman, et. al. discovered an enhancement in the Raman scattering signal of pyridine over a rough silver substrate, Surface Enhanced Raman Spectroscopy (SERS) has become a powerful tool for the characterization of a wide range of inorganic and biologically relevant analytes.[7,56,68-72] The main advantage of SERS is an extremely large enhancement of the Raman signal of an analyte when adsorbed at or near the surface of certain noble metal structures with nanoscale features. Theoretical

predictions or experimental realizations for the level of SERS enhancements vary greatly in reports. As discussed in section 1.3.1, two models for enhancement have matured to the point of acceptance in their general forms.[4,29,70,71] The electromagnetic model involves very large laser-induced electromagnetic fields near the noble metal surface, and the chemical model involves changes in analyte polarizability or energy levels due to metal-analyte interactions. Under certain circumstances, these enhancement mechanisms permit single molecule detection by SERS.[46,73,75]

SERS potential for extremely low detection limits, in conjunction with the capability of Raman spectroscopy to provide structural information, has made it a very promising tool for biomedical and environmental applications.[4,59,76-78] Despite these advantages, SERS has not become a routine technique due to limitations in analytical figures of merit such as reproducibility and dynamic range. An underlying and often underestimated cause for these limitations is that relevant analytes are often sensitive to thermal and photolytic processes inherent to SERS.[79] Continuous irradiation of the laser beam over the SERS substrate can promote the rapid decomposition or fragmentation of the sample analytes, which significantly broadens and reduces the intensity of observed spectral bands. Alteration of the observable bands may lead to a misinterpretation of analytical data.[79-81] In addition, the SERS substrate may undergo chemical or morphological changes. In Raman microscopy, these problems are sometimes compensated by rastering the laser beam with a rotating mirror, defocusing the

laser beam, or by using a neutral density filter to reduce the power of the incident beam at the surface of the SERS active substrate. These techniques tend to improve the spectral quality of Raman bands, but at the expense of the sensitivity. In addition, Raman microscopes are incapable of reproducibly matching defocusing conditions. Kiefer and Bernstein proposed the use of a rotary cell to minimize the thermal and photodecomposition effects under Resonance Raman (RR) conditions.[81] This technique enhances the quality of the observed spectra and provides a means to analyze samples that are normally destroyed under static conditions.[81-83]

In this chapter we present the use of a Sample Translation Technique (STT) for the minimization of band broadening and thermal and photolytic decomposition effects in SERS experiments. The sample translation is accomplished by spinning the sample and monitoring off-center to create translational rates of roughly 10^5 μm/sec. Under these conditions, the effective residence time of analytes and substrate within the irradiated zone is dramatically decreased without reducing spectral acquisition time or the density of analyte in the zone at any given instant. Spectra of naproxen USP, riboflavin, rhodamine 6G (R6G), folic acid and 4-aminothiophenol (4-ATP), using silver island on glass and silver-polydimethylsiloxane (Ag-PDMS) composite substrates, all showed improvements upon spinning at laser powers as low as 4.2(±0.1) mW.

STT is developed as a tool for kinetic studies of thermal and photosensitive materials decomposition processes. Substantial differences in the

SERS spectra of the analytes under stationary and translating conditions are demonstrated and discussed. The potential benefits of STT for improved qualitative and quantitative analysis are also presented.

2.2 Experimental

2.2.1 Instrumentation

All the SERS spectra were acquired using a LabRam Spectrograph from JY-Horiba. The instrument uses an Olympus microscope with a 10X (0.25 n. a.) objective to deliver up to 8.9±(0.1) mW of the 632.8nm line from an electrically cooled He-Ne laser. The confocal hole and slit of the instrument were opened to 500 μm and 200 μm, respectively. All spectra were acquired in a 180° scattering geometry with a 2936 cm^{-1} spectral window centered at 1700 cm^{-1}. The scatter was dispersed with a 600 groove/mm grating, imaged with a 1024 x 256 thermoelectrically cooled CCD camera, and processed using Labspec 4.03 software. A computer controlled x-y-z stage was used to adjust the focusing of the microscope objective as well as the positioning of the laser spot under stationary and translating conditions. The translation of the sample was performed by using a spinning platen via a direct drive AC motor connected to a variable resistor to regulate the spin rate in the range of 200-2500 rpm (Figure 2.1).

The SERS active substrates were prepared with a physical vapor deposition chamber from Cooke Vacuum Products, Inc. The chamber was set

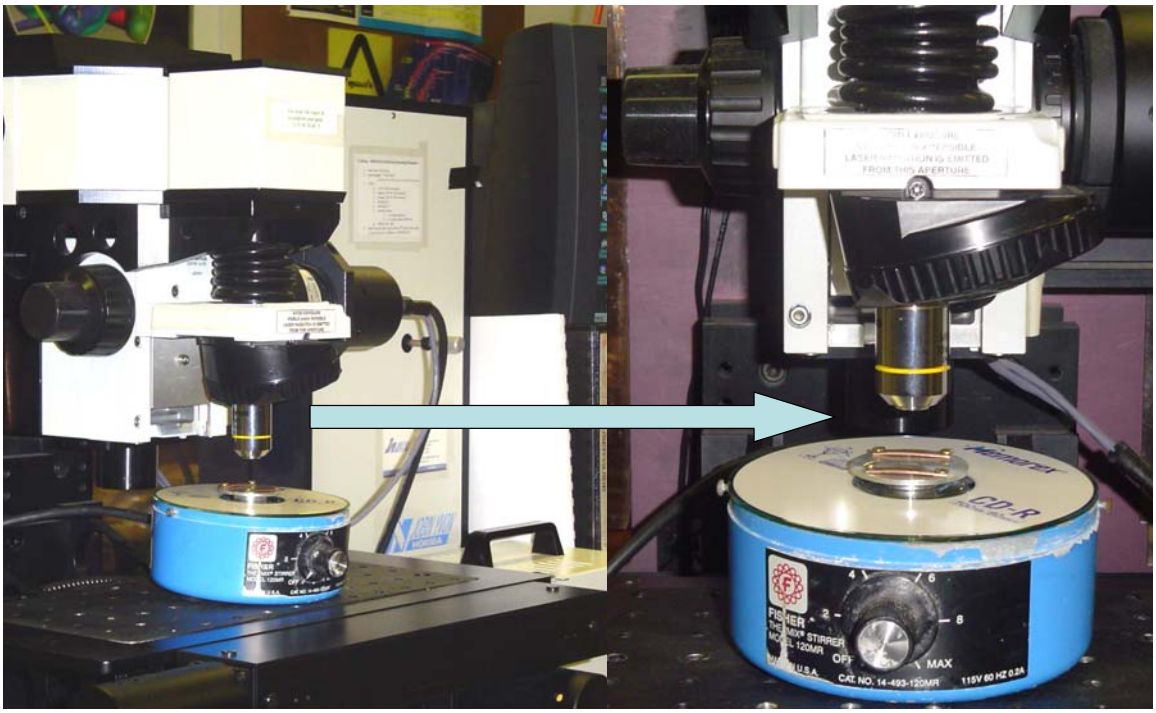

Figure 2.1 Lab-Ram setup with the prototype sample translation accessory. The STT probe consists of an AC variable speed motor (2500 rpm max) from Fisher Scientific.

to operate at a base pressure of ~10^{-7} torr. Samples were mounted 24 cm above and normal to the effusive source. Average mass thickness and deposition rates were measured for each film with a quartz-crystal microbalance.

2.2.2 Preparation of the SERS active substrates

The polydimethylsiloxane (PDMS) substrates were prepared by the addition of Silgard-184 curing agent (Dow Corning) and its elastomer in a 1:10 mass-to-mass ratio. The substrate was thoroughly combined and then degassed under high vacuum conditions for 15 minutes. Once all the entrapped air was removed, the samples were cast over the surface of a flow injection analysis (FIA) mold and placed in the oven at 70°C for 30 minutes. The PDMS substrates were removed from the molds and stored at room temperature until they gained full mechanical strength (24 hours). The FIA mold allows the preparation of an 18-PDMS well array capable of containing up to 50 µL of sample in each well. Each array was brought to high vacuum conditions for 15 minutes and then coated with an average thickness of 18.0 nm of 99.999% Silver (Alfa Aesar, MA), via physical vapor deposition (PVD) at a rate of 1.0 Å/s. The substrates were held under high vacuum conditions in the PVD system for 15 minutes to equilibrate. The Ag-PDMS substrates were stored in a vacuum desiccator prior to use.

Ag-islands on glass films were prepared by cleaning a series of standard glass microscope slides with a 5% (v/v) KOH solution in ethanol for five minutes.

The slides were subsequently rinsed with deionized (18ΩBarnstead E-Pure) water and dried under N_2. Once dried, an average thickness of 7.0 nm film of Ag was deposited at a rate 1.0 Angstroms per second. The Ag-glass films were held under high vacuum conditions in the PVD system for 15 minutes to equilibrate, and subsequently stored under vacuum in a dessicator.

2.2.3 Sample preparation and data analysis

A series of $1x10^{-2}$ M stock solutions of 4-ATP (90+% Aldrich), riboflavin (98+% Aldrich), naproxen USP (98+% ICN Biomedicals), folic acid (98+% Aldrich), R6G (98%+ Allied Chemicals), 4-chlorobenzoic acid (A.C.S, Eastman), ketoprofen (98+% Sigma), Tetracaine (98+% ICN Biomedicals), and 8-hydroxyquinoline (98+% Sigma) were prepared with deionized water (18ΩBarnstead E-Pure) and 1% DMSO (99.9% Acros Inc.). These stock solutions were used to prepare a series of aqueous standards in the $1x10^{-4}$ - $3x10^{-6}$ M range.

A 50 µL aliquot of each sample solution was transferred to a precisely centered Ag-glass or, more commonly, Ag-PDMS well and covered with a glass cover slip. The samples were generally spun at ~400 rpm and the beam was aligned relative to the dead center of the surface. The maximum SERS signal of the analyte was obtained by re-focusing the laser beam at this point. Once the signal was brought to focus, the SERS spectra of the sample were acquired by moving the stage at 50 µm intervals (1 s acquisition per step) to a maximum

distance of 1500 μm from dead center under spinning and stationary conditions. A series of experiments were performed to explore the effects of continuous irradiation of the laser beam by acquiring 100 spectra of the sample under spinning and stationary conditions at ~500 μm and ~550 μm, respectively, from dead center. The R6G standards were used to generate a working curve in order to estimate the linear range of the substrate as well its saturation profile.

2.3 Results and discussion

Silver islands on glass has become a standard substrate for SERS due to the ease of preparation, good signal enhancement for a wide variety of analytes, and minimization of background signal relative to its colloidal counterparts. In principle, deposition of Ag on elastomers such as PDMS can create a three-dimensional structure of embedded Ag clusters, thereby increasing the effective surface area for SERS. Researchers have discovered recently that Ag-PDMS composites possess unique optical properties including SERS capabilities.[52] The elastomeric properties of PDMS allow for the fabrication of substrates with different shapes and dimensions such as microtiter wells for SERS. The hydrophobic nature of PDMS enhances the adsorption of organic molecules to a close proximity with the silver clusters, thus augmenting the intensity of the SERS signals.

Naproxen sodium is among the few relatively insoluble drugs (63 μM at 25°C) that have been successful on the pharmaceutical market.[84] Its large

production and consumption by the public makes it a potential contaminant in wastewaters.[85-86] As a naphthalene derivative, naproxen is susceptible to easily photo-decompose by the incident laser beam. The Raman spectral information for naphthalene is also well discussed in the literature. As a result, naproxen was considered a good analyte for the study of laser irradiation effects under spinning and stationary conditions.

The temporal degradation of the naproxen SERS signal under stationary conditions is shown in Figure 2.2. During these experiments it was observed a dramatic broadening of the SERS bands within the region covering 1200-1600 cm^{-1} as a function of the irradiation time. The appearance of two broad bands around 1607 and 1358 cm^{-1} are normally attributed to the G and D bands of graphitic carbon.[87-89] The changes in the SERS signal of naproxen within this region are consistent with the formation of graphite at the surface of the substrate. This led us to suspect that the observed changes in spectral features were due mostly to the thermal and photolytic decomposition of the drug.

A continuous translation of the Labram x-y-z stage during spectral acquisition was considered to minimize these effects. Unfortunately, our instrument does not currently have the capability to collect a spectrum while continuously translating the stage. As an alternate approach, samples were spun as described above. This approach has proven to be effective under conventional Raman since it minimizes the laser irradiation effects by decreasing the residency time of the laser beam on the sample.[81-83] It was expected that

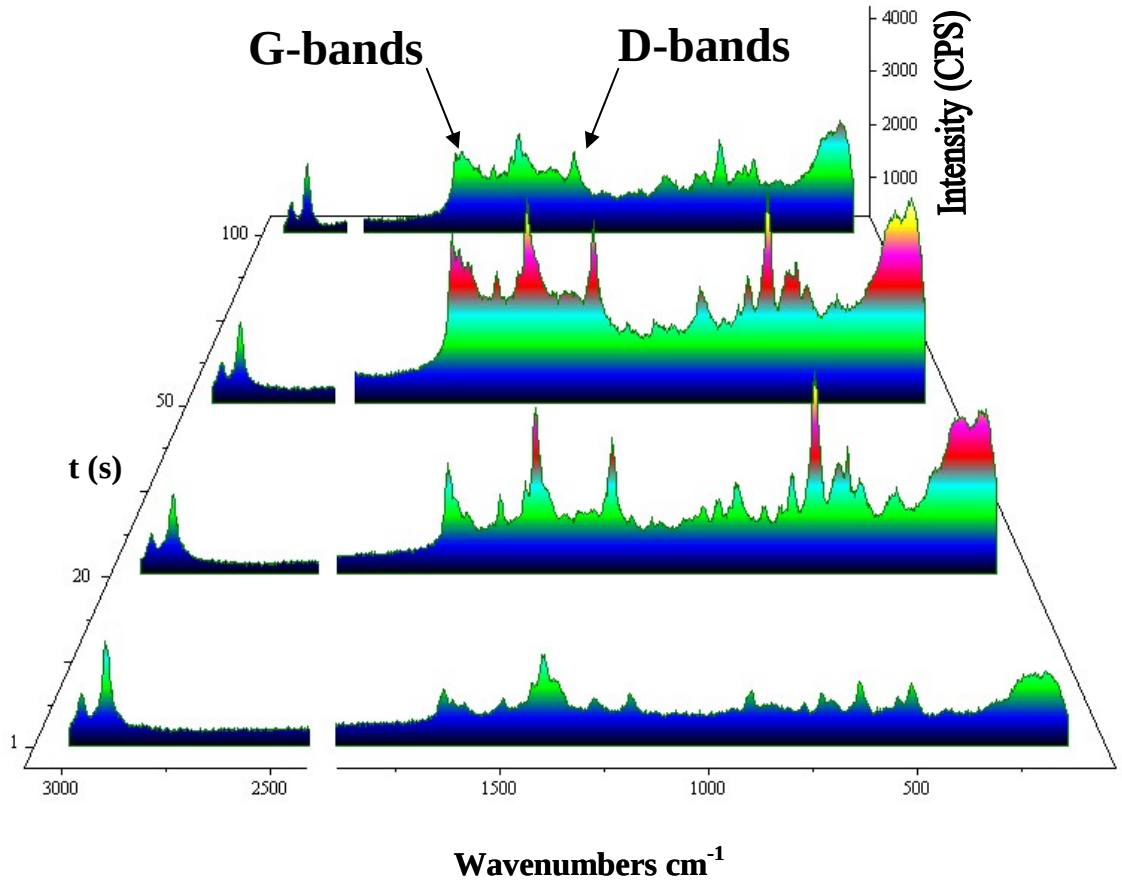

Figure 2.2 Signal degradation profile for a 1.0x10^{-4}M solution of naproxen USP under stationary conditions on Ag-PDMS.

even greater benefits should be realized with a surface-based technique. Typical conditions involve spinning at 400 rpm (~ 7 revolutions per second), acquiring signals for one second, and positioning the illuminated region 500 μm off center. Under these conditions, the effective duty cycle for 1 second interval an estimated spot size of 20 μm is only about 0.6 %. The spinning of the sample also compensates for microscopic aberrations of the substrate by generating a solid of revolution that is viewed by the detector as a uniformly distributed surface. STT also shows a significant improvement in the reproducibility of the analytical signals of 4-ATP relative to those obtained by mapping the surface of the substrate (Figure 2.3). The technique also exhibits a significant decrease in the SERS bandwidths of a series of solutions of naproxen, riboflavin, R6G, 4-ATP, and folic acid in 1% DMSO (Figure 2.4). STT also increases the intensity of the observed bands of other pharmaceutical and environmentally relevant compounds (Figure 2.5). Bands that are not observed under stationary conditions can be detected with STT.

The extent of the laser damage under spinning and stationary conditions was studied by capturing the images of the SERS active surface prior to and after the laser irradiation. The results demonstrated that permanent damage of the substrates occurred even after a one second irradiation of the sample with 8.9±(0.1) mW of the 632.8 nm line of the He-Ne laser (Figure 2.6). The diameter of the affected areas was estimated by using the measuring features available in Labspec. The results showed a visible damage of approximately 25 μm in

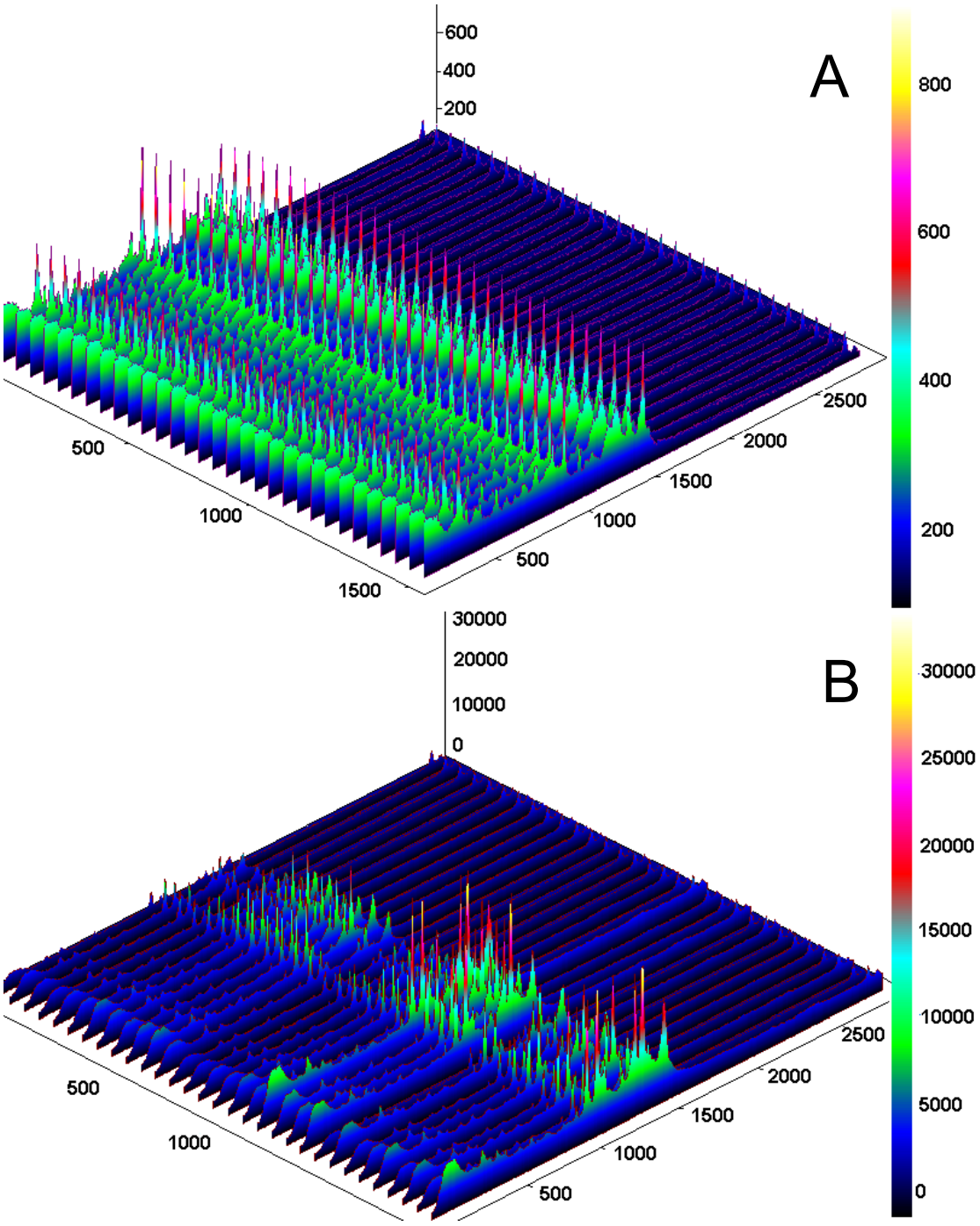

Figure 2.3 Differences in the 4-ATP signals under (A) STT and (B) traditional SERS mapping conditions.

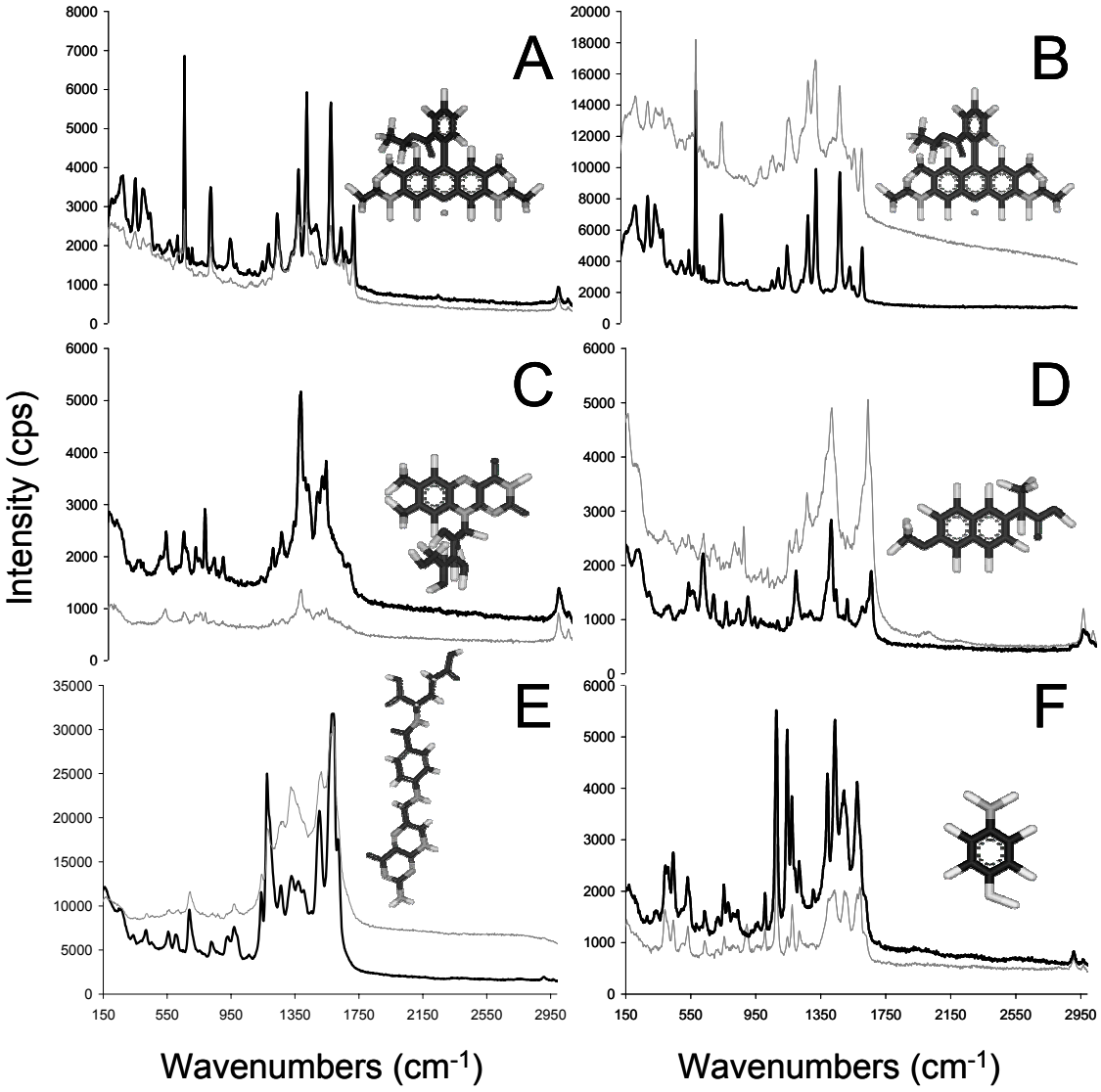

Figure 2.4 Laser irradiation effects under spinning (bold line), and stationary (light line) conditions: A. 1.0x10^{-4}M rhodamine-6 G on PDMS; B. 3.0x10^{-6}M rhodamine-6 G on glass; C. 1.0x10^{-4}M riboflavin on PDMS; D. 1.0x10^{-4}M naproxen on PDMS; E. 9.0x10^{-5}M folic acid on PDMS; F. 3.0x10^{-6}M 4-aminothiophenol on PDMS (all 1.0 s acquisition).

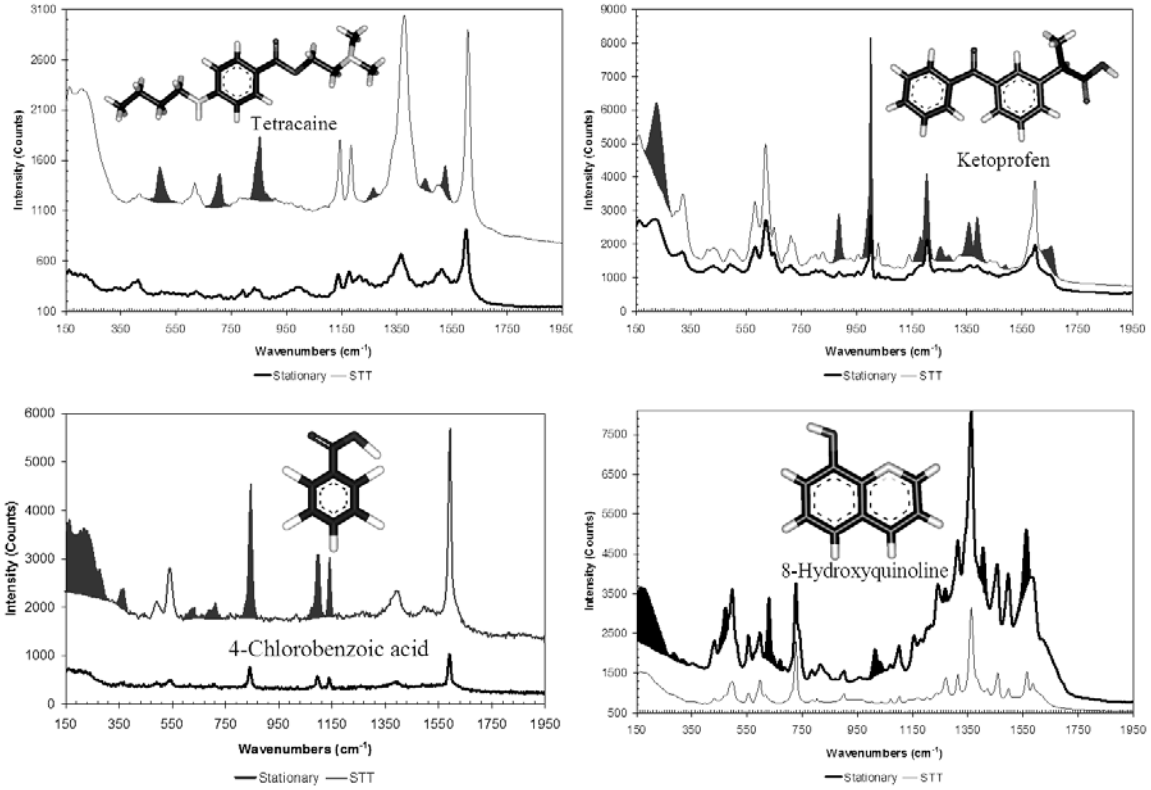

Figure 2.5 Spinning (light line), and stationary (bold line), SERS spectra of a series of 1.0×10^{-4}M solutions of tetracaine, ketoprofen, 4-chlorobenzoic acid, and 8-hydroxyquinoline on PDMS (all 1.0 s acquisition).

Note: The highlighted areas correspond to some of the regions were changes in the observed signals occur.

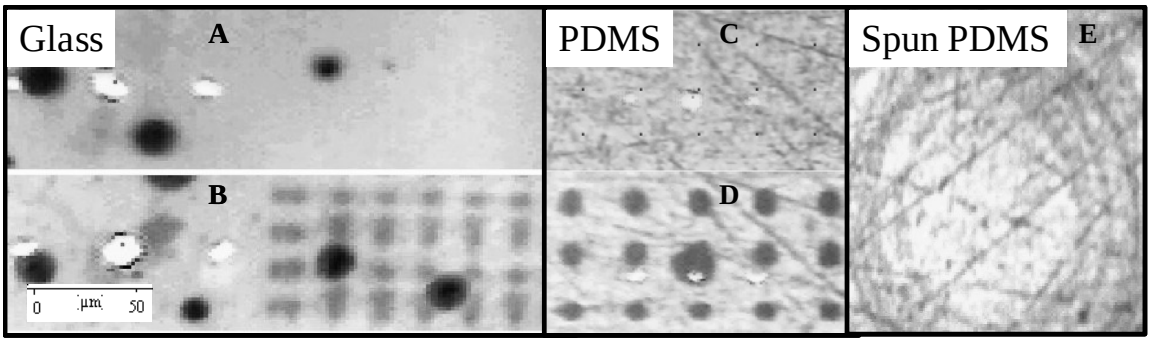

Figure 2.6 Damage to the substrate surface after being irradiated with 8.9 ±(0.1) mW (632.8 nm He-Ne laser): A. Ag-glass surface prior to irradiation; B. Ag-glass surface after the irradiation; C. Ag-PDMS surface prior to irradiation; D. Ag-PDMS surface after irradiation; E. Ag-PDMS surface after irradiation under spinning conditions (the concentric circles correspond to photolytic damage of the surface upon an extended irradiation of the beam.

diameter at the regions that were temporarily irradiated by the laser beam (note the square grid of irradiated spots), and a 50 μm area at the continuously irradiated region (note the darker random spots). This effect occurs even at powers as low as 2.5±(0.1) mW under stationary conditions. The damage was decreased by more than 30% (to about 17 μm), by spinning the sample at approximately 400 rpm with the maximum laser power (note the concentric rings in Figure 2.6 E). This decrease in apparent damage is a direct result of the decreased residency time of the laser beam at a given region of the substrate, which minimizes the heating of the surface as well as the photo-excitation of individual analyte molecules. The effects of the laser irradiation time under spinning and stationary conditions were studied using a 1.0×10^{-4} M solution of naproxen (d-2-(6-methoxy-2-naphthyl)propionic acid) in 1%DMSO. Naproxen is susceptible to thermal and photolytic decomposition under the experimental conditions. Naproxen Raman shift assignments were performed by comparing its conventional Raman spectrum (Figure 2.7) to the data available for naphthalene. The naphthalene, methoxy, and the isopropionic acid modes of naproxen are summarized in Table 2.1.

As expected, most of the vibrational modes of the drug corresponded fairly well to those observed in the literature for naphthalene. The stationary SERS results for the diluted naproxen sample show the disappearance of the 2650 cm^{-1} and the 1768 cm^{-1} bands that are attributed to the carboxylic acid overtone and a carboxylic acid hydrogen bond dimer modes, respectively. The

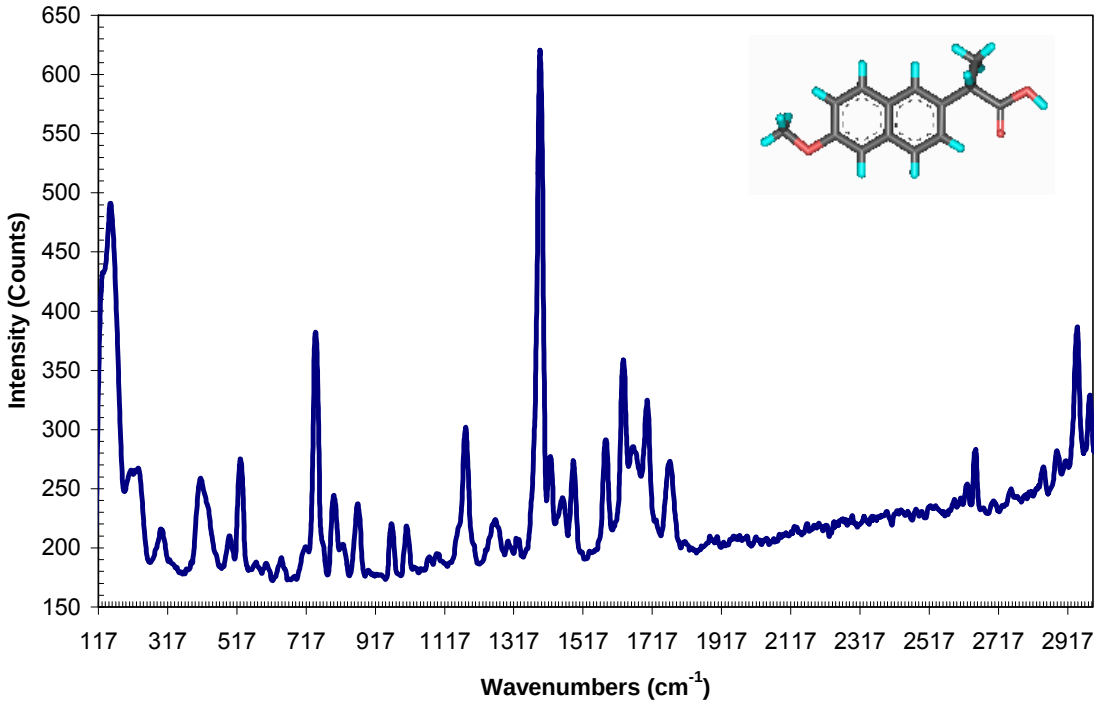

Figure 2.7 Raman spectrum of solid naproxen in a glass capillary (1.0 s acquisition).

Table 2.1 Characterization of the SERS and conventional Raman spectra of naproxen USP.

Solid Raman	$1x10^{-4}$ M Spinning (SERS)	$1x10^{-4}$ M Stationary (SERS)	Naphthalene Assignments (see ref. 90)	Assignments [a,b]
2982				ν CH_3
	2970	2970		ν CH_3 Si-OH from PDMS
	2910	2910		ν CH_3 from PDMS
2944				ν CH_3 Stretch from the ether
2889				ν CH_3 Stretch
2841				ν CH Stretch
2650				COOH overtone
1768				COOH hydrogen bond dimmer
1670				ν Aryl-C
1634	1634	1628	1628	B_{3g} v_{39}
		1607		G_2 band of amorphous C
1582	1587	Overlapped	1576	A_g v_3
		1579		G_1 band of amorphous C; A_g v_3; $\nu CH\text{-}COO^-$
1488.0	1488.0	1485		δ O-CH_3, overlapped with A_g v_4
1464.4			1464	A_g v_4
1393	1390	1390	1383	A_g v_5
		1358		D band for amorphous carbon; B_{2u} v_{32}
1324				ν Aryl-O
1267	1267	1267	1267	B_{1u} v_{21}
1175	1178	1178	1147	A_g v_6
1079	1076	1070		ν O-CH_3
1003			1021, (1011)	Ag_{v7}, (B_{2u} v_{35})
		975	968	B_{3u} v_{45}
963	934	922	951	B_{3g} v_{43}
	890			τ Isopropionic acid
864				ν C-O-C
	835	835		τ Isopropionic acid -Ag complex
799	792	Obscured		CH π for 2,6 substituted naphthalene; PDMS ν O-$SiCH_3$
745	761	761	764	A_g v_8 from the Naphthalene ring
	715	715		PDMS ν R-Si-R
	683	683		PDMS ν Si-OH
643				Ring Asymmetric Stretch
	623	620		PDMS τ R-SiOH-R
		557		ν Ag-CH Stretch
527	534	527	513	A_g V9, PDMS Si band
	497	497		B_{3g} v_{44}
415	408			δ COC

[a] The vibrational modes were abbreviated as Sym. ν, symmetric stretch ; Asym. ν, asymmetric stretch; δ, in plane bend; γ, out of pane bend; π, wagging; τ, torsion. The ring vibrations were assigned relative to the vibrational modes of Naphthalene under D_{2h} symmetry. [b] The assignments were made relative to the data from references 90-93.

Aryl-C stretch band at 1670 cm^{-1} was possibly obscured within the B_{3g} v_{39} band typical on β substituted naphthalene. The ether C-O-C stretch, the Aryl-O stretch from the methoxy substituent, and the A_g v_4, and the A_g v_6 bands of the naphthalene ring were absent under spinning and stationary conditions (see Table 2.1). However, as seen in the table, most of the conventional Raman spectral features of naproxen were observed under spinning conditions. A minimal degradation of the SERS intensity of the analyte was observed under spinning conditions. Similarly, a minimal change in bandwidth of the SERS signals occurred after irradiation for 115 seconds under STT when compared against those observed under stationary conditions (Figures 2.8, 2.9). Nevertheless, there was no significant contribution from the sample matrix or the SERS substrate to the background signal (Figure 2.8). In contrast, significant changes in the observed spectral features occurred under stationary SERS conditions (Figures 2.10). These changes include a significant increase in the bandwidth of its SERS signals, the absence of bands that were present under spinning conditions, as well as the formation of bands that were absent under spinning conditions.

The time vs. bandwidth changes of the A_g v_5 band at 1390 cm^{-1} of the drug were automatically measured by LabRam computer (Figure 2.11). The data show an increase of over 400 cm^{-1} in the apparent width of this band under stationary conditions. This effect is dramatically reduced upon spinning were the changes in the apparent width of this band are less than 24 cm^{-1}. The increased

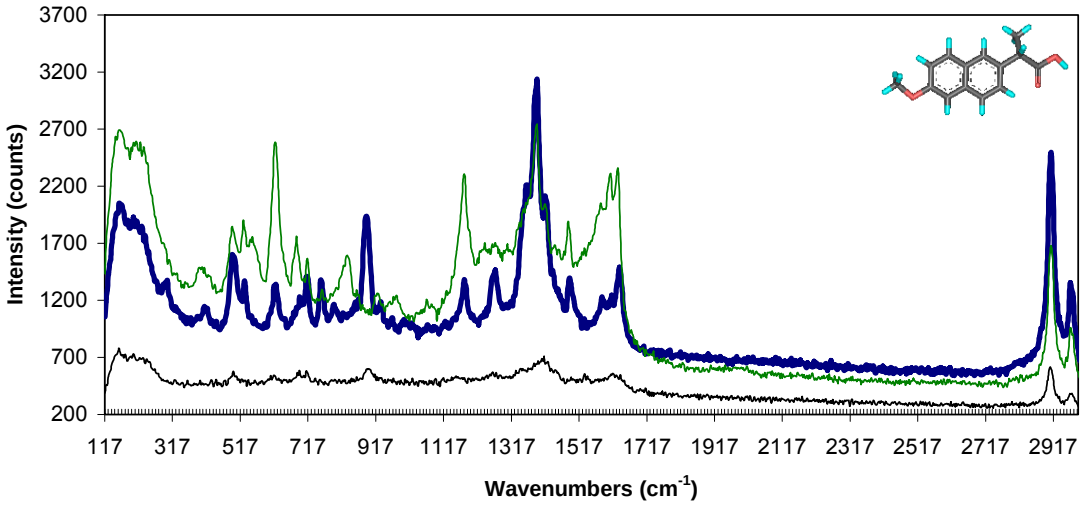

Figure 2.8 One-second snapshot of the SERS spectra of a 1.0x10-4 M solution of naproxen in 1%DMSO/Water over 18.0 nm Ag-PDMS after 115 s of irradiation; spinning at 400 rpm (bold line), stationary (gray line), background (dashed).

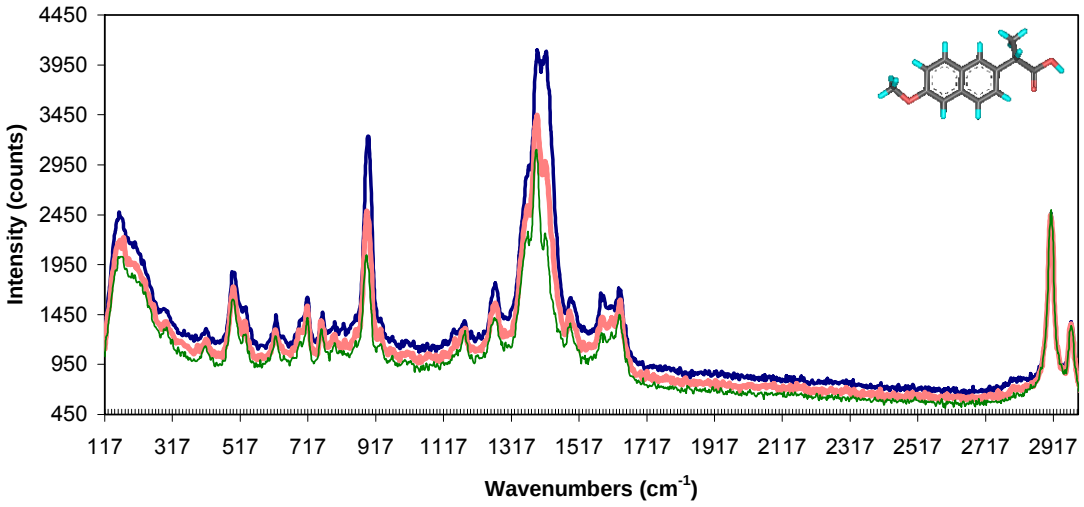

Figure 2.9 Changes in the spectral features of naproxen under spinning conditions: 1.0 s acquisition after 1 s (bold line), 30 s (bold-gray line), and 90 s (dashed line) of irradiation.

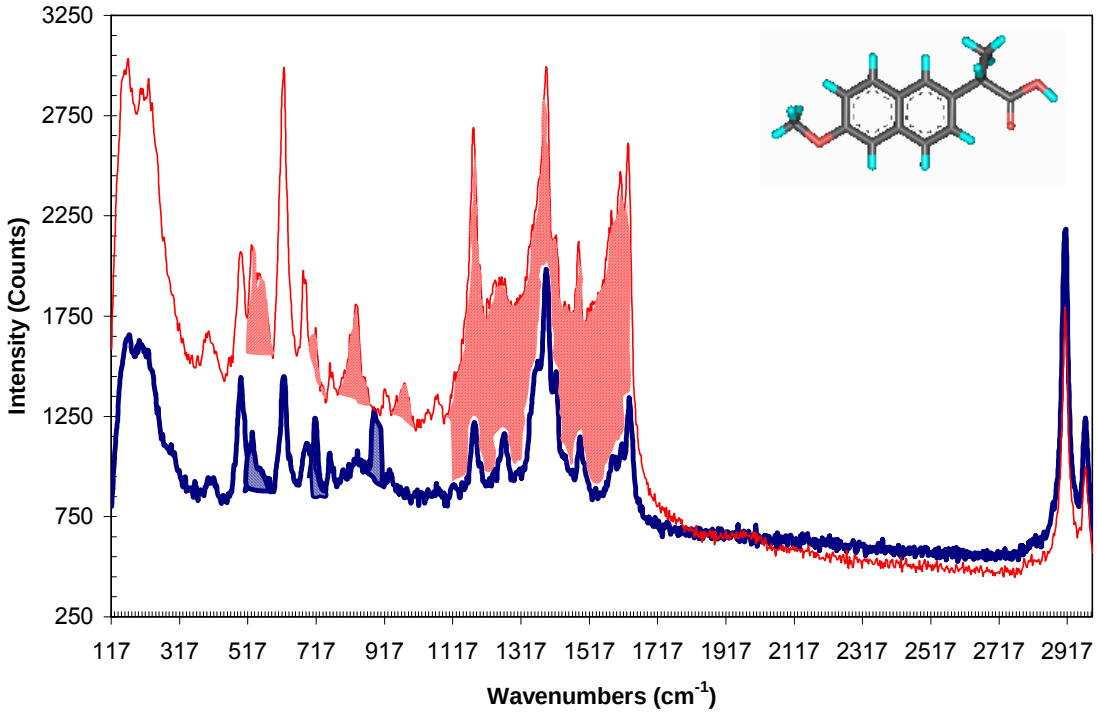

Figure 2.10 Changes in the spectral features of naproxen under stationary conditions: 1.0 s acquisition after 1 s (bold line) and 115 s (light line) of irradiation. The shaded areas correspond to the altered bands during the irradiation. Note that after 115 s the photodecomposition of the analyte is evidenced by the presence of graphitic bands. The appearances of naproxen bands on top of these bands are the result of the diffusion of intact molecules of the analyte from the bulk solution onto the irradiated area.

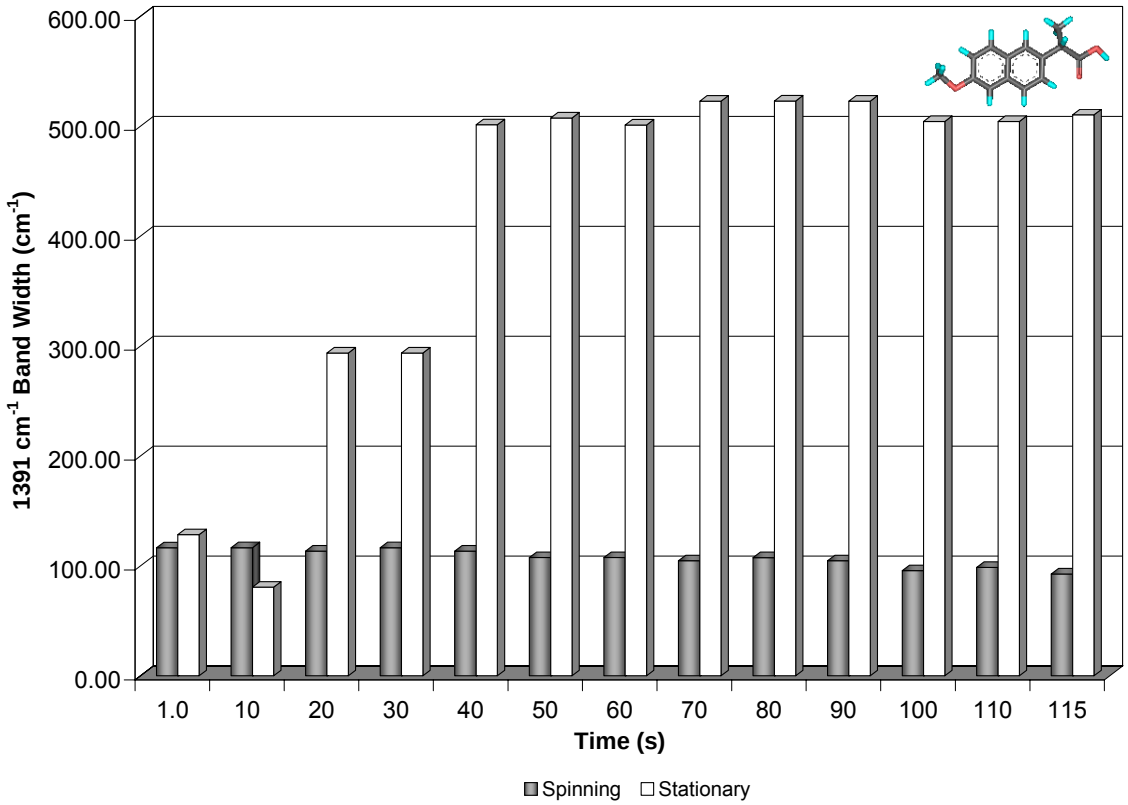

Figure 2.11 Changes in the 1391 cm^{-1} bandwidth of naproxen (1x10-4 M) under spinning and stationary conditions. Note: the changes under stationary conditions are the result of the graphitic bands of the analyte due to photodecomposition and the diffusion of intact molecules of the analyte from the bulk solution.

bandwidth is partly a consequence of the overlap of the naproxen bands and the multi-component graphitic D bands formed in the region of 1200-1460 cm^{-1} as well as the graphitic G bands near 1600 cm^{-1}. Consequently, the presence of the graphitic bands greatly diminishes the spectral resolution within this region. The presence of the naproxen bands on top of the graphitic carbon indicates the diffusion of intact molecules of the analyte from the bulk solution to the irradiated area. The graphitic bands are consistent with those observed by Dumont et. al. and reported in the literature as amorphous graphite bands.[87-88] The impact of changes in band profiles under stationary SERS conditions on the quantitative aspects of SERS are obvious.

Another important difference in the stationary SERS spectra of naproxen was the absence of the isopropionic acid band at 890 cm^{-1} band and the increased intensity of the 835 cm^{-1} band under stationary conditions. The band at 890 cm^{-1} has been attributed to the reaction of the isopropionic acid group with the SERS active substrate to form a silver-isopropylcarboxylate-R complex in a mechanism similar to the one observed during the Hunsdiecker reaction.[94] This interaction mechanism has been proposed by Paniker et. al. on their SERS studies of 4-aminosalicylic acid by FT-Raman.[95] The proposed naproxen-silver complex has been recently reported by Ali et. al.[96] The aforementioned effects demonstrate the thermal and photolytic changes that probably lead ultimately to the fragmentation of the drug.

Interestingly, it was visually observed that incomplete “healing” of the Ag-PDMS substrate (see darkened regions in Figure 2.6) occurred with time after modest irradiation conditions. Although there were some background features of the Ag-PDMS composite material (see above), these features show negligible changes with prolonged irradiation. However, the SERS activity of the darkened spots in Figure 2.6 was diminish relative to that of a pristine substrate. In one experiment, the substrate was irradiated for one minute with the substrate either dry or with solvent present. Subsequently, a solution of naproxen was added and spectra were acquired. These spectra were a factor of 3-10 times less intense than when the substrate was moved from the irradiated spot (for both the dry or solvent cases), but did not show the appreciable broadening and graphitic bands that were observed when irradiation was performed in the presence of naproxen.

A similar study was performed for 4-ATP. Due to its strong SERS activity, a 3.0×10^{-6} M standard solution of 4-ATP in 1%DMSO was used. At a proper concentration, this analyte reacts irreversibly with silver to form a “self-assembled monolayer” at the surface of the SERS active substrate.[91] The stability of the silver-sulfur bond, as well as its relatively simple structure, makes 4-ATP an interesting analyte to study laser irradiation effects on our substrates. The characterization and band assignments of the 4-ATP under spinning and stationary conditions were performed via available literature and are summarized in Table 2.2.

Table 2.2 Characterization of the SERS spectra of 4-aminothiophenol.

$3x10^{-6}$ M Spinning (SERS)	$3x10^{-6}$ M Stationary (SERS)	Literature[see ref. 91] Values Raman/(SERS)	Assignments [a,b]
2572	2577	2565	ν Ar-SH
2281			Overtone NH_2^+
1936			Overtone for benzene derivatives
1628		1620	ν CC, 8a (a_1), δ NH_2, ring quadrant ν
1576	1582	1572 (1573)	ν CC, 8b (b_2), ring quadrant ν
1503			Quadrant ν p-substituted benzene
	1489	1490	Quadrant ν, 19a (a_1) for mono substituted Benzenes
1476	1479	1480 (1472)	ν CC + δ CH, 19a (a_1) p-substituted
1441	1438	1445 (1440)	19b (b_2), νCC+δCH
1393	1393	1391(1403)	δCH+νCC, 3 (b_2), quadrant ν p-substituted benzene
1303	1306	1310 (1306)	14 (b_2), ν CC+δ CH, Aryl-NH_2 ν
1284		1280	7a'(a_1), ν CH
1246	1245		Ar-NH_2 ν
1218	1215		Ring Quadrant Sym. ν
1192	1190	1206 (1190)	Ring Quadrant Asym. ν
1172	1174	1173	δ CH, 9a (a_1)
1144	1144	1142 (1142)	δ CH, 19b (b_2), νCN
1073	1076	1089 (1077)	ν CS, 7a(a_1)
1007	1007	1011(1006)	γ CC+γ CCC, 18_a (a_1)
960	967	960 (950)	Cs 17 a (a_2), δ NH_3
922	920	(921)	δ C-S, π CH, 5b (b_1)
882			π CH disubstituted benzene, mono substituted NH_2
861	861		π CH for monosubstituted benzene
838	841	830	π CH, 10a(a_2)
818	823	820	π CH, 11 (b_1)
806	809	799	ν CH, ν CS, ν CC, 1(a_1), γ NH_2, PDMS ν O-$SiCH_3$
758	758		CH 10b(b_2)
715	715	699 (719)	PDMS ν R-Si-R, 4 (b_1), π CH+π CS+π CC
633	633	634	12(a_1), γ CCC, τ R-SiOH-R
530	533	521	16 (b_1), PDMS Si band
490	493		τ S-H
443	443	463	γ CCC, 6a (a_1)
405	398	396 (406)	16a (a_2), γ CC, δ CH+δ CS,
337		321	δ CN+δ CS, 18b (b_2)
278		256	δ CN+δ CS, 9b(b_2)
195	204	213	ν Ag-S
162	158	154	π CN+π CS+τ CC

[a] The vibrational modes were abbreviated as ν, stretching; δ,and γ, bending; π, wagging; τ, torsion. The ring vibrations were assigned relative to the vibrational modes of a para-substituted benzene with C_{2v} symmetry. [b] The assignments were made relative to the available data for p-substituted benzenes and 4-aminothiophenol from references 1,91-93,100

Similar to naproxen, 4-ATP had a minimal degradation of the SERS intensity and bandwidths under spinning conditions. Significant changes of the spectral features of 4-ATP were observed under stationary conditions (Figure 2.12). These changes include an increase of the widths of the 1441 and 1073 cm^{-1} bands, from 29.7 to 35.6 cm^{-1}, and from 24.9 cm^{-1} to 31.2 cm^{-1}, respectively, when comparing spinning to stationary SERS conditions. Bands that were present under spinning conditions disappeared or changed their relative intensities under stationary conditions.

The results for the 4-ATP sample under stationary conditions display the disappearance of the 1628, 337, and 278 cm^{-1} bands as well as a decrease in the intensity of the 1246 cm^{-1} band relative to the initial spectrum under spinning conditions. These are attributed to vibrational modes of the amino group in 4-ATP (Table 2.2). These observations strongly suggest a cleavage of the amino group due to the laser irradiation. This was supported by the disappearance of the band at 1503 cm^{-1} that was attributed to a quadrant stretching mode characteristic of p-substituted benzenes. Further evidence is seen in the decreased intensity of the 1503, 1192, 1172, 758, 530 and 464 cm^{-1} bands under stationary conditions. These bands are mostly ring vibrational modes for p-substituted benzenes. The presence of residual intact 4-ATP molecules and the C_{2v} symmetry of benzenethiol and 4-ATP complicate the observation of this phenomenon under stationary conditions. The increased bandwidths in the 1200-1600 cm^{-1} region indicates the eventual formation of graphitic bands from

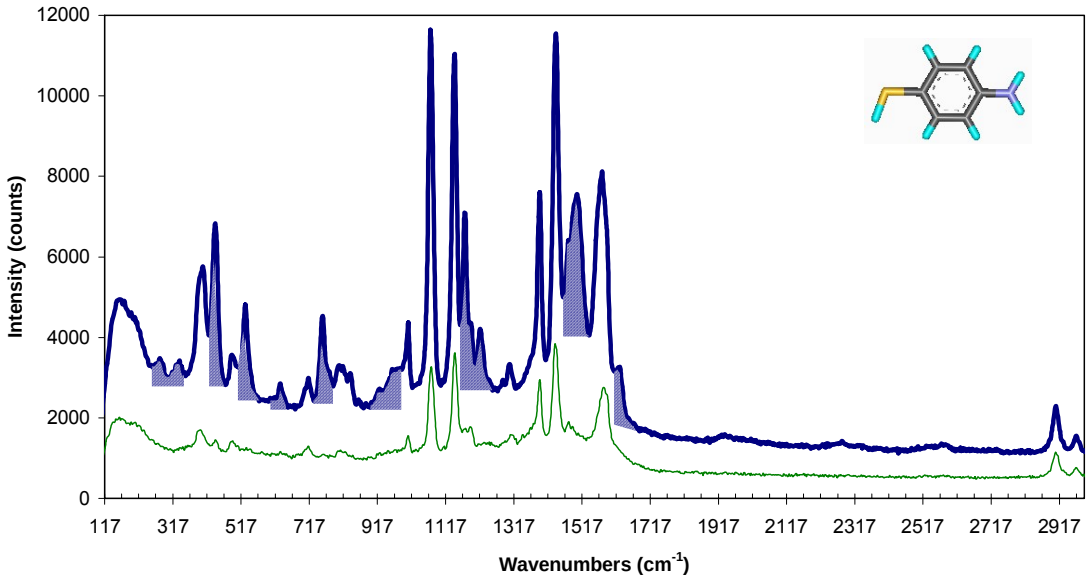

Figure 2.12 Changes in the spectral features of 4-ATP under stationary conditions: 1.0 s acquisition after 1 s (bold line), 114 s (gray line). The shaded areas correspond to the altered bands during the irradiation.

thermal decomposition. These spectral changes limit the use of stationary SERS for quantititation and increase the risk of qualitative misinterpretation of the analytical data.

Rhodamine 6G (R6G) is a fluorescent dye whose Raman signal is modestly resonant enhanced at 632.8 nm. The SERS spectra of a $1.0x10^{-4}$ M solution of R6G under spinning and stationary conditions are reported on Figure 2.13. As in the previous cases, a significant broadening of the bands in the 1200-1600 cm^{-1} graphitic region under stationary conditions indicate the rapid photo-thermal decomposition of the dye. Photo-thermal changes in the relative intensities of the bands under stationary conditions were observed with laser powers as low as 2.1 mW. Emory, et. al. has recently studied the photodecomposition of single Rhodamine 6G molecules on silver nanoparticles.[97] The photoproduct was identified as graphitic carbon based on the appearance of bread SERS vibrational bands at 1592 cm-1 and 1340 cm^{-1}. It is interesting to speculate that the intermittent fluorescence ("blinking") of R6G at or near single molecule detection conditions, as reported by Nie[73] and others, may occasionally include the photo-thermal decomposition effects seen in this work with bulk concentrations of the dye.

Since R6G is among the most SERS active analytes reported in the literature, its detection at concentrations as low as 10^{-12} M under SERS conditions is possible.[101] This makes R6G an ideal analyte to study the effectiveness of Ag-PDMS substrates for quantitative determinations with STT.

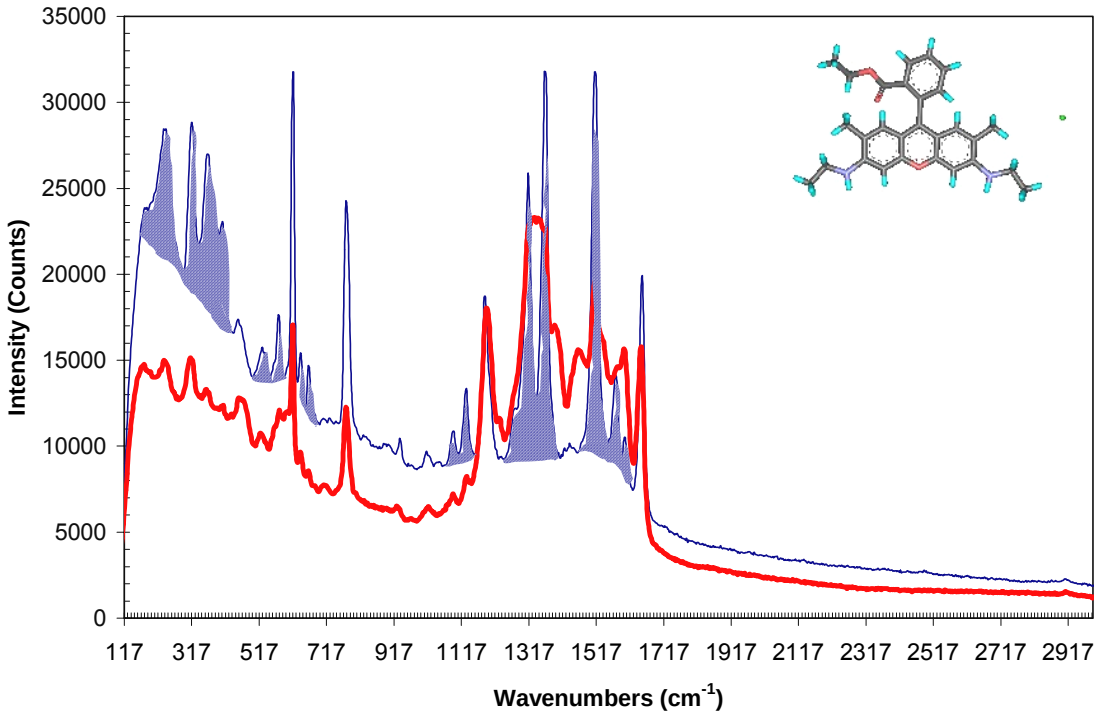

Figure 2.13 Changes in the spectral features of R6G under stationary conditions: 1.0 s acquisition after 1 s (bold line), 110 s (gray line) of irradiation. The shaded areas correspond to the altered bands during the irradiation.

Figure 2.14 shows the Ag-PDMS working curve for a series of R6G standards from $3x10^{-6}$ to $1x10^{-4}$ M in 1% DMSO under spinning conditions. The results suggest a saturation of the Ag-PDMS SERS active substrate at very low concentrations (above $1x10^{-5}$M), in contrast to concentrations above $7x10^{-6}$M for our previous results with the Ag island on glass substrates. The data show a coefficient of variation lower than 5% and a correlation coefficient of 0.99, below the saturation point. The saturation of the substrate at levels above $1x10^{-5}$ M seems to be a consequence of the large amount of analyte present in the wells (50 µL) per sample and the concentrating effect of the PDMS material. At the moment of this publication our group is working on the optimization of our design to increase its linear range.

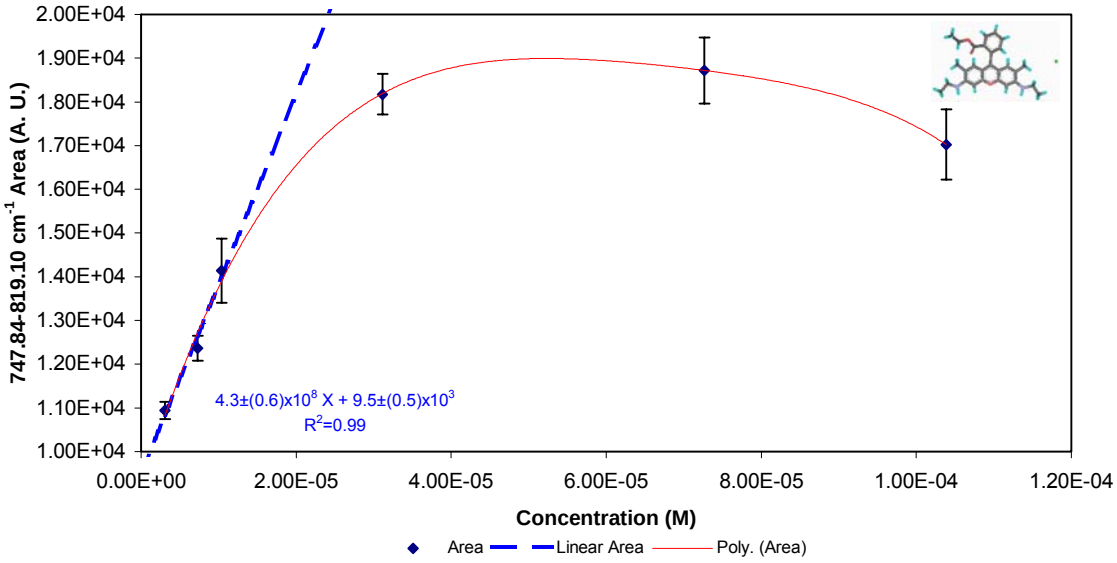

Figure 2.14 Working curve of R6G (N=5) under spinning conditions.

CHAPTER 3

Improving the analytical figures of merit of SERS for the analysis of model environmental pollutants

This chapter is a revised version of an article under the same name published in the Journal of Raman Spectroscopy by Marco A. De Jesús, Kathleen S. Giesfeldt, and Michael J. Sepaniak:

De Jesús, M. A.; Giesfeldt, K. S.; Sepaniak, M. J.; **"Improving the Analytical Figures of Merit of SERS for the Analysis of Model Environmental Pollutants."**; Journal of Raman Spectroscopy (MS#z3023) in press.

My use of "we" in this chapter refers to my co-authors and myself. My primary contributions to this article included: (A) design of the project and development of the experimental protocols to study the sorption of model pollutants by SERS (B) design and fabrication of a series of metallized-PDMS microtiter well plates, (C) design of the experimental methods and protocols, (D) collection and statistical analysis of the analytical data (E) collection and interpretation of the cited literature, (F) most of the writing.

3.1 Introduction

The presence of aromatic pollutants in natural water has become an issue of prime importance to the international community.[102-104] Chemicals such as amino aromatic compounds, poly-aromatic hydrocarbons (PAH´s), phenolics, and naphthalene derivatives are present in aquatic environments as a result of their use as pesticides or as raw materials for industrial processes.[105-107] The potential persistence and toxicological effects of these chemicals and their biodegradation products are major concerns for regulatory agencies in the United

States and the European Union.[105,107] As a result, a maximum concentration limit (MCL) of less than 1 μg/L has been set for the majority of these pollutants in drinking water.[109] Such detection limits impose a real analytical challenge for the development of instrumental techniques capable of selectively detecting trace and ultra-trace amounts of these pollutants in aqueous media.

Most of the EPA-approved methods for the detection of aromatic pollutants in water rely on techniques such as headspace analysis, purge and trap, solid-phase extraction (SPE), and liquid-liquid extraction to promote the pre-concentration of sample analytes prior to subsequent analysis via gas chromatography (GC) or liquid chromatography (LC).[102,103] These methods often require complex and time-consuming protocols in order to cope with the potential sample loss and cross-contamination during the sample preparation and detection steps. This complexity has led to the development of new analytical protocols, such as solid phase micro-extraction (SPME), in order to simplify and accelerate the analysis.[110] Regardless of these advancements, the detection of the eluting species often relies on information-limited techniques such as electrochemical detection, flame ionization detection, fluorescence, or UV-vis spectrophotometry. The lack of detailed structural information obtained by these detection schemes greatly limits their use for the unequivocal identification of the chemical constituents in complex samples. Nuclear magnetic resonance (NMR), infrared (IR), and Raman spectroscopy are analytical techniques that can provide considerably more structural information than the aforementioned

approaches.[111-113] The use of NMR for the detection of trace pollutants has been limited due to the inherent costs, solvent requirements, and the relatively low sensitivity of the technique. Although FT-IR has been employed in the detection of organic contaminants in the gas phase, its use for trace analysis has been limited due to low sensitivity and a general incompatibility with aqueous media. Recent advances in optical and laser technology, in addition to the low polarizability of water, have made Raman spectroscopy one of the most promising tools for the spectroscopic analysis of organic pollutants in aqueous media. However, its use as a routine analytical tool for the detection of organic compounds has been limited due to the very small cross-sections of the Raman scattering process and thermal and photolytic processes induced by the radiation sources.

Surface Enhanced Raman Spectroscopy (SERS) has proven to be a viable approach to improve the sensitivity of Raman signals for the detection of pharmaceutically and environmentally relevant compounds.[4,78,115] The extremely large enhancement of the Raman signal upon the positioning of the sample analytes on or very near the surface of certain noble metal structures with nanoscale features has greatly improved the sensitivity of the technique. Nevertheless, a dichotomy surrounding SERS as an analytical technique is evident. On one hand the ultimate in sensitive analysis, the acquisition of distinctive spectra of single molecules, has been reported by several groups.[73,116-117] On the other hand, a search of the literature over the period of

1904-2003, via the SciFinder scholar search engine, and based on the key words *trace analysis*, revealed that only 0.29% of the flagged reports involved SERS. A clear contributing factor to this dichotomy is that only a miniscule fraction of significant organic chemicals and possible adsorption sites on most SERS substrates can exploit the full power of resonant, chemical and electromagnetic surface enhancement factors. Notwithstanding the uniqueness of single molecule detection, both in its power for certain important studies and its lack of general applicability, SERS has not seen general use for more traditional trace analysis because of limitations in the analytical figures of merit of the technique, such as reproducibility and dynamic range.

A key factor in improving the analytical capabilities of SERS resides in the performance characteristics of the SERS-active substrate. Considerable work has been done in the area of substrate design. Among the approaches are silver islands on glass,[43] colliodal silver solutions,[118] colloidal particles encapsulated in sol-gels,[58] silver coated microspheres,[53] metallized polymers,[52] and more regular structures such as those created by nanosphere lithography.[119]

The inhomogeneous adsorption of the analyte onto traditional SERS substrates, such as colloidal silver and silver-islands films, in combination with their susceptibility to oxidation upon contact with water and other oxidizing agents, are among the variables that contribute to these poor figures of merit. Our research group has recently demonstrated the use of metallized polymers such as silver-polydimethylsiloxane (PDMS) as substrates for SERS

applications.[52] These novel metal-polymer nanocomposites have proven to be effective in reducing the oxidation of the metal nanoparticles and exhibit unique optical and pre-concentrating properties that make them a promising alternative for the detection of aromatic pollutants in water.

In the previous chapter we demonstrated that relevant analytes are commonly sensitive to the thermal and photolytic processes inherent to SERS. Continuous irradiation of the laser beam over the SERS substrate can promote the decomposition or fragmentation of the sample analytes, altering the observed spectral bands and greatly affecting the reproducibility of the observed signals.[80,81,120] In 1971, Kiefer and Bernstein used a rotary cell to minimize these effects under Resonance Raman (RR) conditions.[81] This technique allowed the study of analytes that were destroyed with exposure to the laser radiation, which allowed a significant enhancement of the observed spectral features.[81-83]

Our research group has extended recently this technique to SERS by rapidly translating both sample and SERS active substrate (see chapter 2). This new version of the sample translation technique (STT) dramatically decreased the effective residence time of both analytes and substrates within the irradiated zone without reducing spectral acquisition time or the power density at any given instant.[120] In addition, the rapid translation of the sample creates a solid area of revolution that averages out microscopic aberrations often seen in SERS substrates.

In this chapter we discuss the use of silver-polydimethylsiloxane nanocomposites (Ag-PDMS) for the qualitative and quantitative analysis of model environmental pollutants in water via STT-SERS. The analytical response characteristics of 4-aminobenzoic acid (4-ABA), 4-hydroxybenzoic acid (4-OHBA), 4-chlorobenzoic acid (4-ClBA), 4-aminothiophenol (4-ATP), and phenolphthalein (PHT) are studied and reported. The effects of different experimental variables such as laser power, laser irradiation time, and translation rate on the SERS signals of the above mentioned analytes are discussed. The use of pH to promote the selective sorption of 1,5-diaminonaphthalene (1,5-DAN), 1,5-dihydroxynaphthalene (1,5-DHN), and 4-ABA is also presented. The term sorption is used to indicate that variable degrees of adsorption and absorption (partitioning) may be involved. The impact of these variables on the precision and accuracy of the analytical results and the potential use of the technique for the direct analysis of environmental pollutants in water are presented.

3.2 Experimental

3.2.1 Instrumentation

All SERS spectra were acquired using a modified version of a LabRam Spectrograph from JY-Horiba (Figure 3.1). The instrument uses an Olympus BX-40 microscope with a 10X (0.25 NA, ∞) objective that delivers up to 8.9 mW of the 632.8 nm line from an electrically-cooled He-Ne laser. The acquisition

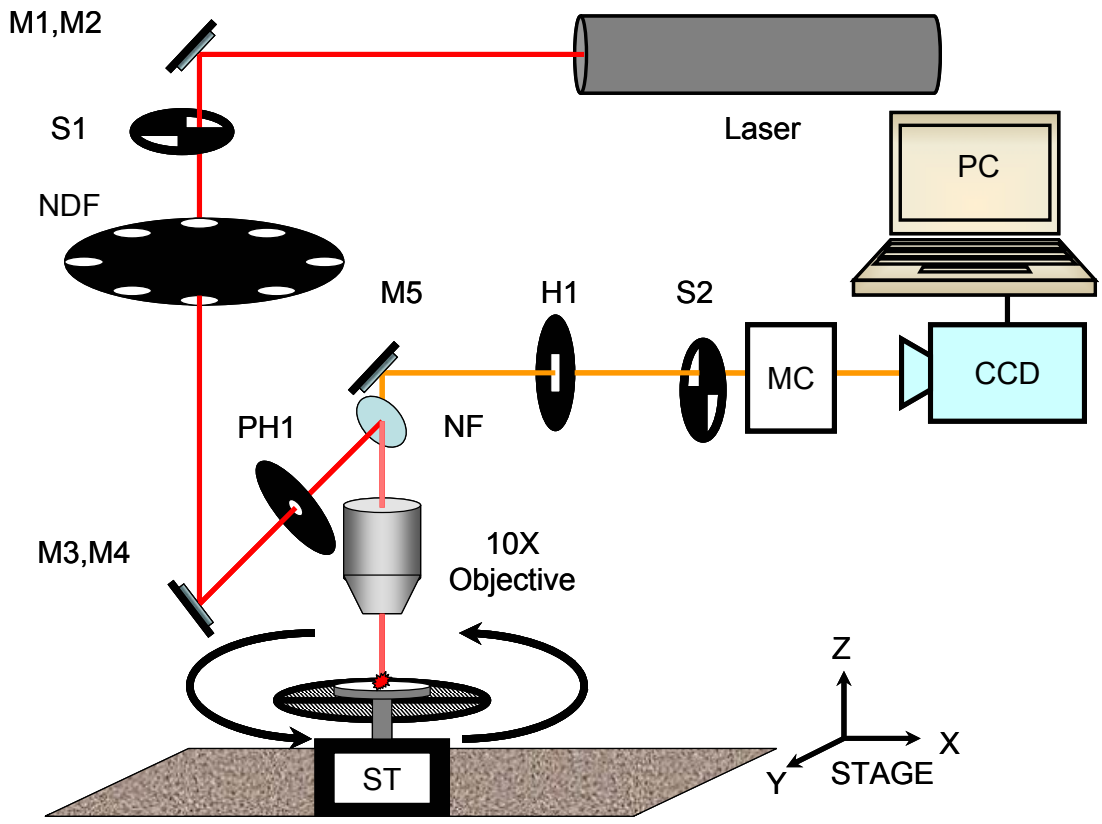

Figure 3.1 Schematic representation of the Raman instrument: 20 mW (8.9±(0.1) at the sample) He-Ne laser at 632.8 nm, external mirrors (M1, M2), synchronous mechanical shutters (S1, S2), neutral density filter wheel (NDF), internal mirrors (M3-M6), notch filter (NF), confocal pinhole and hole (PH1, H1), 10 x microscope objective, 600 g/mm monochromator (MC), 1024x256 Peltier cooled CCD camera (CCD), XYZ stage, and sample translator (ST).

parameters were adjusted as described in chapter 2. The slit and hole were opened to 500 μm and 200 μm, respectively. All spectra were acquired in a 180° scattering geometry with a 2936 cm^{-1} spectral window centered at 1700 cm^{-1}. The scatter was dispersed with a 600 groove/mm grating, imaged with a 1024 x 256 thermoelectrically cooled CCD camera, and processed with Labspec 4.03 software. A computer controlled x-y-z stage was used to adjust the focusing of the microscope objective as well as the positioning of the laser spot under stationary and translating conditions. Two improvements in the basic spectrometer hardware (see sections 1.2.6.3 and 2.2.1), include the addition of a mechanical shutter at the exit of the laser and prior to the entrance of the internal optics of the instrument, and the use of a Stanford SR-540 chopper for the fast translation (via spinning) of the samples during the experiments (Figure 3.2). The addition of a shutter at the exit of the laser minimizes the laser irradiation effects by exposing the samples to the incident beam only while the instrument is collecting data. In this work, all sample acquisition times were 1 second. The SR-540 chopper allows the translation of the sample at spin rates up to 8000 rpm.

The SERS active substrates were prepared with a physical vapor deposition chamber from Cooke Vacuum Products, Inc. The chamber was set to operate at a base pressure of 1.0 ±(0.5) 10^{-6} torr. Samples were mounted 24 cm above and normal to the effusive source. Average mass thickness and deposition rates were measured for each film with a quartz-crystal microbalance.

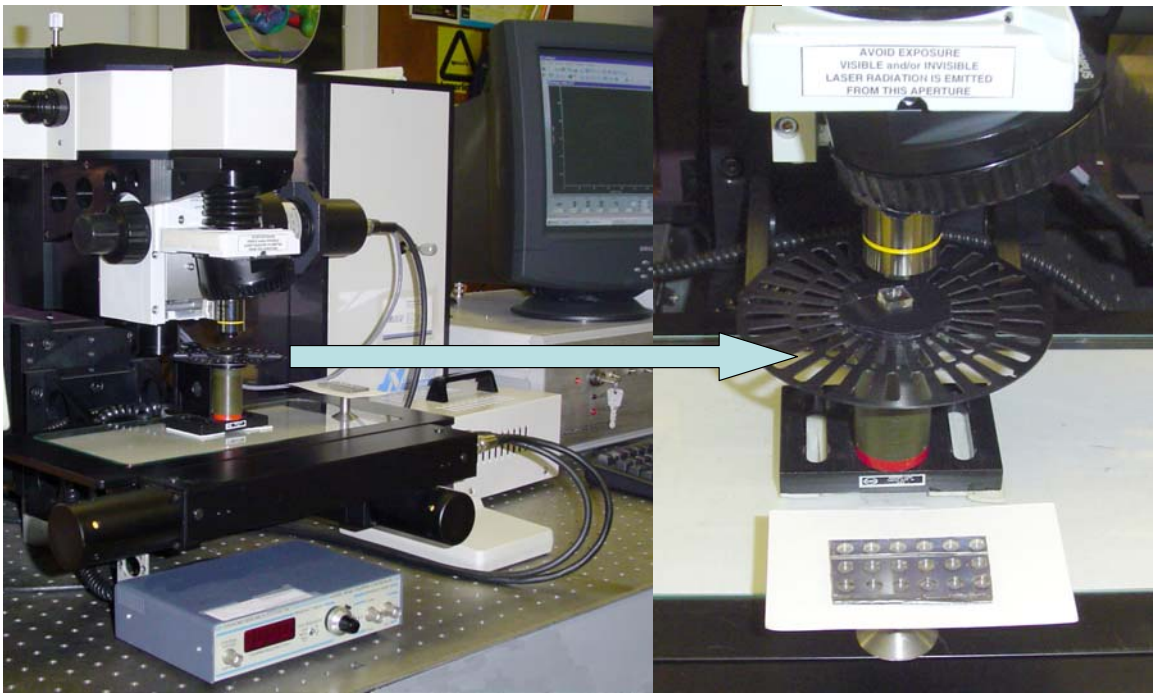

Figure 3.2 Graphical representation of the Lab-Ram setup with a Stanford SR-540 chopper.

3.2.2 Preparation of the SERS-active substrates

The polydimethylsiloxane (PDMS) substrates were prepared by the addition of Sylgard-184 curing agent (Dow Corning) and its elastomer in a 1:10 mass-to-mass ratio as discussed in chapter 2. The substrate was thoroughly combined and then degassed under moderate vacuum conditions (10^{-4} torr) for 15 minutes. Once all the entrapped air was removed, the samples were cast over the surface of a mold constructed from sanded Lego® platform and placed in the oven at 70°C for 30 minutes. The PDMS substrates were removed from the molds and stored at room temperature until the PDMS gained full mechanical strength (24 hours). The mold allows the preparation of a 28 x 28 array of 50 µL PDMS wells in a platform that resembles a microtiter plate. Each array was brought to high vacuum conditions ($1.0 \pm (0.5) \times 10^{-6}$ torr) and then coated with an average thickness of 19.0 ±(0.2) nm of 99.999% Ag (Alfa Aesar, MA), via physical vapor deposition (PVD) at a rate of 1.0 Å/s. The substrates were held under high vacuum conditions in the PVD system for 15 minutes to equilibrate. The Ag-PDMS substrates were stored in a vacuum desiccator held at 10^{-4} torr in the dark prior to use.

3.2.3 Sample preparation and data analysis

A series of 1×10^{-4} M stock solutions of 4-ATP (90+%, Aldrich), 4-ABA (analytical grade, Nutritional Biomedicals), 4-OHBA (98+%, Sigma), 4-ClBA (analytical grade, Eastman Organics), 1,5-DAN (97+% Aldrich), and 1,5-DHN

(97%+, Aldrich) were prepared with deionized water (18ΩBarnstead E-Pure) and 1% Methanol (99.9%, Acros Inc.). These stock solutions were used to prepare a series of calibration standards within the $1x10^{-4}$ to $1x10^{-8}$ M range. Nitric acid (Trace metal, Fisher) and sodium hydroxide (99%, Mallinkrodt), were used to adjust the alkalinity of a series of 1,5-DAN, 4-ABA, and 1,5-DHN solutions (all $1.0x10^{-4}$ M). The samples were used to study the changes in the SERS signal of these analytes as a function of the pH.

A 50 µL aliquot of each sample solution was transferred to the Ag-PDMS well, precisely centered on the top of the sample translator, and covered with a glass cover slip. The samples were generally spun at 2000 rpm and the spectrophotometer light microscope images were aligned relative to dead center of the bottom of the microtiter well. The point of maximum SERS signal was obtained by fine-focusing the microscope objective after moving the illuminated spot 150 µm off-center. Once the signal was brought into focus the SERS spectra of the sample were acquired by moving the stage at 50 µm intervals (1 spectral acquisition per step) to a maximum distance of 1400 µm from the dead center. The Ag-PDMS substrates were exposed to the sample matrix for approximately two minutes prior the collection of the analytical data. Corrections of the baseline and the background were performed in order to compensate for the changes in refractive index of the sample solutions and the optical background signal from the substrate.

3.3 Results and discussion

The contamination of our natural water resources with aromatic pollutants such as phenols and benzoic acid derivatives has become a problem of global significance. This study uses phenolphthalein (PHT), 1,5-diaminonaphthalene (1,5-DAN), 1,5-dihydroxynaphthalene (1,5-DHN) and four para-substituted aromatic compounds: 4-chlorobenzoic acid (4-ClBA), 4-aminobenzoic acid (4-ABA), 4-hydroxybenzoic acid (4-OHBA) and 4-aminothiophenol (4-ATP) as model systems for polyaromatic, chlorinated, amino aromatic, phenolic, and thiolated pollutants in water.

Some of these chemicals such as chlorinated aromatic compounds have been widely used as preservative agents, pesticides, bactericides and fungicides. They can also be generated as part of the biodegradative pathway of chlorinated pesticides such as chlorophenols and polychlorinated biphenyls (PCB´s), and the chlorine treatment of potable water.[121,122] Chlorinated aromatics show high environmental persistence and toxicity, including carcinogenic and endocrine disrupting activities.[123] Hydroxy-aromatic compounds also exhibit similar bacteriological and fungicidal activity, with the characteristic of being considerably more water soluble than their chlorinated counterparts. Aromatic amines constitute an important group of environmental pollutants due to their potential presence in industrial wastes and their role in the degradation pathway of nitroaromatic compounds. Their intrinsic alkalinity and metal binding

capabilities are important topics in the study of the dissolution of metals and organic matter in water.[124]

Most of the traditional detection schemes for these chemicals are based on information-limited techniques such as fluorescence, UV-Vis spectrophotometry, and flame ionization detection. The potential presence of positional isomers and other byproducts with minute structural differences make these detection methods unsuitable for the unequivocal identification of these chemicals in complex mixtures. An alternative to these traditional detection schemes is the use of SERS for the detection of aromatic pollutants in water. The tremendous enhancement of the Raman signal under SERS conditions and the low polarizability of water make SERS a promising tool for trace analysis in aqueous media. However, the susceptibility of the sample analytes to photo-react upon exposure to the incident laser beam and the fast oxidation and inhomogeneity of the substrates under SERS conditions has limited its use as a routine tool for environmental analysis. The present studies aim to demonstrate that these fundamental problems can be surmounted with Ag-PDMS substrates in combination with the STT technique.[120]

Ag-PDMS nanocomposite substrates offer important characteristics such as low cost, simple preparation, superior SERS signals, and low background features. The metallization of PDMS via physical vapor deposition also creates a three-dimensional structure of imbedded silver clusters that increases the effective surface area for SERS.[52,120] The elastomeric properties of PDMS

permit the fabrication of substrates with different shapes and dimensions such as microtiter wells (Figure 3.3). Furthermore, the hydrophobic character of PDMS serves as a protective coating that reduces chemical attack of the silver nanoparticles by sample matrix components, thereby extending the useful lifetime of the substrates. The extracting capabilities of PDMS also enhance the distribution of organic molecules in close proximity to the silver nanoparticles, which considerably augments the intensity of the SERS signals in comparison to traditional silver island films (Figure 3.4). The effective thickness of the embedded nanoparticle film can alter the morphology of the silver clusters, therefore affecting the SERS activity of the substrate. A previous analysis of the Ag-PDMS nanocomposites indicates that these substrates exhibit a maximum SERS response at an effective average silver film thickness of approximately 20 nm (Figure 3.5).[52] XPS and conductivity studies demonstrate that the silver nanoparticles formed under these conditions exist largely as isolated particles or small clusters of particles with most of the silver particles embedded just below the surface of the PDMS (see Figure 3.3).[52]

An important and often underestimated parameter in SERS is the influence of the laser beam on both analyte and substrate. Recent experiments have demonstrated that even under conditions of modest power density (typically 1 – 3 kW/cm^2) the appearance SERS spectra and the band resolution of the analytes can be significantly altered.[120] Further studies with 1.0 $x10^{-5}$ M solutions of 4-ABA and 1,5-DAN under stationary conditions showed considerable

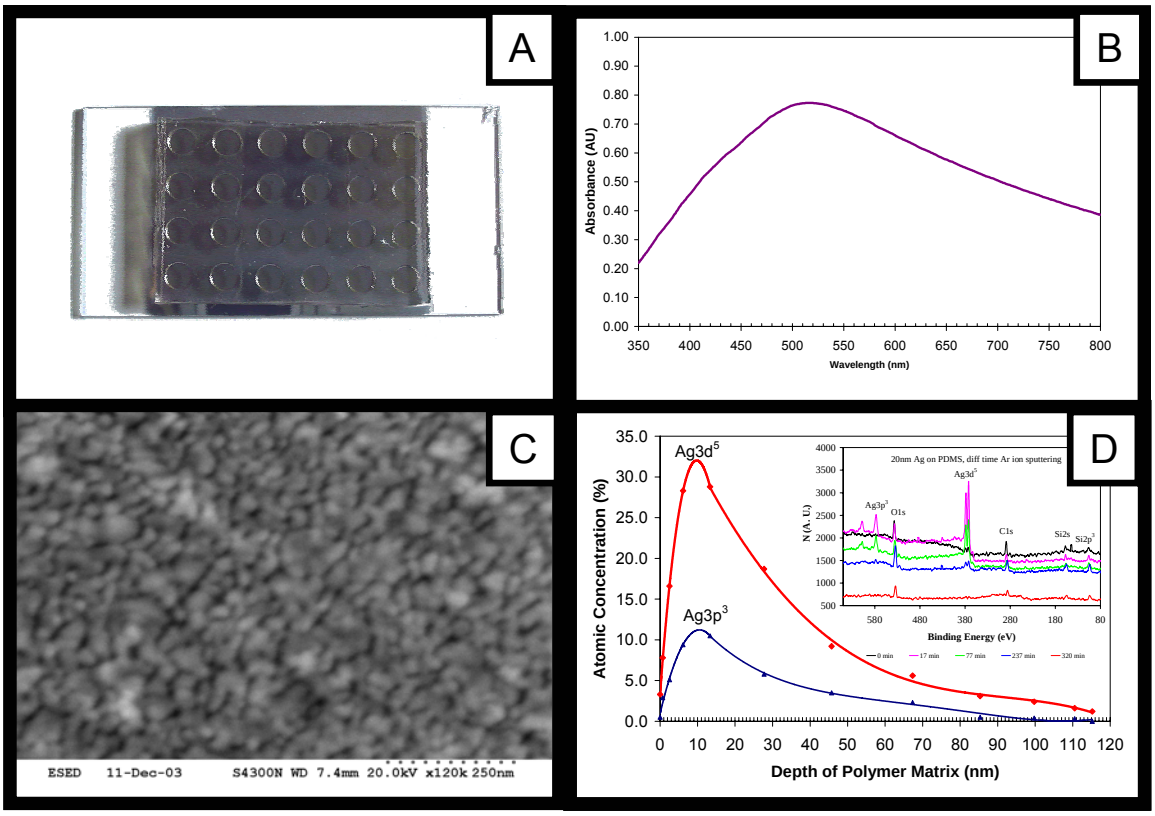

Figure 3.3 Characterization of the Ag-PDMS nanocomposites: Ag-PDMS microtiter plate (A); optical extinction spectra (B); SEM image of a well bottom (C); XPS depth profile (D).

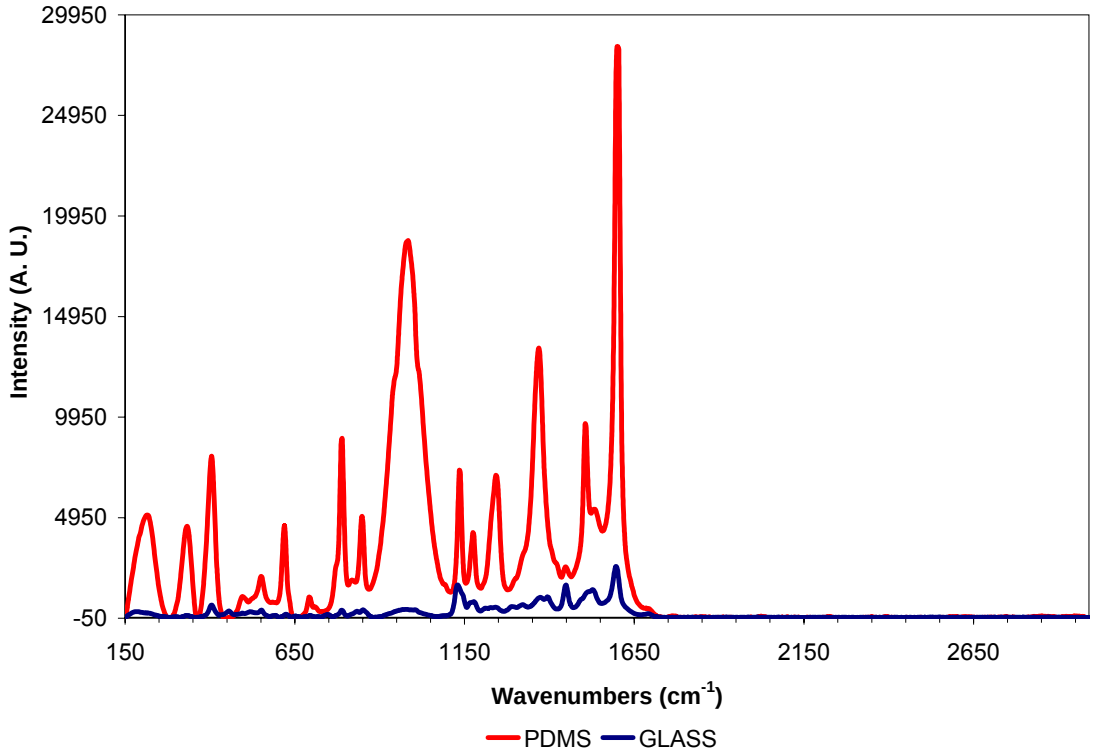

Figure 3.4 Enhancement of the SERS signal of a $1.0x10^{-5}$ M solutions of 4-aminobenzoic acid (4-ABA) during the irradiation with 2.2±(0.1) mW of the 632.81 nm radiation from a He-Ne laser onto Ag-PDMS, and conventional silver islands films.

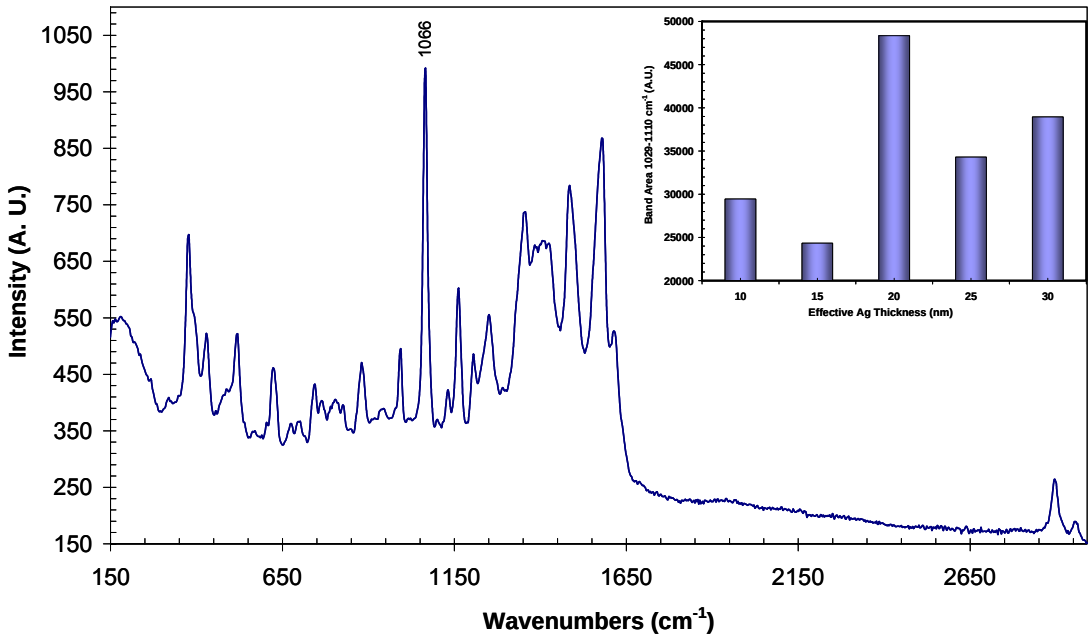

Figure 3.5 Changes in the 1066 cm^{-1} SERS signal of 4-ATP ($1.0x10^{-5}$ M) as a function of the effective Ag film thickness.

changes in their spectral features as a function of the irradiation time (Figure 3.6). In the 4-ABA case, a decrease in the intensity of the symmetric stretching (1251 cm^{-1}), and in plane deformation modes of the carboxyl group (623 cm^{-1}), were observed. These changes suggest that some of the adsorbed molecules lose the carboxylic acid group of 4-ABA upon their exposure to the incident laser beam. Such a process can involve a series of complex radical reactions similar to the ones observed during the Hunsdiecker reaction.[94] Shaw, et. al. have shown that the continuous irradiation of 4-ABA with ultraviolet and visible radiation can lead to the dimerization of the molecule to form either 4-amino-4'-carboxydiphenylamine or 4-amino-3-[(4-carboxyphenyl)amino]-benzoic acid.[125]

Our results show a decrease in the intensity of the bands at 790, 408, and 337 cm^{-1}, which suggests a reduction in the number of para-substituted molecules at the surface of the substrate. In contrast, increases in the signals at 1602, 1452, and 1135 cm^{-1} upon irradiation are indicative of the addition of a second aromatic ring to the molecule. These bands are split into doublets and are at positions indicative of meta substitution. The shift in the maximum SERS signals at 1508, 1369, and 850 cm^{-1} to 1494, 1396, and 838 cm^{-1} respectively, also supports the meta substitution of 4-ABA (i.e., the formation of 4-amino-3-[(4-carboxyphenyl)amino]-benzoic acid) under these conditions. Thus, in addition to analyte decomposition, SERS conditions can give rise to the formation of species that are more complex than the original analyte, and such occurrences can be diagnosed *in situ* and in real time.

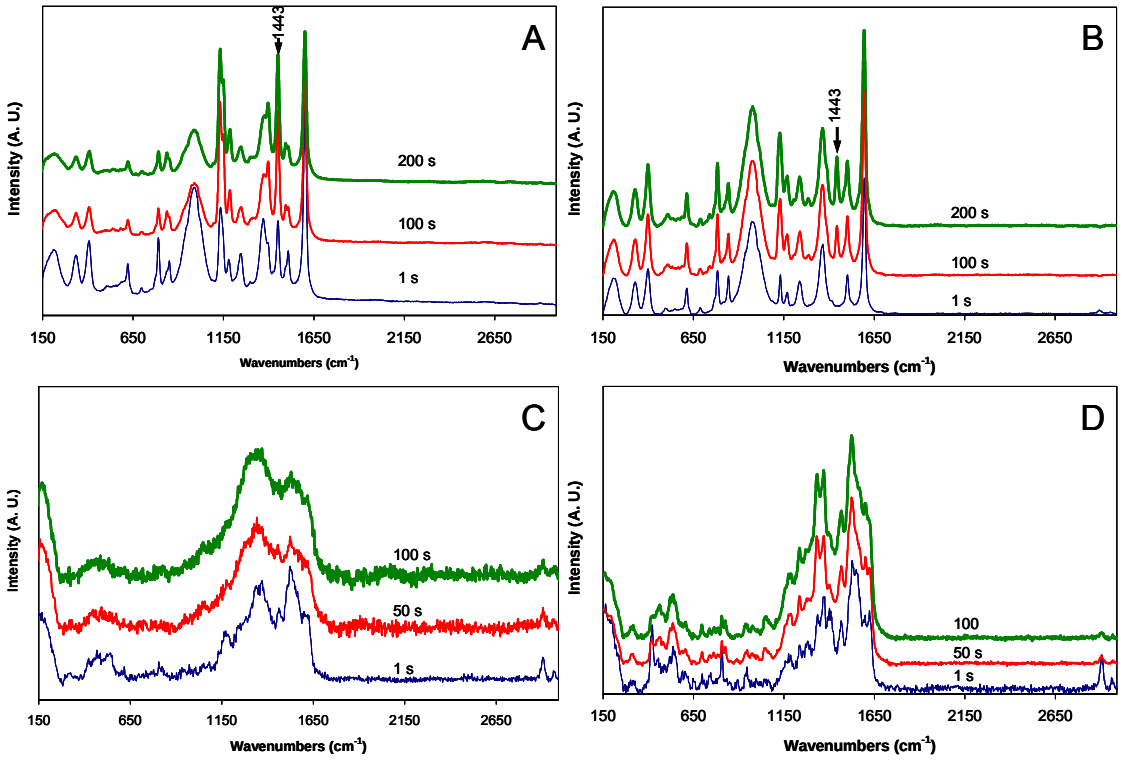

Figure 3.6 Spectral profiles of a 1.0x10^{-4} M solution of 4-ABA and 1,5-DAN as a function of the irradiation time: (A) 4-ABA, stationary, (B) 4-ABA, STT, (C) 1,5-DAN, stationary, (D) 1,5-DAN, STT. All samples were continuously irradiated with 8.9 mW.

The chemical transformation of the analyte as a function of the irradiation time is even more prominent for highly photosensitive compounds such as 1,5-DAN, where the exposure to the incident laser beam promotes the rapid decomposition of the analyte (Figure 3.6 C). Under these conditions, the continuous irradiation of the sample leads to the formation of two broad bands in the 1150-1650 cm^{-1} region. These bands are normally attributed to the G and D bands of graphitic carbon.[126] Such dramatic changes in the analytical signal upon laser irradiation has greatly limited the use of SERS for qualitative and quantitative applications. The rapid translation of the sample at 2000 RPM minimizes these effects and allows the use of laser powers up to 8.9 mW with minor changes in the observed vibrational modes and the band areas of the analytes, which is significant for analytical applications (Figure 3.6 B, D).

An analysis of 4-ABA decomposition rate as a function of the incident laser power was conducted under stationary and STT conditions. The results are plotted in Figure 3.7 as the growth of the band at 1443 cm^{-1} (see above). Under stationary conditions and at the highest laser power tested (8.9 mW), the growth of that band is so rapid that the pixel saturation point of the CCD is reached in less than a second (Figure 3.7 A). The continuous irradiation of the sample further broadens the 1443 cm^{-1} band that becomes saturated above $1.5x10^5$ area units/s. A decrease of the incident power to 0.89 mW is required to lower the reaction rate to 87 area units/s. The translation of the sample at 2000 RPM induces dramatic changes in the apparent formation of 4-amino-3-[(4-

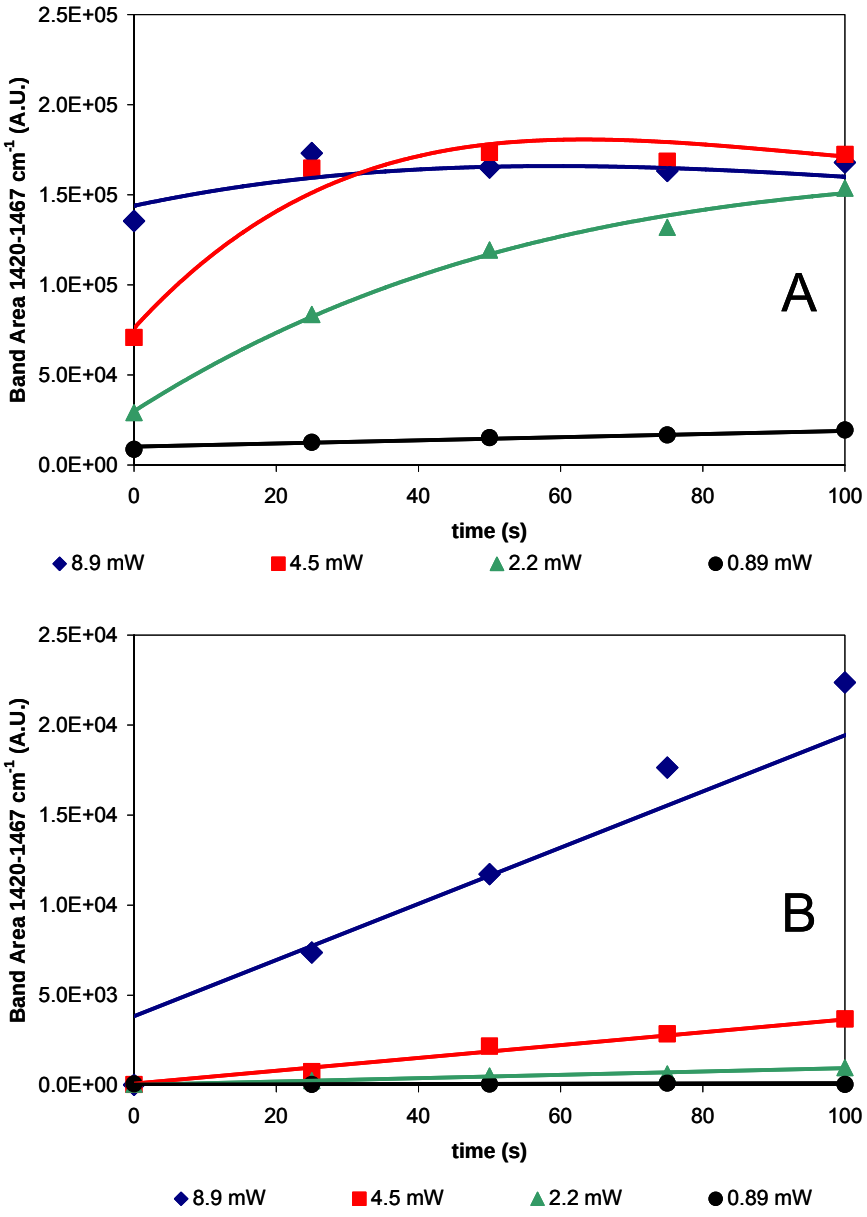

Figure 3.7 Changes in the analytical response of the 1443 cm^{-1} band of 4-ABA ($1.0x10^{-4}$ M) as a function of the incident laser power: (A) stationary, (B) STT.

carboxyphenyl)amino]-benzoic acid (Figure 3.7 B). At an incident power of the laser beam of 2.2 mW, the rate of change of the 1443 cm^{-1} band is an acceptable 9.3 area units/s, with the band still exhibiting a very good signal-to-noise ratio. This dramatic reduction in the sample decomposition permits the collection of SERS spectra that resemble the signals observed by conventional Raman spectrometry at high analyte concentrations. Consequently, STT-SERS provides an excellent means to generate spectral libraries for the qualitative identification of aromatic compounds in aqueous media.

Since translation of the sample minimizes the detrimental effects of laser irradiation, the question arises as to what is an appropriate translation rate. As a point of reference, when the incident laser beam is positioned 1 mm from the dead center, 1000 RPM corresponds to a linear velocity of approximately 104 mm/s. An analysis of the translation rate effects on the 643 cm^{-1} signal of 4-ATP ($1.0x10^{-5}$ M) in the range from 0-6000 rpm at a laser power of 2.2 mW was performed (Figure 3.8 A). This spectral region was selected since it exhibits only small thermal and photolytic effects which result in a reduction in band area. The results show that under stationary conditions, 4-ATP decomposes in less than one second (Figure 3.8 B). These effects decrease considerably when the translation process is initiated. Once the rotation rate produces multiple cycles per acquisition time, the duty cycle for measurements with STT-SERS remains constant with changing RPM and is roughly equal to the focused laser beam spot size divided by the circumference of irradiated circle (generally < 1%). For a

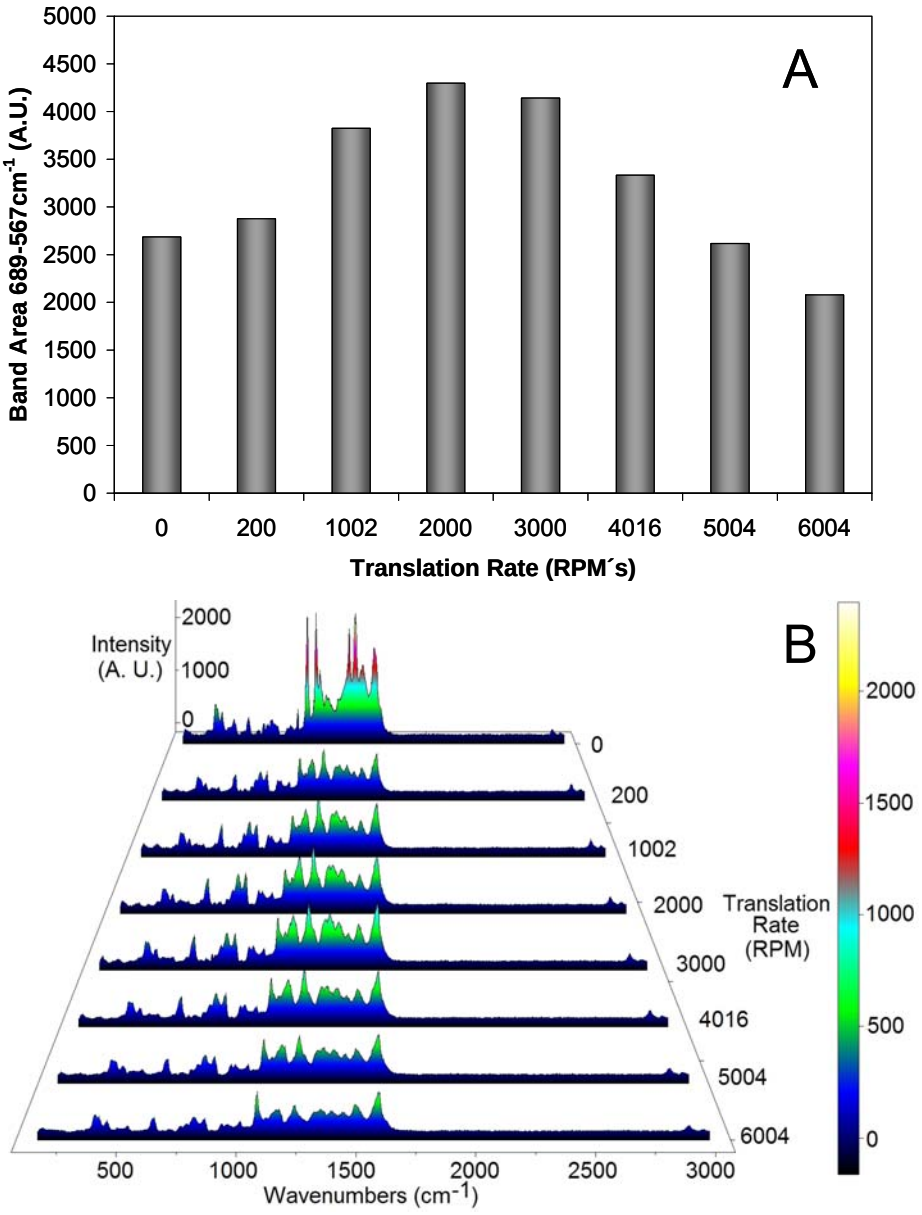

Figure 3.8 Influence of the translation rate on spectra of 4-ATP (1.0×10^{-5} M) with 2.2 mW laser power: (A) area of band centered around 640 cm^{-1}, (B) overall spectral profiles.

given probed substrate location, however, the irradiation and recovery times between cycles both decrease with increasing RPM. Our results indicate that a maximum SERS response for p-ATP occurs at a rate of 2000 RPM (Figure 3.8 A) and, under the conditions employed, this corresponds to irradiation and recovery times of 0.3 ms and 30 ms, respectively. Long irradiation times are expected to be detrimental and long recovery times are expected to be advantageous, thereby giving rise to the optimum observed in the figure.

The fast acquisition time of STT-SERS in combination with the small changes in the spectral features of the analyte makes the technique useful for the qualitative identification of a family of compounds such as benzoic acid derivatives (Figure 3.9). Our experiments show clear differences in the intensity ratios as well as the band profiles of 4-ABA, 4-OHBA, and 4-ClBA under STT conditions. Such spectral differences provide a fast and relatively simple method for the identification of the analyte.

Our initial studies using Ag-PDMS microtiter wells under STT conditions demonstrated improvements in SERS spectral reproducibility and band resolution (see section 2.3).[120] Ag-PDMS substrates also exhibit minimal background features that can be easily subtracted from the analytical signal. Current studies using a 1.0×10^{-5} M solution of phenolphthalein as a model polyaromatic compound and Ag-PDMS titer wells show an intra-well relative standard deviation (RSD) of less than 6.5% (N=21) and an inter-well RSD of less than 10% (N=4) using the 915 cm^{-1} band. Figure 3.10 shows the reproducibility

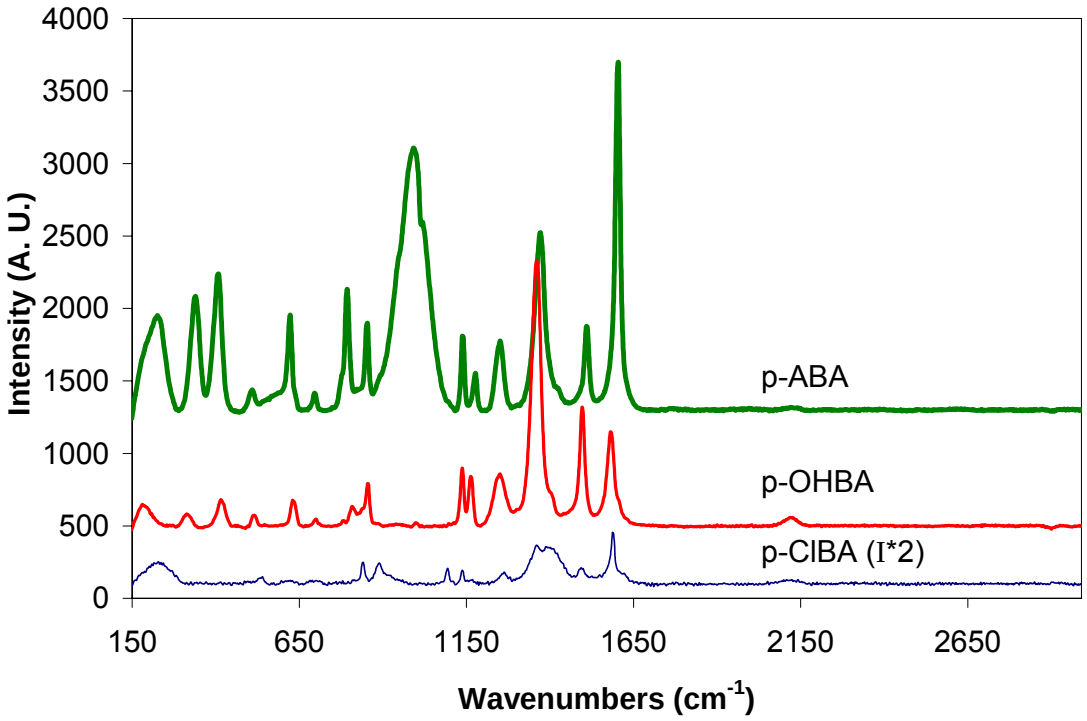

Figure 3.9 Differences in spectral features for a series of benzoic acid derivatives: 4-ABA, 4-OHBA, 4-ClBA. All the samples were 1.0×10^{-5} M and analyzed via STT at 2000 rpm with an incident laser power of 2.2 mW.

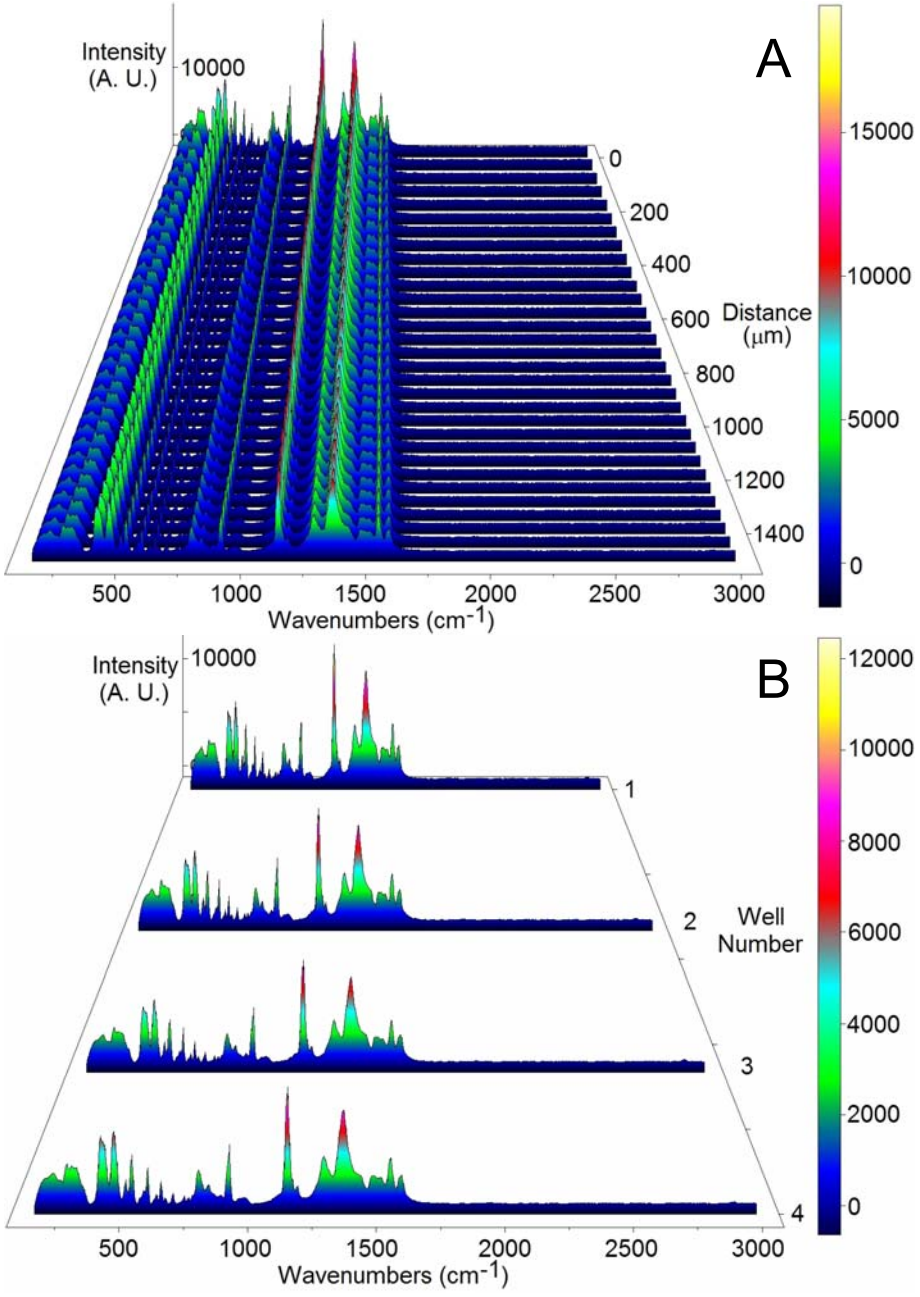

Figure 3.10 Reproducibility of the SERS-STT signal of PHT (1.0×10^{-5} M) in Ag-PDMS microtiter wells: (A) intra-well reproducibility for a 50 μm step size from 400 to 1400 μm (N=21), (B) inter-well reproducibility (N=4).

of the entire phenolphthalein spectrum under STT conditions.

The simple, economical and compact design of the Ag-PDMS microtiter wells results in disposable SERS substrates. This prevents the cross-contamination of the samples during analysis, which is particularly important for environmental applications. It is often possible to release analytes that are adsorbed onto the metal by adjusting the pH of the solution or by rinsing with different solvents (e.g. methanol or acetonitrile). However, the process often accelerates the oxidation of the substrate and results in an incomplete removal of the analyte. Certain analytes, such as thiols and carboxylic acids, covalently bind (chemisorb) to the silver. This, in combination with the extracting capabilities of PDMS limits its application as a reversible, re-usable substrate.

The limited number of adsorption sites and the rapid decay of the enhanced electromagnetic field with distance from the SERS-active surface, set the maximum loading capacity of the substrate close to that of an effective monolayer of analyte on that surface. Our studies with Ag-island films deposited onto 50 μL glass-bottomed microtiter wells indicated that the surface becomes saturated after the addition of 50 μL, 1.0×10^{-6} M solutions of aromatic compound such as 4-ABA or 4-ATP. At the saturation point working curves exhibit severe roll-over. With the Ag-PDMS nanocomposites, the encapsulated nature of the silver within the polymer increases the available surface area for SERS and extends the saturation point of the substrates for 4-ABA up to approximately 1.0×10^{-5} M (Figure 3.11). Further studies with a series of standard solutions of

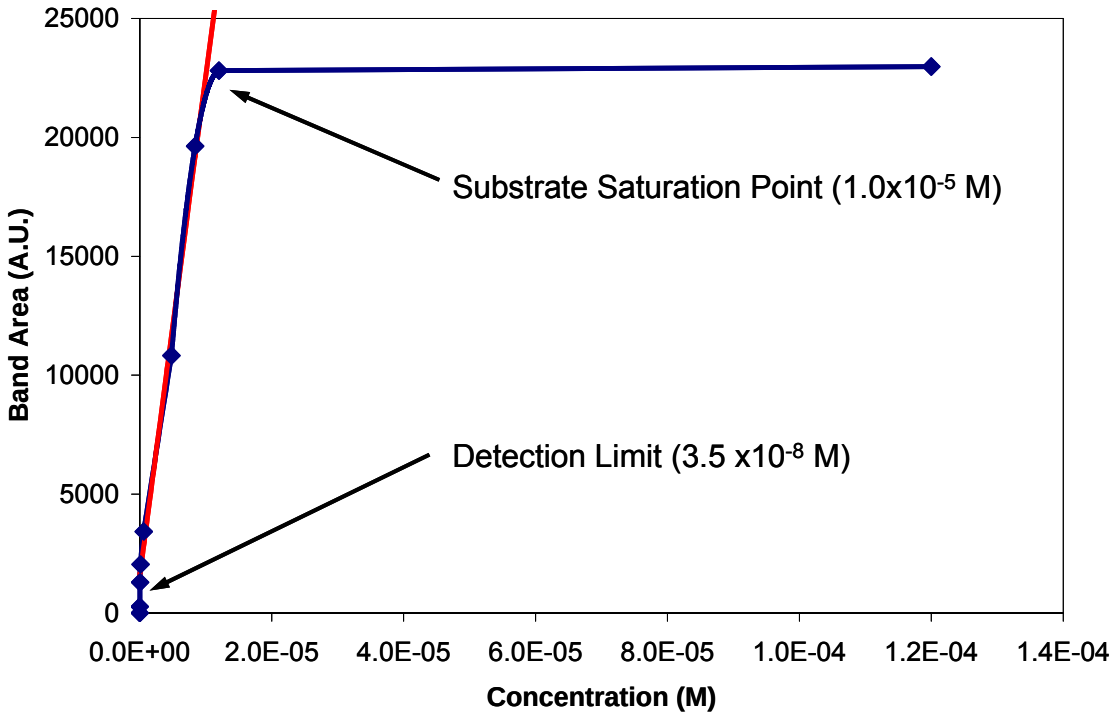

Figure 3.11 Working curve for 4-ABA using the Ag-PDMS nanocomposites.

4-OHBA, 4-ClBA, and PHT within the $1x10^{-8}$ to $1x10^{-6}$ M range were conducted to determine limits of detection (LOD), sensitivity (slope of the working curve), and linearity (R^2) from the LOD to $1x10^{-6}$ M. The data for these four compounds appears in Table 3.1. These results demonstrate that Ag-PDMS nanocomposites are a promising type of SERS substrate for the qualitative and the quantitative analysis of aromatic pollutants in aqueous media.

The acid-base properties of the sample analytes can be exploited to enhance their sorption with the substrate. The changes in the SERS signal of 1,5-DAN, 4-ABA, and 1,5-DHN (all $1.0x10^{-4}$ M), as a function of pH are shown on Figure 3.12 A-C. The maximum SERS signal for these chemicals was observed at pH values of 3.12, 5.23, and 6.98, respectively. An analysis of the distribution equilibria indicates that the dominant species under these conditions corresponds to the fully protonated 1,5-DAN, deprotonated 4-ABA, and neutral 1,5-DHN.

The effect of pH on the SERS signals of analytes can involve a number of factors when using the Ag-PDMS substrates. Converting the analyte to a form that facilitates interaction with the silver surface would be expected to enhance signals. For example, the deprotonated carboxyl group of 4-ABA may interact with the silver nanoparticles by acting as a soft Lewis base.[123] However, pH may also influence the sorption of the analyte into the PDMS phase, as well as the chemical state of the silver and PDMS surfaces. As an example of the latter surface effect, PDMS has surface silanol groups for which the distribution

Table 3.1 Regression results for the working curves of 4-ABA, 4-OHBA, 4-ClBA, and phenolphthalein using Ag-PDMS nanocomposites.

Compound	Slope (Area Units/M)	R^2	LOD
4-ABA	$2.1x10^{9}$	0.99	$3.5x10^{-8}$
4-OHBA	$5.8x10^{9}$	1.00	$2.9x10^{-8}$
4-ClBA	$3.0x10^{9}$	0.98	$5.9x10^{-8}$
PHT	$1.9x10^{10}$	1.00	$5.5x10^{-8}$

Note: LOD was calculated as the signal equivalent to 3 times the standard deviation of the blank for N=21. A linear relation was observed in the range from the LOD to 10^{-6} M.

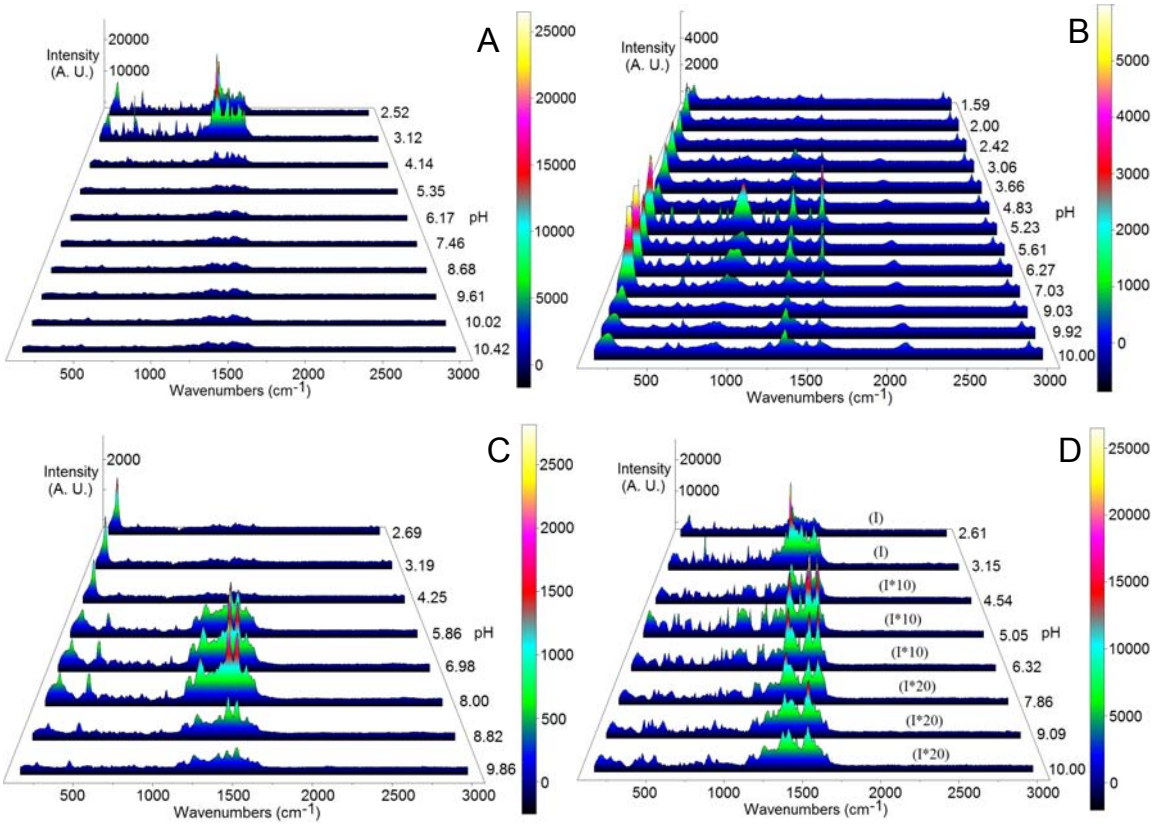

Figure 3.12 Influence of pH on the adsorption of: (A) 1,5-DAN, (B) 4-ABA, (C) 1,5-DHN, (D) mixture of 1,5-DAN, 4-ABA, and 1,5-DHN. All the samples were 1.0x10-4 M and analyzed via STT at 2000 rpm with an incident laser power of 2.2 mW.

between protonated and ionic forms can be expected to influence the accessibility of the underlying silver surface to certain analytes. The dependence of the SERS signal of 1,5-DAN, 4-ABA, and 1,5-DHN on pH can be exploited to promote the selective detection of these analytes in a mixture. The pH dependent changes in the SERS responses for a solution containing $1.0x10^{-4}$ M each of 1,5-DAN, 4-ABA, and 1,5-DHN are shown in Figure 3.12 D. The majority of the spectral features observed at pH 3.15, such as the bands at 1576, 1348, and 510 cm^{-1}, are consistent with those previously observed for 1,5-DAN. The absence of characteristic bands for 4-ABA and 1,5-DHN at 1605, and 1464 cm^{-1}, respectively, indicates that their influence at this pH is negligible. The SERS spectrum at pH 5.05 clearly shows the characteristic bands for 4-ABA (e.g. 1605, 1372, 982, 412 and 442 cm^{-1}). The spectrum also shows some residual bands from the 1,5-DAN , while there was no significant influence of 1,5-DHN on the SERS signal at this pH. The relatively low signal magnitude of 4-ABA may be a result of chemical interactions with the other components in the sample and the competition for available sites at the surface of the Ag-PDMS nanocomposites. The absence of the bands at 510, 934, and 1303 cm^{-1} for 1,5-DAN at pH 9.09, suggests a negligible distribution of the analyte at this pH. Consequently, most of the observed features such as the bands at 1458, 1181, 1156, and 463 cm^{-1} are due to selective detection of 1,5-DHN. The ionic state of the analytes can be altered by adjusting the pH of the mixture. This permits the selective-sorption of the analytes to the metal. The simple adjustment of pH offers a promising tool

for SERS to circumvent the competitive adsorption processes commonly observed in mixtures. The results demonstrate that Ag-PDMS nanocomposites can be used for the analysis of aromatic compounds over a wide pH range with possible benefits in analytical selectivity. This may extend the applications of SERS-STT in environmental analysis.

It is important to consider how the changes in pH affects the thermal and photolytic processes commonly observed in SERS. 4-ABA is highly susceptible to photodecomposition upon its exposure to UV-VIS radiation, which contributes to its previous use as a sun-block agent. Our previous studies with 4-ABA indicates that this drug can participate in series of dimerization reactions similar to the ones described by Shaw et. al.[125] The changes in spectral features of 4-ABA upon its continuous irradiation (250 s), with 2.1 mW of the 632.8 line of the He-Ne laser are presented in Figure 3.13. The results shows minor differences in the Raman shift of the 4-ABA photoproducts as a function of pH, which suggest that the decomposition of the analyte is not directly dependent upon pH.

The observed spectral profiles show an increase in the signal at 1452 cm^{-1} with the increased irradiation time. This has been attributed to a combination band resulting from the chemisorption of 4-ABA onto the Ag surface. This band is not observed under normal STT conditions (2000 RPM´s and 1 s of laser irradiation at 2.1 mW), indicating that 4-ABA is only physisorbed onto the Ag nanoparticles under routine STT-SERS conditions. The change in SERS intensity for the bands at 1508, 1369, and 850 cm^{-1}, as well as, the enhancement

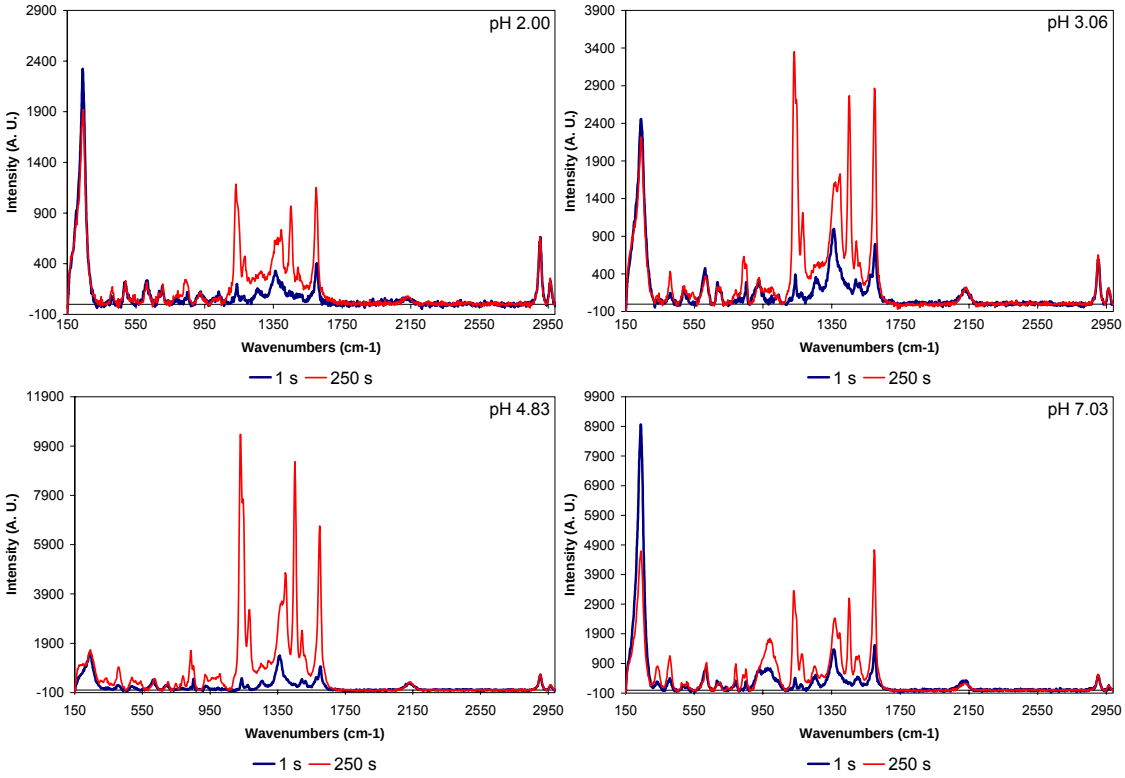

Figure 3.13 pH effects on the photodecomposition of 4-ABA after the continuous irradiation of the sample with 2.2 mW of the 632.8 line of a He-Ne laser. All the samples were 1.0×10^{-4} M and analyzed via STT at 2000 rpm and a total irradiation time of 250s.

of the bands at 1494, 1396, and 838 cm^{-1} are also indicative of the chemisorption and subsequent photodecomposition of 4-ABA upon irradiation. In theory, the chemisorption of the carboxyl group to the Ag surface and the presence of an amine group at the "para" position, activates the "meta" sites of the benzene ring. This is consistent with our initial studies of 4-ABA that suggest the formation of a meta-substituted derivative of 4-ABA similar to the 4-amino-3-[(4-carboxyphenyl)amino]-benzoic) proposed by Shaw, et. al.[125]

Further studies suggest that the enhancement of the signals at 1599, 1452, and 1132 cm^{-1} upon laser irradiation could not be entirely justified by the mere chemisorption of 4-ABA onto the substrate. An analysis of the Raman shift of this bands indicate the addition of second aromatic ring at the "meta" position of 4-ABA. These bands will correspond to the 8b(b"), 19a (b"), and 9b (b") modes of a m-substituted benzene. The decrease in the SERS photodecomposition signals of 4-ABA at pH 2.00, particularly the band at 991 cm^{-1}, suggests that the protonated form of the acid is adsorbed less efficiently onto the substrate than its conjugated base. The increased nitric acid concentration also contributes to the partial etching of the silver nanoparticles, thus lowering their overall SERS activity at low pH. Nonetheless, the increased concentration of the nitrate ion can promote a competitive interaction for the substrate active sites, which induces the more rapid oxidation of the substrate as evidenced by the enhancement of the band at 219 cm^{-1} (Figure 3.12).

CHAPTER 4

Factors affecting the sorption of model environmental pollutants onto silver polydimethylsiloxane nanocomposite Raman substrates

This chapter is a revised version of an article under the same name published in Applied Spectroscopy by Marco A. De Jesús, Kathleen S. Giesfeldt, and Michael J. Sepaniak:

De Jesús, M. A.; Giesfeldt, K. S.; Sepaniak, M. J.; **"Factors Affecting the Sorption of Model Environmental Pollutants onto Silver Polydimethylsiloxane Nanocomposite Raman Substrates."**; Applied Spectroscopy (Under Revision).

My use of "we" in this chapter refers to my co-authors and myself. My primary contributions to this article included: (A) design of the project and development the experimental protocols to study the sorption of model pollutants by SERS (B) design and fabrication of a series of metalized-PDMS microtiter well plates, (C) design of the experimental methods and protocols, (D) collection and interpretation of the analytical data (E) collection and interpretation of the cited literature, (F) most of the writing.

4.1 Introduction

As mentioned in the previous chapter, the increased presence and persistence of aromatic pollutants in natural water has become a problem of major importance in environmental sciences.[102-104] These chemicals are often present in our water resources as a result of the natural degradation of organic matter and their use in agricultural and pharmaceutical processes.[128] Many of these compounds, such as phenolics, naphthalene derivatives, and aromatic acids are rapidly trapped by humic substances and suspended organic mater,

which increases their presence in and toxicological effects to the environment.[129] These compounds can also act as Lewis bases, which allow them to serve as promoters for the dissolution of heavy metals in water. These processes often depend upon the pH of the sample, as well as the matrix composition. Therefore, the study of how these variables can affect the sorptive and decomposition properties of these chemicals onto surfaces can provide new insights about their fate in the environment.[130]

A considerable number of environmentally and pharmaceutically relevant aromatic compounds are ionizable in aqueous media. The ability of these chemicals to bind to metallic surfaces makes SERS a promising tool for the analysis of pharmaceutically and environmentally relevant compounds.[4,76,78] The considerable amount of structural information attainable through SERS, in combination with tremendous enhancement of the Raman signals, make it an attractive technique for the analysis of trace aromatic pollutants in aqueous media.[131] Despite these advantages, SERS has not become a routine technique due to limitations in analytical figures of merit such as signal reproducibility, robustness, ruggedness and linear dynamic range. Consequently, considerable work has been done in the area of substrate design in an attempt to lessen these limitations. These studies have led to the creation of a wide variety of SERS active substrates such as silver islands on glass,[43] colloidal silver solutions,[132] colloidal particles encapsulated in sol-gels,[58] silver coated microspheres,[53]

metallized polymers,[52] as well as more regular structures such as those created by nanosphere lithography.[119]

It is well known that the surface of silver and other noble metal nanocomposites can induce the catalytic transformation of adsorbed molecules. Some of the most common catalytic processes that have been reported on noble metal surfaces involve the oxidation, decarboxylation, and polymerization of the molecules that are in close proximity to the metal nanoparticles.[120,133-137] This has been considered as a contributing factor to the changes in spectral profiles often observed in SERS.[129] Another important and often underestimated complication in SERS is the influence that pH and matrix composition can exert on the sorption of analytes onto the substrates. Several researchers have reported that changes in pH and electrolyte composition can considerably alter the reactivity of the metallic surface, as well as the efficiency of the adsorbate-metal interactions.[37,138-141] Most of these studies have focused on the application of hydrogels[141], and silver colloids.[37,140] Studies that evaluate pH and ionic effects on physical vapor deposited films such as silver-island films are scarce.[142,143] Therefore, further studies are required to better understand how these variables affect the SERS activity of the substrate and the binding of the analyte to the metal . These studies are important for the implementation of SERS as a routine analytical tool.

In the past two chapters we demonstrated the use of metallized polymers such as Ag-PDMS as substrates for SERS applications.[52] These novel metal-

polymer nanocomposites exhibit unique optical and sorption properties that make them a promising alternative to more traditional substrates for the detection of aromatic pollutants in water.[52,137] In addition, the use of these metal-polymer nanocomposites have proven to promote the selective sorption of a series of model environmental pollutants as a function of pH.[137] The term sorption is often used to indicate the different variables that can influence the interaction of the analytes with a given substrate or phase. On Ag-PDMS, this process is thought to occur via the combined action of: (a) the absorption (partitioning) of the analyte into the PDMS phase, and (b) the adsorption (either by physisorption or chemisorption) of the analytes onto the silver nanoparticles.

This chapter is devoted to identifing which variables can maximize the interactions between sample analytes and these novel substrates. An analysis of the factors controlling the sorption of a series of model pollutants as a function of pH are presented and discussed. Our studies also consider the effects that environmentally significant anions such as chloride, fluoride, carbonate, and phosphate have on SERS signals. These experiments demonstrate that the presence of naturally occurring anions such as chloride, carbonate and phosphate can considerably alter the SERS activity of the substrates. The use of liquid chromatography for the removal of these and other matrix interferences from natural water samples is presented.

4.2 Experimental

4.2.1 Instrumentation

All SERS spectra were acquired using a modified version of a LabRam Spectrograph from JY-Horiba. The instrument set-up has been described previously (see section 3.2).[137] In general terms the instrument uses an Olympus BX-40 microscope with a 10X (0.25 NA, ∞) objective that delivers up to 8.9 mW of the 632.8 nm line from an electrically cooled He-Ne laser. All spectra were acquired in a 180° scattering geometry with a 2936 cm^{-1} spectral window centered at 1747 cm^{-1}. The scatter was dispersed with a 600 groove/mm grating, imaged with a 1024 x 256 thermoelectrically cooled CCD camera, and processed with Labspec 4.03 software. A computer controlled x-y-z stage was used to adjust the focusing of the microscope objective as well as the positioning of the laser spot under stationary and translating conditions. A Stanford SR-540 chopper was used to prevent the photodecomposition of the analyte by spinning the substrate (usually at 2000 rpm). The radial mapping of the spun surface allows a faster and more efficient interrogation of the SERS active surface. In this work, all sample acquisition times were set to 1 second.

The SERS active substrates were prepared with a physical vapor deposition chamber from Cooke Vacuum Products, Inc. The chamber was set to operate at a base pressure of 1.0 $\pm(0.5)x10^{-6}$ torr. Samples were mounted 25 cm above and normal to the effusive source. Average mass thickness and deposition rates were measured for each film with a quartz-crystal microbalance.

4.2.2 Preparation of the SERS-active substrates

Ag-PDMS substrates were prepared by the addition of Sylgard-184 curing agent (Dow Corning) and its elastomer in a 1:10 mass-to-mass ratio. The curing conditions can be found elsewhere.[120,137] The substrates were produced as a 28x28 micro-well array that was negatively cast from the surface of a Lego® platform. Each well has a maximum loading volume of 50 µL. The arrays were metalized with 19.0 ± (0.2) nm of 99.999% Ag (Alfa Aesar, MA), under high vacuum conditions ($1x10^{-6}$ torr). Once prepared, the SERS active substrates were stored in a vacuum desiccator held at 10^{-4} torr in the dark prior its use. Under these conditions, the substrates typically remain with a quantitative-grade SERS activity for up to five days. After this period, they remain good for qualitative applications for about two weeks.

Ag island films on glass were prepared by cleaning a series of standard microscope slides with a 5% (v/v) KOH solution in ethanol for five minutes. The slides were subsequently rinsed with deionized (18 Ω Barnstead E-Pure) water and dried under N_2. Once dried, Ag film with average thickness of 7.0 ± (0.2) nm was deposited. The Ag-glass films were stored under vacuum as described above. These films have a useful life span of 24 and 72 hours for quantitative and qualitative applications, respectively.

4.2.3 Sample preparation

4.2.3.1 pH studies

A series of $1x10^{-4}$ M stock solutions of 4-aminobenzoic acid (98+%, Sigma), phenolphthalein (titrimetric grade, Fisher), benzoic acid (A.C.S. grade, Fisher), 1,5-diaminonaphthalene (97+% Aldrich), 1,7-dihydroxynaphthalene (98+%, Aldrich), 1,5-dihydroxinaphthalene (97%+, Aldrich), and 4-nitrophenol (A.C.S. grade, Fisher), were prepared with deionized water (18Ω Barnstead E-Pure) and 1% methanol (99.9%, Acros Inc. (when necessary)). Nitric acid (Trace Metal, Fisher) and sodium hydroxide (99%, Mallinkrodt), were used to prepare a series of 0.1 M standard solutions to adjust the alkalinity of the analytical samples. These samples were used to titrate 25 mL aliquots of the sample analytes within the pH range of 2-10.

4.2.3.2 Inorganic anion studies

Stock solutions ($1x10^{-2}$ M) of sodium chloride (A.C.S, Fisher), sodium carbonate (99%, Acros), sodium sulfate (99%, Mallinkodt), sodium nitrate (99%, Sigma) and sodium phosphate monobasic (99%, Sigma), were prepared in deionized water (18Ω Barnstead E-Pure). Then a series of standard solutions ($1x10^{-3}$-$1x10^{-6}$ M) of each electrolyte was prepared in a $1x10^{-5}$ M solution of 4-hydroxybenzoic acid (98%+, Aldrich). These samples were used to study the effects of different metal anions on the SERS signal of 4-hydroxybenzoic acid, on silver islands and Ag-PDMS nanocomposites.

4.2.3.3 HPLC-extraction conditions

Natural water samples (1L each) were obtained from the Second Creek area in downtown Knoxville, TN. The samples were filtered using a 0.45 μm nylon filter to remove of the suspended organic matter. Two solutions of 4-ABA ($1.4x10^{-4}$ M, and $1.2x10^{-6}$ M), were prepared in natural water. New standard solutions of 4-ABA ($1.4x10^{-4}$ M, and $1.2x10^{-6}$ M), were also prepared to serve as reference solutions. The $1.2x10^{-6}$ M samples were directly analyzed via SERS to demonstrate the matrix composition effects to the substrates. Conversely, a 20 μL aliquot of the $1.4x10^{-4}$ M samples was eluted at 2.0 mL/min under isocratic conditions (40% Acetonitrile/60% water), using an Agilent-1100 high performance liquid chromatograph, to separate the analyte from the remaining components of the matrix. A Supelcosil ABZ+ column (15 cm x 4mm x 5 μm) was used as the stationary phase (Supelco, Co.). The detection wavelength and temperature were set to 280 nm and 25°C, respectively. The eluted fractions were collected into 2-dram vials (Fisher, Co.) for subsequent analysis via SERS.

4.2.4 Data acquisition and analysis

A 50 μL aliquot of each sample solution was transferred to a Ag-PDMS well that was precisely centered on the top of the sample translator and covered with a glass cover slip. The samples were spun at 2000 rpm to minimize the photodecomposition of the sample upon irradiation.[137] The spectrophotometer light microscope images of each well were used to centralize each well relative to

the rotation axis. The point of maximum SERS signal was obtained by fine-focusing the microscope objective after moving the illuminated spot 150 μm off-spinning center. Once the signal was brought into focus the spectroscopic data was collected by moving the stage at 50 μm intervals (1 spectral acquisition per step) from 400 μm to a maximum distance of 1400 μm relative to the spinning center (N=21). The average spectrum of each experiment was used for the interpretation of the analytical results. The Ag-PDMS substrates were exposed to the sample matrix for approximately two minutes prior the collection of the analytical data.

For the studies of the effects of inorganic ions on Ag-island films, a 50 μl aliquot of each sample was spotted on the surface of an Ag-coated glass slide. The optical microscope images of the samples were focused relative to glass surface. Then the point of maximum SERS signal was obtained by fine-focusing the microscope objective. Once the signal was brought into focus, the SERS spectra of the sample were acquired by mapping a 150 x 350 μm area below the initial focal point (N=21), at 50 μm intervals (1 spectral acquisition per step). The substrates were not spun because the analyte under study (4-hydroxybenzoic acid), is not susceptible to photodecomposition under these conditions. This will also allow us to evaluate how these anions affect the activity of the substrate under conventional SERS conditions.

4.3 Results and discussion

The contamination of our natural water resources by small aromatic pollutants such as phenols and benzoic acid derivatives has become a problem of global significance. This study uses phenolphthalein (PHT), 1,5-diaminonaphthalene (1,5-DAN), 1,5-dihydroxynaphthalene (1,5-DHN), and 1,7-dihydroxynaphthalene (1,7-DHN) as model polyaromatic pollutants. 4-aminobenzoic acid (4-ABA), and 4-nitrophenol (4-NP), were used as nitrogen based pollutants, while benzoic acid and 4-hydroxybenzoic acid (4-OHBA) serve as model aromatic acids and phenols respectively.

Naphthalene derivatives have been widely used as pesticides, drugs, repellents, deodorizers and additives for filmmaking and electronics.[144] These chemicals are also released to the environment as part of coal tar production, wood treatment, and oil spills. Phenols have been widely used as preservative agents, pesticides, bactericides and fungicides.[121] They are also generated as part of the biodegradative pathway of plants and from the processing of olive oil.[124,145] Aromatic amines are commonly present in industrial wastes. They also play an important role in the degradation pathway of nitroaromatic compounds. The intrinsic alkalinities and ability of aromatic amines to bind onto metallic surfaces are important topics in studies of the dissolution of metals and organic matter in water.[124] The persistence and toxicity of the above mentioned compounds is an important topic in environmental sciences.

Surface enhanced Raman spectroscopy has emerged as a promising tool for the analysis of trace amounts of aromatic compounds due to its large enhancement of the Raman signal, and the large amount of structural information that it is inherent to the technique. Despite these advantages, SERS has not been implemented as a routine tool in environmental sciences due to the irreproducible responses that are normally obtained with traditional SERS substrates. These substrates are also prone to oxidation upon contact to water and other oxidizing agents present in the sample matrix. Furthermore, a significant number of environmentally relevant compounds are susceptible to thermal and photolytic decomposition upon exposure to the incident laser beam. Our research group has demonstrated that these fundamental problems can be surmounted to a substantial degree by using Ag-PDMS substrates in combination with a recently developed sample translation technique (STT-SERS).[52,120,137] Ag-PDMS nanocomposites offer several advantages over traditional SERS substrates such as low cost, simple preparation, increased effective surface area of the metal, superior SERS signals, and relatively low background features.[120,137] The elastomeric properties of PDMS permit the fabrication of substrates with different shapes and dimensions such as microtiter wells.[120,137] Furthermore, the hydrophobic character of PDMS reduces the chemical attack of the silver nanoparticles by common oxidizing agents, thereby extending the useful lifetime of the substrates. Our studies with Ag-PDMS indicate that the interaction of the analyte with the SERS substrate is mediated

first by the absorption of the sample into the polymer, followed by its subsequent adsorption onto the silver nanoparticles. Therefore, changes in experimental variables such as pH and matrix composition could significantly alter the absorptive properties of the polymer, and the SERS activity of the metal nanoparticles.

4.3.1 The effects of pH on analyte sorption and SERS activity

The interaction of ionizable aromatic compounds with noble metal surfaces often depends upon the ionic state of the analyte. Consequently, a change in the pH of the sample can promote the conversion of the analyte to a form that associates more or less efficiently with the silver nanoparticles. Such changes could also alter the distribution of the silanol groups commonly present in the polymer, affecting the partition of the analyte at the sample/PDMS interface, and its access to the embedded nanoparticles. These effects are evidenced by the changes in SERS signal of 4-ABA and 1,5-DAN (1.0×10^{-4} M) with pH (Figure 4.1). Among the pHs studied, the 4-ABA signal at pH 5.23 exhibits the maximum SERS intensity. An analysis of the distribution diagram of 4-ABA at this pH indicates that over 66% of the molecules present in the solution exist as the fully deprotonated form of the acid. The conjugate base of 4-ABA can act as a soft Lewis base that can be readily adsorbed onto the silver surface.[145] The considerable enhancement of the bands at 408, 1375, and 1605 cm^{-1}, which are combination bands containing the CO_2^- in-plane bending,

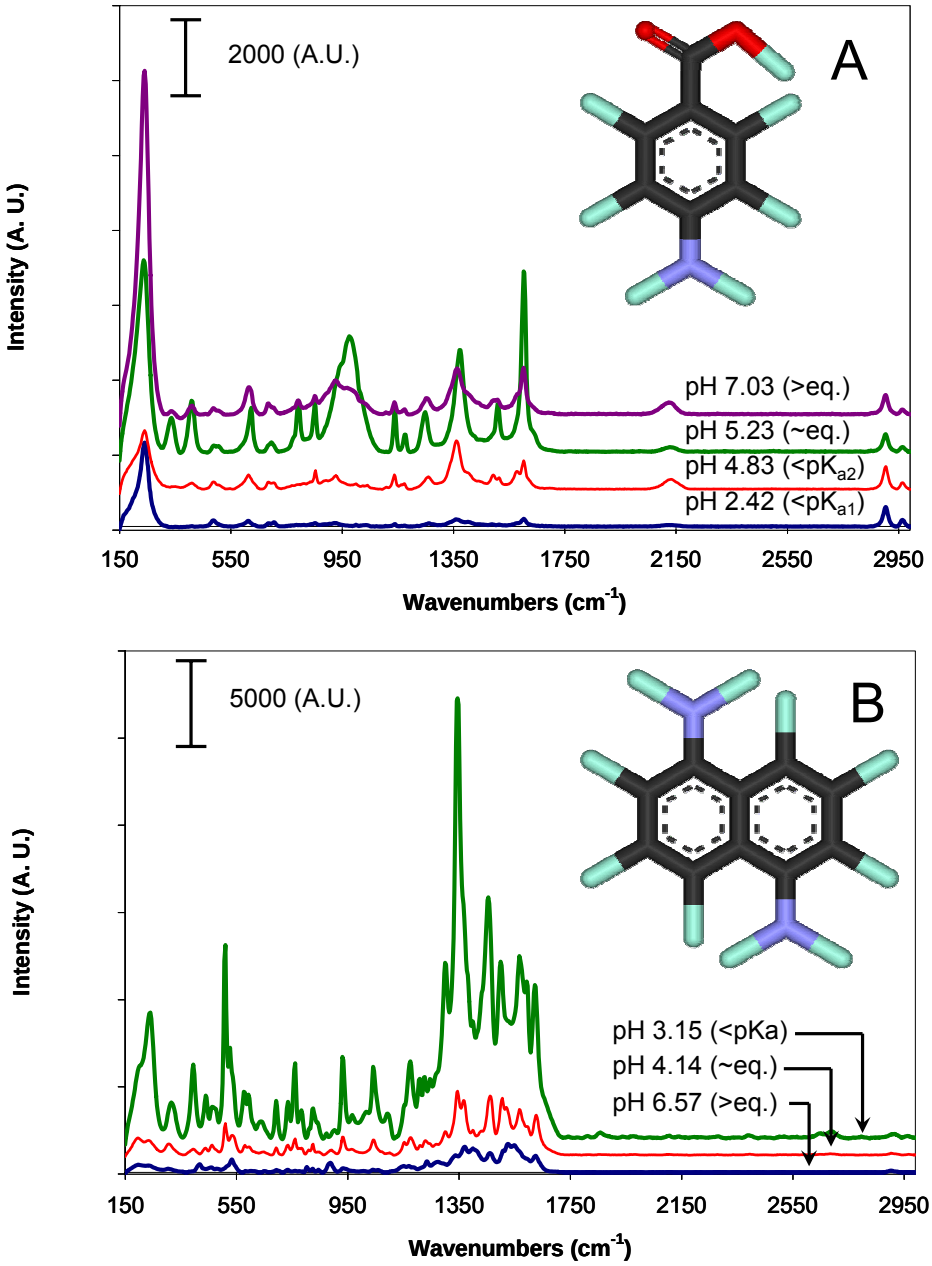

Figure 4.1 Differences in the SERS intensity of (A) 4-ABA (pK_{a1} 2.48, and pK_{a2} 4.90), and (b) 1,5-DAN (pK_{a1} 3.90), as a function of pH. All the samples were $1.0x10^{-4}$ M and analyzed via STT at 2000 rpm with an incident laser power of 2.2 mW.

symmetric CO_2^- stretching, and the asymmetric CO_2^- stretching modes, respectively, provides supportive evidence for this type of interaction. Increasing the pH to 7.03 dramatically reduces the SERS signals of 4-ABA. Conversely, the SERS signal at 219 cm^{-1} is enhanced with the increasing pH. We attribute this band to the in-plane bending mode of AgO in good agreement with the 217 cm^{-1} reported by Geoffrey et. al.[146] The general increase in this band at higher pH values indicates that the silver nanoparticles are being oxidized by the excess hydroxyl ions that diffuse into the PDMS. It also indicates that the hydroxyl ions compete with 4-ABA for the active sites of the substrate, inducing the oxidation of the substrate and the subsequent quenching of its SERS activity. When the pH of the solution is adjusted bellow its pK_{a2} (4.90) and pK_{a1}(2.48), a decrease in the overall signal profile is also observed. This suggests that the protonated form of 4-ABA is adsorbed less efficiently by the silver nanoparticles than its conjugate base.

4-ABA is susceptible to photodecomposition upon exposure to UV-VIS radiation, which contributes to its previous use as a sun-block agent. Our results show only minor differences in the Raman shift of the 4-ABA photoproducts as a function of pH, which suggest that the decomposition of the analyte is not directly dependent upon pH. In theory, the chemisorption of the carbonyl group to the Ag surface and the presence of an amine group at the “para” position, activates the “meta” sites of the benzene ring. This is consistent with our initial studies of 4-ABA that provided evidence of a meta-substituted derivative of 4-ABA.[137]

SERS studies of 1,5-DAN as a function of pH show a considerable increase in signal at pH 3.15 (Figure 4. 1B). At this pH, the dominant species in solution correspond to the fully protonated form of 1,5-DAN. This is evidenced by enhancement of the signals at 931, 1500, and 1567 cm^{-1}, which correspond to combination bands containing the NH^{3+} rocking, NH^{3+} symmetric deformation, and NH^{3+} anti-symmetric deformation modes, respectively. The enhanced adsorption of 1,5-DAN onto silver at low pH may be the result of an increase in the effective hydrogen-bond interactions between the protonated amino groups and the oxygen atoms that are commonly adsorbed to the nanoparticles.[127,137]

Additional studies with a series of $1x10^{-4}$ M solutions of BA, PHT, 1,7-DHN, and 4-NP were performed (Figure 4.2). The spectral profile of BA shows an enhancement in its SERS signal at pH 4.98. This pH is slightly above the pKa of BA, where the equilibrium is dominated by the deprotonated form of the acid in accordance with our observations for 4-ABA case (Figure 4. 3 A). Similar results were obtained for PHT (see Figure 4.3 B), where its highest SERS signal occurs when its conjugate base was the dominant species in solution (pH 9.96). The weak interaction of the alcohols with the metal in combination to the strong Raman signal of the carboxyl moiety for the acids indicate that interaction of aromatic acids with the silver is mediated by the adsorption of their carboxyl groups to the metal nanoparticles. 1,7-DHN was selected as a model of a weakly acidic system (pKa 9.38). As with the carboxyl groups, the deprotonated

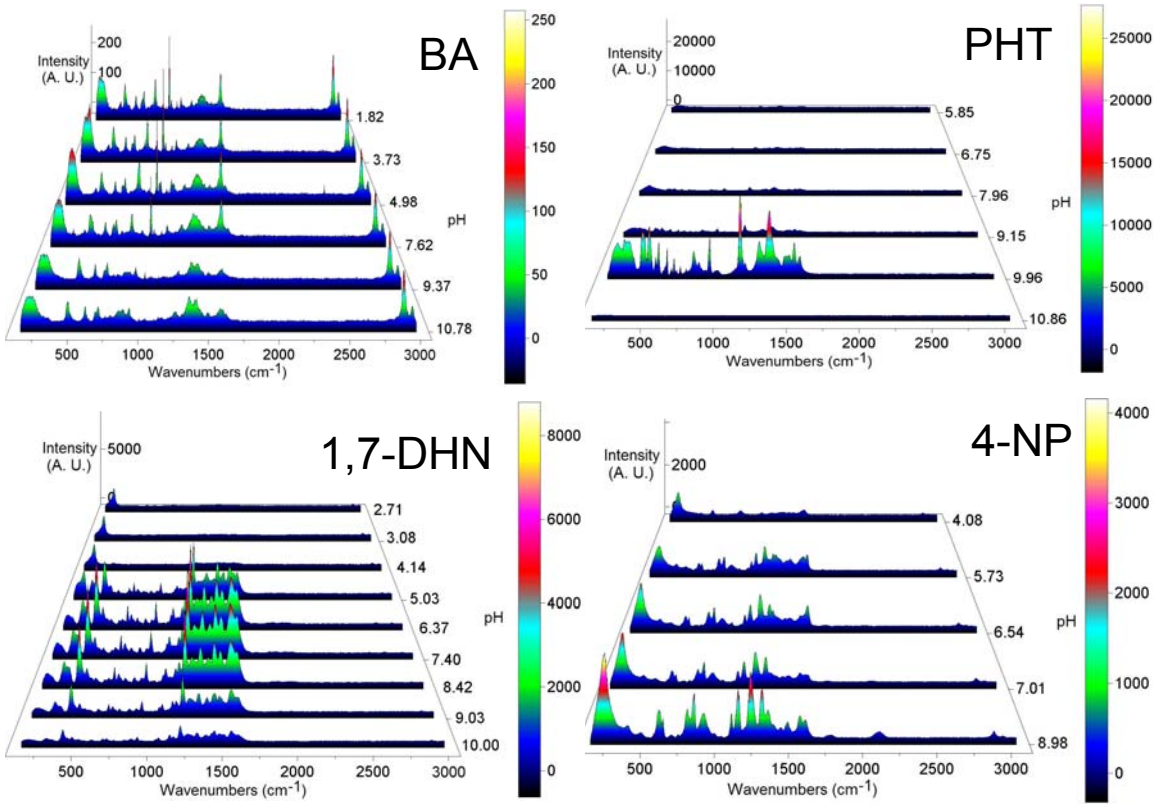

Figure 4.2 Influence of pH on the adsorption of: (A) BA (pKa 4.20), (B) PHT (pKa 9.23), (C) 1,7-DHN (pKa 9.28), and (D) 4-NP (pKa 7.23). All the samples were 1.0x10-4 M and analyzed via STT at 2000 rpm with an incident laser power of 2.2 mW.

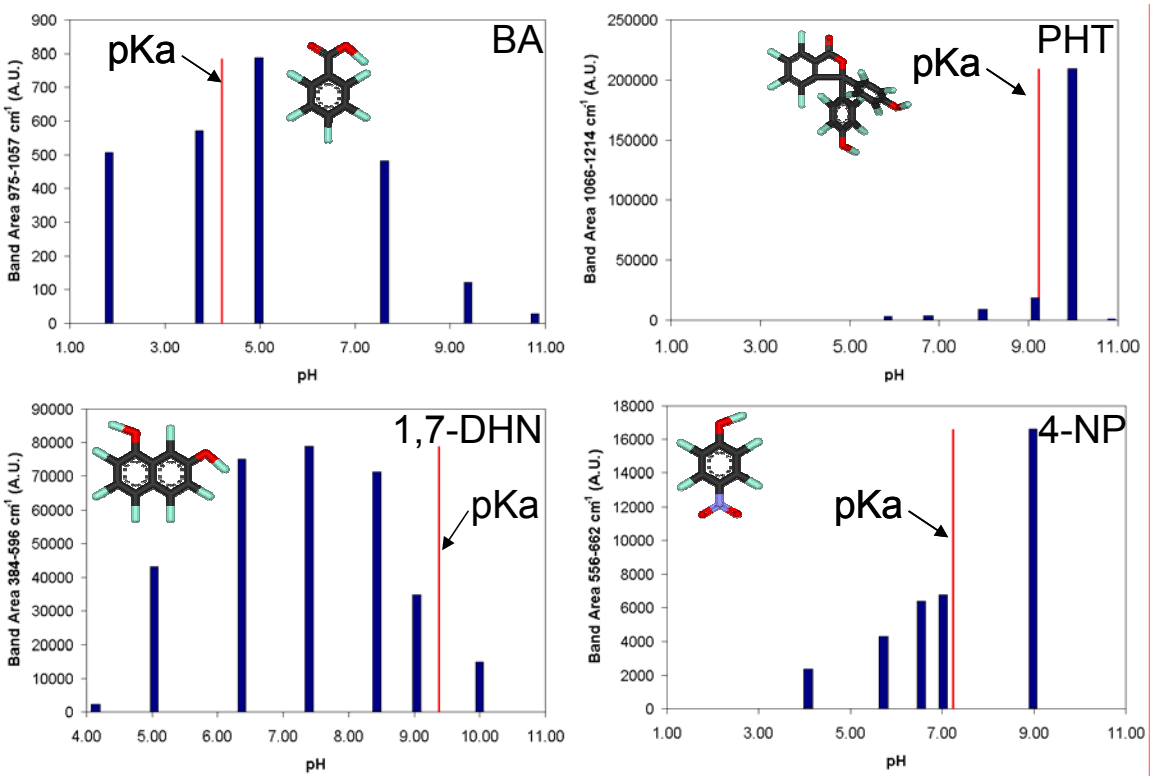

Figure 4.3 Changes in the SERS areas of (A) BA (pK_a 4.20), (B) PHT (pK_a 9.23), (C) 1,7-DHN (pK_a 9.28), and (D) 4-NP (pK_a 7.23) with pH. All the samples were $1.0x10^{-4}$ M and analyzed via STT at 2000 rpm with an incident laser power of 2.2 mW.

form of the hydroxyl group was expected to adsorb more efficiently onto the metal. However, the maximum SERS signal of 1,7-DHN was not observed above its pKa (Figure 4.3 C). Rather it occurred at a lower pH (7.40), at which less than 22% of the 1,7-DHN molecules exist in the deprotonated state. Interestingly, a significant decrease in the SERS signal of the analyte is observed when pH is pushed beyond this point. This could be attributed to two phenomena. First, the weak acid character of the 1,7-DHN hydroxyl groups relative to that of a carboxylic acid result in a less efficient adsorption of the analyte onto the metal. In addition, the increasing hydroxide content in the solution causes the rapid oxidation of the silver surface and quenches the SERS signal of the analyte.

The pH profile of 4-NP provides supportive evidence to these observations. The presence of a nitro group in this model phenol makes its hydroxyl group more acidic (pKa 7.23) than those present in 1,7-DHN. Therefore, 4-NP should exhibit a signal profile more similar to that of a carboxylic acid. The analysis of the spectroscopic data of 4-NP (Figure 4.3 D), shows a significant increase in its SERS signal above the pKa of the analyte (pH 8.98). At this point, over 98% of the 4-NP molecules exist in its deprotonated form. Zhang et. al. recently reported that 4-NP is less susceptible to photodecomposition, at this pH, which also contributes to our observations.[147] Our experiments demonstrate that the maximum enhancement of the SERS signals occurs when the analyte is physisorbed to the surface of the metal nanoparticles. The

observed trends also reveal that an excess amount of sodium hydroxide in the sample matrix reduces the intensity of the SERS signal of the analyte due to the competitive binding between the excess base and the analyte to the metal-nanoparticles.

4.3.2 The effects of sample matrix composition on analyte sorption and SERS activity

In addition to the pH effects, the presence of inorganic anions in the water matrix can alter the aqueous solubility of the analytes and their sorption onto the SERS active substrates. Therefore, a study of the changes in the SERS signal of 4-OHBA in the presence of different inorganic anions was performed for both Ag-PDMS and Ag-island films. Samples were prepared by using a series of sodium salts of the type (NaX), where X was one of the following phosphate, sulfate, carbonate, nitrate, chloride or fluoride. The band area for the region from 1190-1103 cm^{-1} of 4-OHBA was used to monitor the effect of the increased anion concentrations on the sorption of the analyte to the Ag-nanoparticles (Figure 4.4). The results for a "control" sample consisting of 4-OHBA diluted in deionized water shows a two fold higher SERS band area for 4-OHBA with Ag-PDMS vs. Ag-islands on glass, in good agreement with previous studies performed in our laboratories.[52] This has been attributed in part to an increase in the available surface area of the metal nanoparticles embedded into the polymer.[52,120] The hydrophobic character of PDMS is also important since it

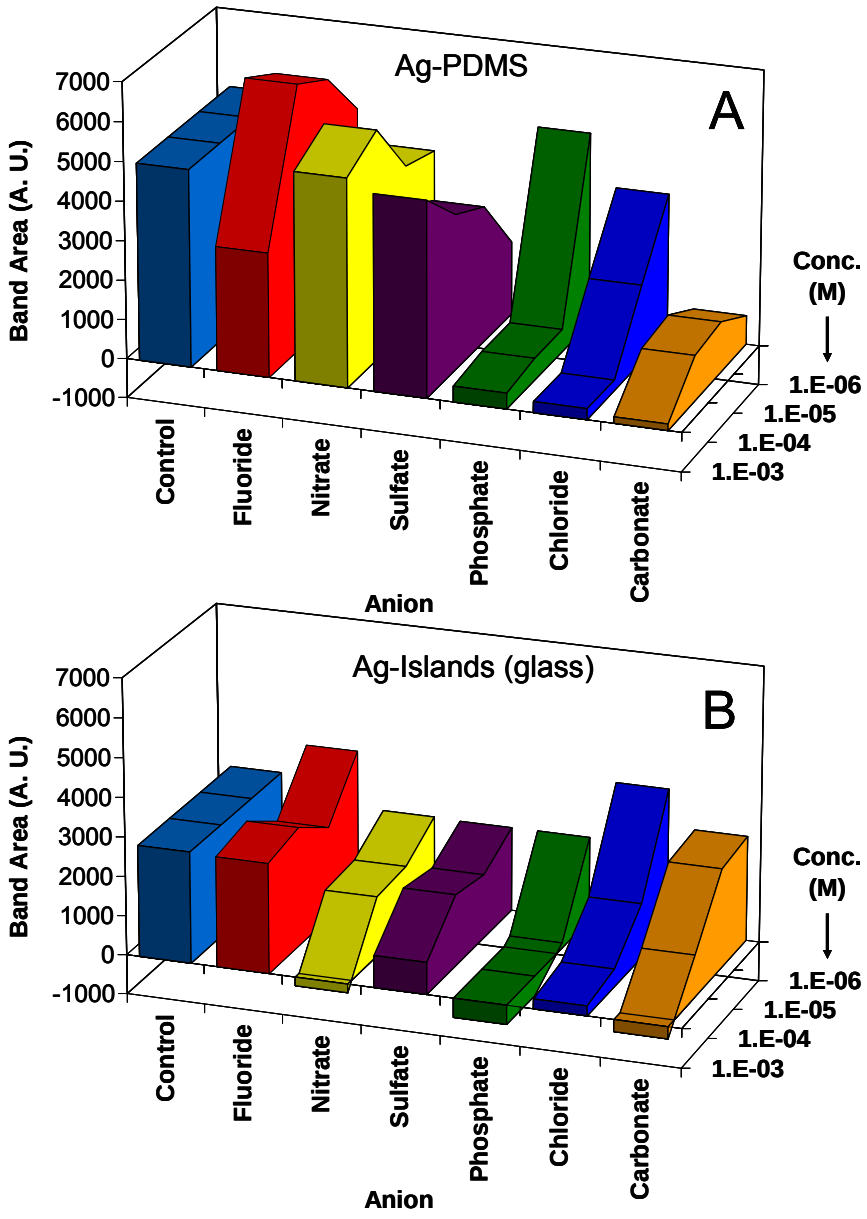

Figure 4.4 Changes in the 1190-1103 cm^{-1} band area of 4-OHBA ($1.0x10^{-5}$ M) with the increased concentration of different inorganic anions: (A) Ag-PDMS, and (b) Ag-islands. All the samples were analyzed via STT at 2000 rpm with an incident laser power of 2.2 mW.

inhibits the oxidation of the silver by limiting its direct contact to water and other oxidizing agents present in the sample matrix.

4.3.2.1 Halide effects

Metal halides such as NaCl and NaBr are often used as signal enhancers for colloidal silver solutions.[73] The mechanisms involved in this enhancement are still not well understood, and are a matter of debate among different research groups.[37,73] This enhancement has been attributed in part to the trapping of analyte into the substrate that promotes the coagulation of colloid around the analyte and increases the number of potential active sites ("hot spots") in the vicinity of the analyte. The competitive binding of these anions to the metal could also result in the removal of the impurities often adsorbed at the surface of the substrate.

Chloride salts can bind to the silver forming stable complexes of AgCl. The formation of these complexes at the surface of the silver nanoparticles is function of the halide concentration and the available surface area of the substrate. Therefore, the presence of these anions in solution could promote a competitive interaction between the analyte and the halogen to bind onto the surface of the substrate. When the metal nanoparticles are "fixed" to a solid support such as glass (Ag-Islands), or PDMS (Ag-PDMS), coagulation effects are not possible and the formation of metal-halide complexes at the surface of the substrate is the predominant event.

An analysis of the spectroscopic data shows a considerable reduction in the CO_2^-asymmetric stretching signal of 4-OHBA at 1639 cm^{-1} upon the addition of sodium chloride. We attribute the reduction in the SERS signal to a competitive interaction between the analyte and the chloride ions for the metal nanoparticles, since the spectroscopic data also shows an increase in the intensity of a band at 239 cm^{-1} with the increasing chloride concentration (Figure 4.5). Inspection of the conventional Raman spectrum of solid silver chloride indicates that this band corresponds to the formation of AgCl at the surface of the silver nanoparticles. Andryushechkin, et. al., have reported that the formation of AgCl on silver surfaces occurs when the concentration of the halogen is beyond the monolayer threshold of the substrate. [149,150] The addition of $1.0x10^{-6}$ M NaCl increases the SERS signals of 4-OHBA, indicating that concentration of the halogen at this point was below the monolayer-coverage of the substrate. At this concentration, the adsorption of the chloride ion to the substrate surface could promote desorption of weakly bound impurities such as trace amounts of carbonate from the deionized water and silicone oil from the physical vapor deposition (PVD) process. Beyond this point, a rapid decrease in the 4-OHBA SERS signal occurs. The increased intensity of the band at 239 cm^{-1} confirms the formation of AgCl at the surface of the nanoparticles, which is associated with the quenching of the SERS activity of the substrate. Studies with 4-ABA also demonstrate the formation of AgCl with the addition of $1.68x10^{-5}$ M NaCl (Figure 4.6).

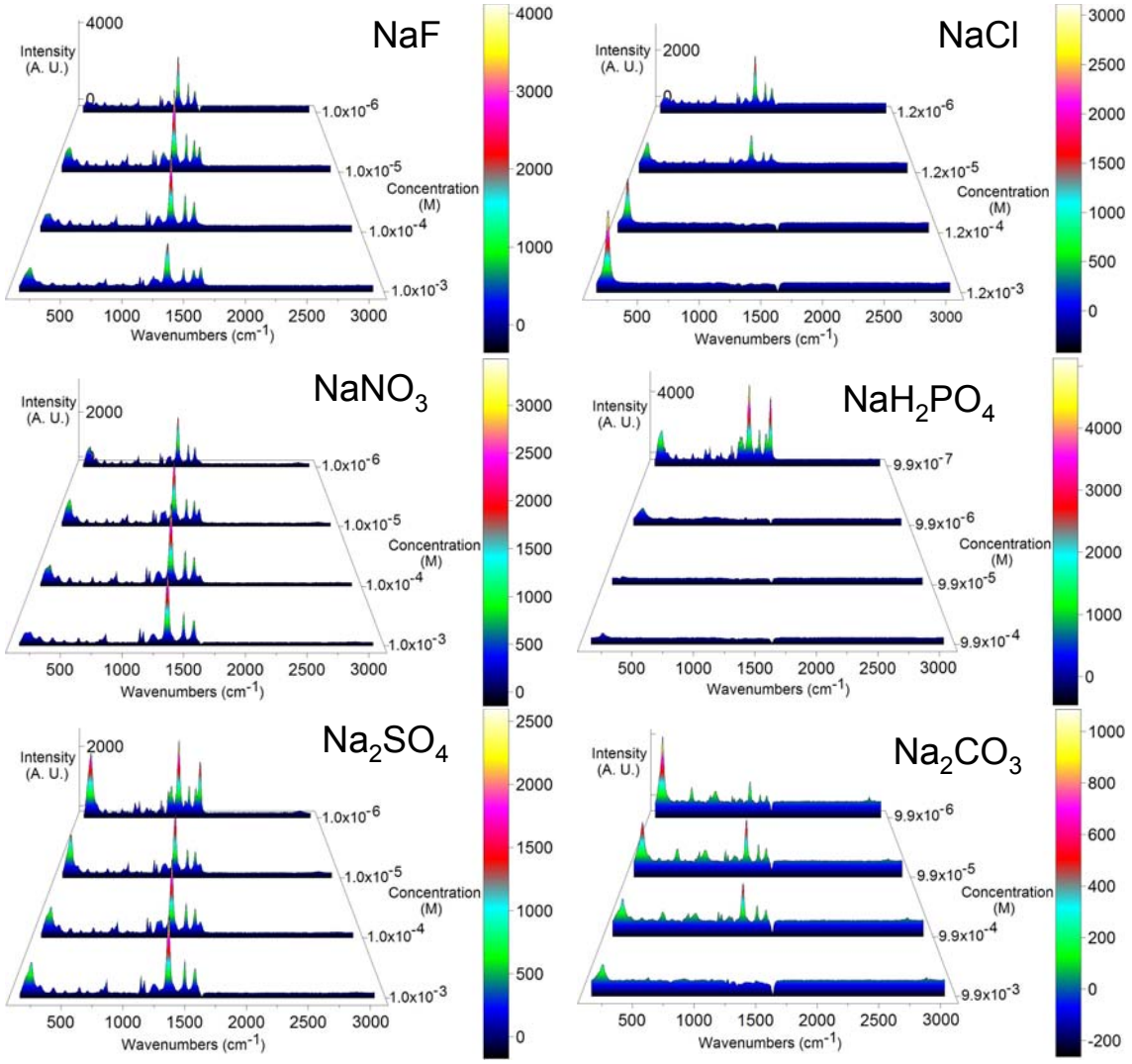

Figure 4.5 Changes in the SERS signal of 4-OHBA on Ag-PDMS upon the increased anion concentration. The spectra were baseline and background corrected after its collection at 2000 rpm with an incident laser power of 2.2 mW.

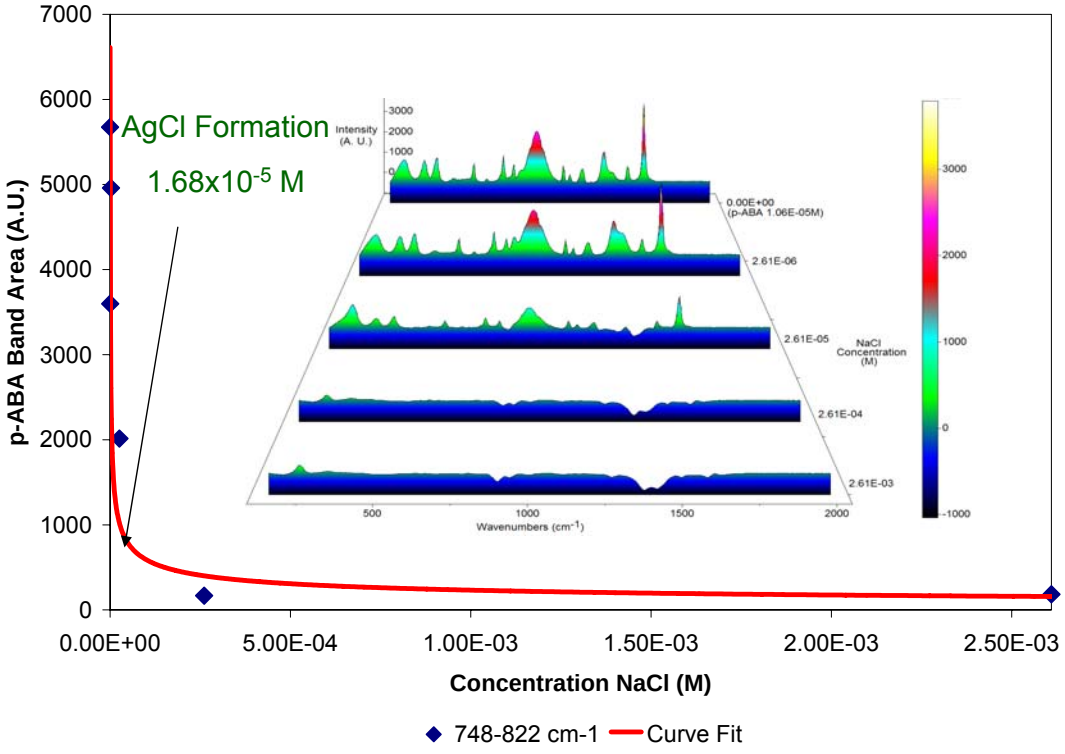

Figure 4.6 Changes in the SERS signal of 4-ABA on Ag-PDMS upon the increased concentration of NaCl.

Interestingly, the addition of moderate amounts of NaF ($1x10^{-6}$ to $1x10^{-4}$ M), result in an increased SERS signal of 4-OHBA on Ag-PDMS. In the case of Ag-islands on glass, this enhancement was only observed upon the addition of $1x10^{-6}$ M NaF. Beyond this concentration, the SERS signal of the analyte decreases due to the competitive interaction between the analyte and the excess fluoride. The changes in the 4-OHBA band at 1639 cm^{-1}, for fluoride vs. chloride indicate that fluoride competes less efficiently for the metal than the latter. The increased signal of the analyte upon the fluoride addition in the range of $1x10^{-6}$-$1x10^{-4}$ M for the Ag-PDMS nanocomposites could be a result of the influence of the NaF on the distribution (partition) of the analyte into the polymer.

4.3.2.2 Other naturally occurring anions

Inorganic anions such as nitrate, sulfate, carbonate and phosphate are often present in natural water samples. Their presence in aqueous environments plays an important role in the dissolution of metal ions, humic substances, and aromatic compounds. Our experiments indicate that the addition of sodium phosphate at a concentration greater than $1x10^{-6}$ M result in the rapid oxidation of silver on both Ag-PDMS and Ag-islands films (see Figure 4.4). The process depends on the concentration of the dissolved ion, which determines its effective surface coverage of the metal particles. The negative spectral features observed upon background correction have been attributed to the removal of the oxides and oils commonly present at the surface of the substrate (see Figure 4.5).

Sodium carbonate also quenches the SERS activity of the substrate (Figure 4.4). Because the effect is less dramatic than with phosphate we believe that this occurs due to the competitive adsorption between the carbonate ion and the analyte for the active sites of the substrates. Our data also demonstrates that this effect is considerably more pronounced for the Ag-PDMS nanocomposites than for the Ag-island films. PDMS is known to easily absorb carbon dioxide into its bulk structure. Therefore, it is possible that PDMS pre-concentrates the carbonate ions near the metal nanoparticles, thus compromising the adsorption of 4-OHBA onto the substrate. The changes in the SERS signals of 4-OHBA upon the addition of sulfate and nitrate also demonstrate the competitive nature of these interactions (see figure 4.4). In these cases the effect is less pronounced for the Ag-PDMS substrates than for the Ag-islands.

4.3.3 Structural effects on the sorption to Ag-PDMS

Early in this chapter we noted that the adsorption of the analyte onto the metal nanoparticles is an important factor to maximize the enhancement of its Raman signals. For poly-substituted aromatic compounds such as those present in this study, the spatial location of the substituents can affect the spatial orientation of the molecule relative to the SERS electromagnetic field as well as the effective binding of the analyte to the metallic surface. In addition positional isomers can exhibit different polarizabilities due to differences in molecular and

intra-molecular interactions. These variables could result in considerable differences in the enhancement of their Raman signals in SERS.

A study of the differences in the SERS signal of the positional isomers of several di-substituted benzenes shows a significant difference in the intensity of their SERS signal based on the spatial orientation of the substituents (Figure 4.7). The study shows that aminobenzoic acid derivatives exhibit an increase in SERS signal in the order of 4-ABA>3-ABA>2-ABA. The spectroscopic data also show an increase in the SERS signal 1605 cm^{-1} in this same order. This suggest that the carbonyl group of 4-ABA interacts more efficiently with the silver particles than the other isomers. An enhancement of the bands at 1508, 1372, 1138, and 991 cm^{-1} which are attributed to the 19a(a´), 19b(a´), 18b(a´), and 17 a(a") modes of a para substituted benzene indicates that the molecule is oriented parallel to the surface of the metal (see Figure 4.7).[151] The reduction in the intensity of these bands for 3-OHBA, particularly on the "b" modes suggest that the molecule is slightly tilted relative to the metal surface. The effect is even more pronounced in the case of 2-ABA. The closeness of these amino and carboxyl groups in 2-ABA may create a permanent hydrogen-bond between two groups, that could affect the binding of the carboxyl group to the metal. This is evidenced by the low intensity of the CO_2^- in-plane bending signal of 2-ABA at 1605 cm^{-1}.

Suh, et. al. demonstrate that the orientation of aromatic carboxylic acids can also be determined by comparing the SERS intensities at 1385 cm^{-1}

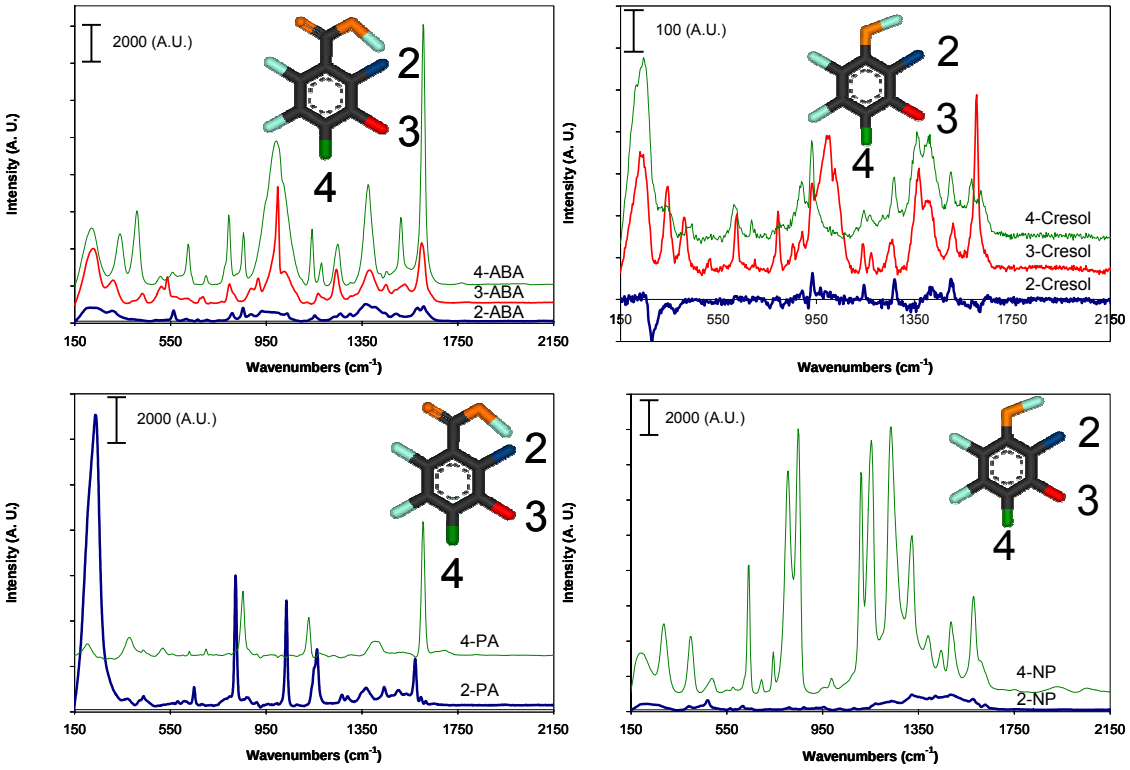

Figure 4.7 Positional isomer effects in the SERS signal of a series of aminobenzoic acid derivatives (ABA), cresols, phthalic acid (PA) and nitrophenol (NP).

(ν_s COO^-), and the 850 (δ COO^-) bands of the carboxyl groups.[151] His work shows that aromatic acids are adsorbed flat onto the metal when the intensity of the ν_s COO^- band is greater than the δ COO^- band and the degree of tilting correlates with the increase intensity of the latter. Our experiments show an increase in the increase intensity in the 850 cm^{-1} band of these analytes in the order of 4-ABA>3-ABA>2-ABA in agreement with the observations of Suh. et. al. Similar trends have also been observed for other systems such as cresols, phthalic acid derivatives, and nitro-phenols (see Figure 4.7).

4.3.4 Analysis of amino aromatic compounds via HPLC SERS

The diversity and relatively high concentrations of inorganic ions in real environmental samples impose significant limitations to the use of SERS as an analytical tool in environmental chemistry. Furthermore, the ability of other interfering agents such as microorganisms and humic substances, to trap organic matter into their bulk structure, as well as their potential contributions to the SERS background, considerably limit SERS use for trace analysis. These problems are evidenced by the differences in the SERS signal for a series of 4-ABA solutions prepared in deionized water and natural water (Figure 4.8 A,B). Our results show that the constituents of the water matrix limit the adsorption of 4-OHBA to the substrates and also promote the oxidation of the silver nanoparticles. Consequently, the use of a method to selectively and conveniently remove the matrix interferences from the analytes is required.

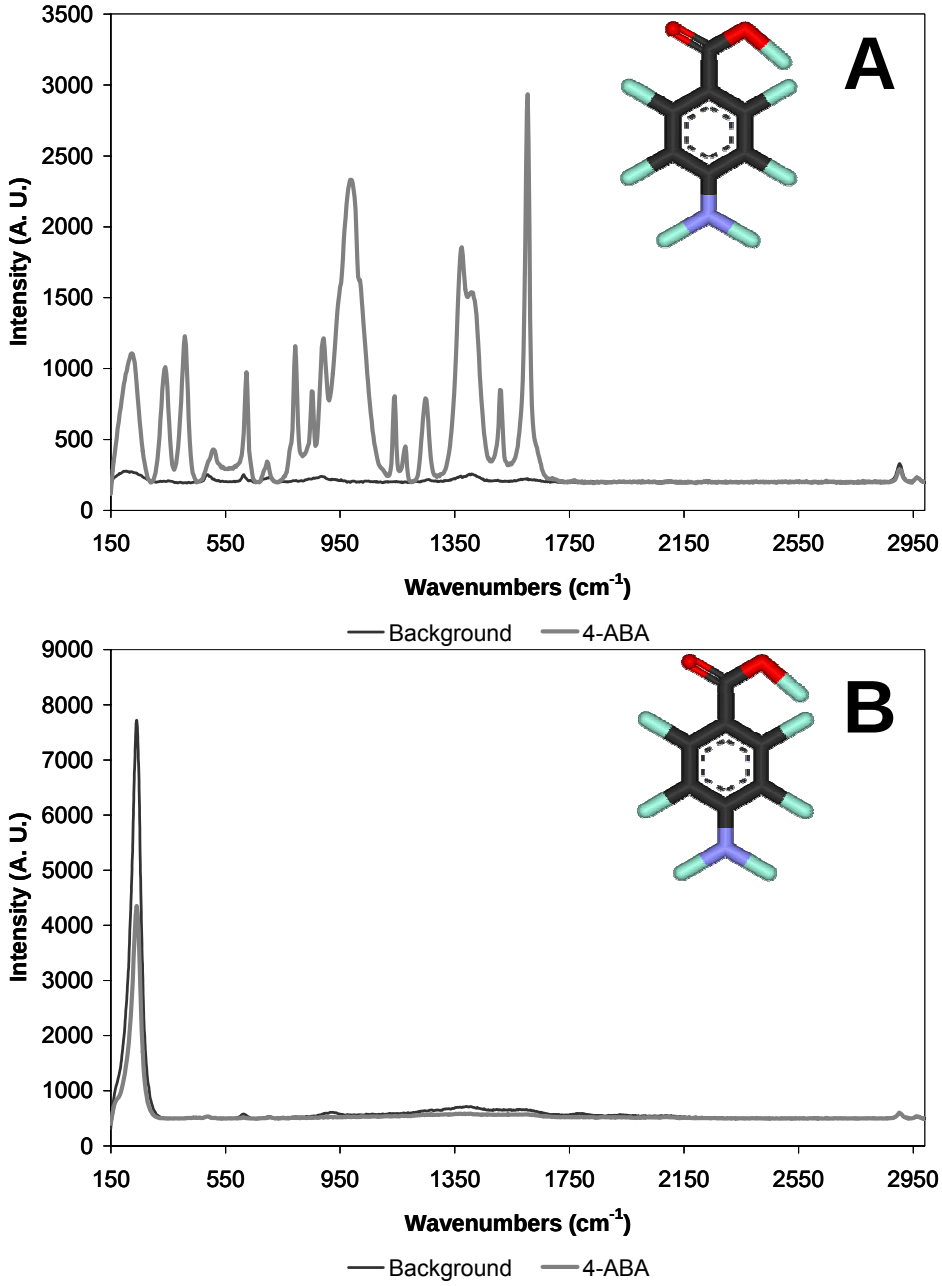

Figure 4.8 SERS spectra of 4-ABA (1.0×10^{-6} M) in deionized water (A) and creek water (B). The creek and DI-water background are shown in gray for clarity.

Recently, liquid chromatography phases have been effective in removing matrix interferences from environmental samples. The selective elution of two 4-ABA solutions (1.4 $x10^{-4}$ M in natural and DI water) was accomplished by injecting a 20μL aliquot of each sample onto a SupelcosilABZ+® liquid chromatography column and eluting with a 40% acetonitrile-60% water mobile phase. The eluted fractions were collected in glass vials, transferred to Ag-PDMS wells, and analyzed via STT-SERS without further treatment (Figure 4.9). The intensity and spectral features obtained from the natural water sample were very comparable to those observed in deionized water. The technique has also proven to be effective in the separation and characterization of mixtures of amino aromatic compounds in aqueous media (see Figure 4.10 and table 4.1). These results demonstrate that the combination of this separation (or isolation) technique with SERS detection could be an effective tool for the analysis of environmental pollutants in natural water. HPLC is a powerful and well established separation technique for the analysis of pesticides and other environmentally relevant compounds. The combination of these two techniques has shown significant potential for the separation and analysis of organic compounds in aqueous media.[152,153]

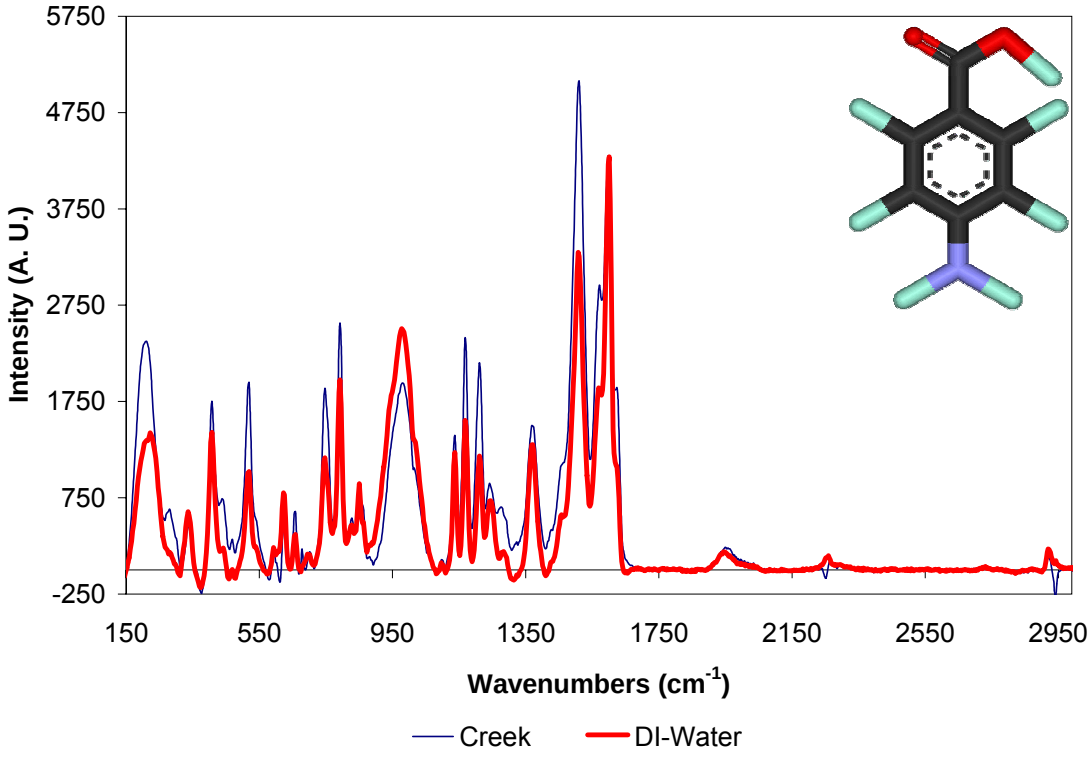

Figure 4.9 Baseline and background corrected SERS spectra of the fractions that eluted after injecting 20 μL of 4-ABA (1.0×10^{-4} M): deionized water and creek water. Samples were eluted in a 40% acetonitrile/60% water mixture with UV-detection at 280 nm.

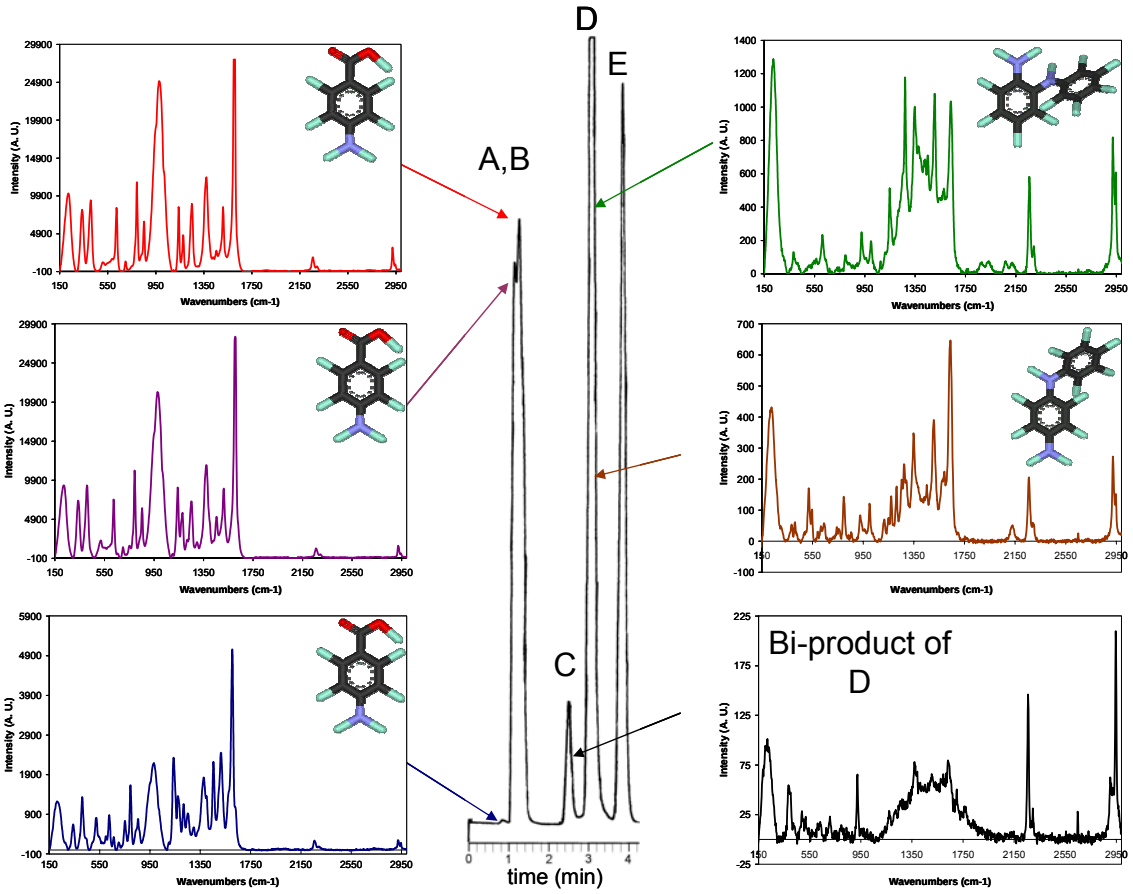

Figure 4.10 HPLC-SERS spectra of the separation of 4-ABA (A,B), 1,4-PDA (D), and 1,2-PDA (E) in a 1.0x10^{-4} M mixture, using the fraction collection approach. The signal at C corresponds to a by-product of 1,4-PDA. The sample consists of a 20 μL aliquot of the mixture eluted in 25% acetonitrile/75% Water with UV detection at 280 nm.

Table 4.1 Chromatographic data for the separation of 4-ABA, 1,4-PDA, and 1,2-PDA in a 1.0×10^{-4} M mixture.

Component	Assignment	Avg. t. (min)	s_t (min)	%RSD (t)	Resolution	
A, B	4-ABA	1.28	0.04	3.21	B,C	3.42
C	Bi-product 1,4-PDA	2.59	0.06	2.45	C,D	1.92
D	1,4-PDA	3.22	0.05	1.64	D,E	2.63
E	1,2-PDA	4.07	0.07	1.66		

CHAPTER 5

Concluding remarks

The use of SERS based methods for routine analysis of environmental and pharmaceutically relevant compounds is still in its early stages. More studies are required in order to gain a better understanding of the experimental variables affecting this technique. In addition, further research is needed for the development of substrates that are more robust and provide better enhancement of the Raman signals. Despite these limitations, surface enhanced Raman spectroscopy has proven to be a promising tool in a wide range of areas such as surface sciences, biophysics, pharmaceutical, and environmental sciences. In the preceding chapters we identified some of the experimental variables that have limited the use of SERS as a routine analytical technique. In addition new methods and protocols have been presented in order to cope with these problems. This chapter provides some conclusions and comments on the future of SERS as an analytical technique.

The continuous irradiation of sample under SERS conditions can induce permanent damage to the substrate surface even at powers as low as 2.1($\pm$0.1) mW. The use of a sample translation technique has proven to minimize substrate damage, as well as thermal and photolytic decomposition of the analyte. In addition, it has shown to be a powerful technique to minimize thermal and photolytic processes commonly observed in SERS. The decreased photo-induced changes in the sample under STT conditions allow the collection of a

SERS spectrum that is similar to the ones observed under conventional Raman conditions.

Improvements in reproducibility under STT conditions also contribute to improvements in sensitivity realized with Ag-PDMS substrates. The STT approach considerably improves the efficiency of the analysis by allowing the rapid and efficient interrogation of the substrate surface. The rapid translation of the sample averages the topographical features of the substrate. This greatly improves the precision of the analytical results. In most cases, the spectral resolution is improved over 20 %, while the signal intensity increases by at least a factor of two. STT also enhances vibrational modes that often are weakly enhanced or even absent under stationary conditions. STT-SERS could be a powerful tool to derive structural information that can be related to the kinetics of thermal and photolytic processes.

The use of Ag-PDMS microtiter wells in combination with STT-SERS has been shown to be a powerful tool for the qualitative and quantitative analysis of aromatic compounds in water at sub-micromolar concentrations. The unique optical and physical properties of Ag-PDMS nanocomposites provide a protective coating for the silver nanoparticles and pre-concentrate the sample analytes in close proximity to the silver. The increased surface area of the Ag-PDMS nanocomposites also extends the technique's linear dynamic range.

The potential for the amino, hydroxy, mercapto, and carboxy-aromatic pollutants to bind onto the surface of the metal nanoparticles makes this technique a promising tool for the qualitative and quantitative analysis of polar-

aromatic pollutants in aqueous media. Such studies can provide new insights into the binding mechanisms of acidic and alkaline pollutants to metallic surfaces. The use of STT-SERS for real time monitoring of chemical changes demonstrates its promise for deriving structural information related to the kinetics of thermal and photolytic processes.

Our studies demonstrate that the effective sorption of model environmental pollutants to Ag-PDMS can be influenced by pH and the presence of inorganic anions in the sample matrix. The experimental results indicate that aromatic acids sorb more efficiently to the substrate when the pH is above the pKa of the analyte. Alternatively, amino aromatic compounds exhibit a better sorption to AgPDMS when the pH is below the pKa of the analyte. The sorption process occurs by the initial partition of the analyte into the polymer, followed by its subsequent adsorption onto the embedded silver-nanoparticles. The results also indicate that the interactions of aromatic acids with the metal are initiated by the physisorption of the carboxyl moiety of the analyte, while amino-aromatic compounds follow a different adsorption mechanism. The presence of inorganic anions can affect the detection of aromatic pollutants in water due to the competition between the anions and the analytes for the active sites of the metal, or the rapid oxidation of the substrate upon contact with the water matrix. These effects can be effectively surmounted by coupling STT-SERS to a separation technique such as HPLC, and presents a promising approach for the use of SERS in the analysis of polarizable environmental pollutants in real samples.

Future studies involving SERS detection should be focused in the rational design of new polymer-based substrates. These studies should involve the preparation of new metal-polymer matrices capable to prevent the oxidation of the metal nanoparticles, while providing a surface for the selective pre-concentration of the analyte at close proximity to the metal. Such matrices should also be suitable for the casting of nano-litographically designed structures at the surface of the substrates. These substrates could provide a more efficient enhancement of the Raman signals. The inherent selectivity and extracting capabilities of these polymer based substrates makes them an attractive alternative for environmental applications.

Another area that desperately needs attention is that of the hyphenation of SERS to a chromatographic technique such as HPLC or CE. These areas require the development of novel sampling techniques and the redesign of the cell compartment of these instruments. The technique also requires the development of an automated and efficient sampling system for post column applications.

In conclusion, it has been demonstrated that the use of Ag-PDMS nanocomposites in combination with STT-SERS is a promising alternative for the analysis of ionizable aromatic compounds of environmental and pharmaceutical significance. STT-SERS is ideal to study the binding-kinetics of aromatic compounds onto metallic surfaces. The technique is also a promising tool for the real-time-monitoring of thermal and photolytic decomposition processes on metallic surfaces. STT-SERS has potential applications in several areas of

pharmaceutical and environmental interest like drug-stability studies, solubility studies, metal-adsorbate interactions and humification processes. The susceptibility of silver to oxidation upon contact with inorganic anions and other matrix components limits the use of STT-SERS for the direct analysis of real samples. The use of HPLC with post-column STT-SERS detection can effectively overcome this limitation. HPLC-SERS is a promising alternative for separation and unequivocal identification of the chemical constituents in real samples. SERS has become one of the fastest growing areas in chemical spectroscopy over the past 15 years. However, further developments needs to occur in order to use SERS as a routine analytical tool.

REFERENCES

1. Colthup, N. B.; Daly, L. H. l.; Wiberley, S. E. (**1990**); **Introduction to infrared an Raman spectroscopy); (1990**), Academic Press, p. 60, Chapters 1-2, 8, 10, 11.
2. Skoog, D. A.; Hooler, F. J.; Nieman, T.; **"Principles of Instrumental Analysis"**; (**1998**), Saunders College Publishing; Chapters 7, 18.
3. Long; Derek A.; **"The Raman Effect": A unified treatment of the theory of Raman scattering by molecules** (**2002**), John Wiley & Sons. Ink; NY Chapters 4-5.
4. Kneipp, K.; Kneipp, H.; Itzkan, I.; Dasari, R. R.; Feld, M. S.; **"Surface-enhanced Raman scattering and biophysics.";** Journal of Physics: Condensed Matter (**2002**),14(18), R597-R624.
5. Vo-Dinh, T.; **"SERS chemical sensors and biosensors" new tools for environmental and biological analysis"**; Sensors ans Actuators B (**1995**) 29, 183-189.
6. Heywang, C.; Chazalet, M.; Saint-Pierre, M. M.; Bolard, J.; **"The passive diffusion of anthracyclines through lipid Langmuir-Blodgett bilayers studied by surface enhanced raman spectroscopy (SERS)"**; Spectroscopy of Biological Molecules: New Directions, European Conference on the Spectroscopy of Biological Molecules, 8th, Enschede, Netherlands (**1999**), Aug. 29-Sept. 2, 339-342.
7. Fleischmann, M.; Hendra, P. J.; McQuillan, A. J.; **"Raman spectra of pyridine adsorbed at a silver electrode."**; Chemical Physics Letters (**1974**), 26(2), 163-166.
8. Kneipp, K.; Kneipp, H.; Itzkan, I.; Dasari, R. R.; Feld, M. S.; **"Ultrasensitive chemical analysis by Raman spectroscopy."**; Chemical Reviews (Washington, D. C.) (**1999**), 99(10), 2957-2975.
9. Xu, H.; Bjerneld, E. J.; Kall, M.; Borjesson, L.; **"Spectroscopy of single hemoglobin molecules by surface enhanced Raman scattering."**; Physical Review Letters (**1999**), 83(21), 4357-4360.
10. Michaels, A. M.; Nirmal, M.; Brus, L. E.; **"Surface Enhanced Raman Spectroscopy of Individual Rhodamine 6G Molecules on Large Ag Nanocrystals."**; Journal of the American Chemical Society (**1999**), 121(43), 9932-9939.
11. Constantino, C. J. L.; Lemma, T.; Antunes, P. A.; Aroca, R.; Analytical Chemistry (**2001**), 73 3674.
12. LaPlant, F.; Ben-Amotz, D.; **"Design and construction of a microscope-based Raman system."**; Review of Scientific Instruments (**1995**), 66(6), 3537-3544.
13. Grand, J.; Kostcheev, S.; Bijeon, J.-L.; De la Chapelle, M. L.; Adam, P.-M.; Rumyantseva, A.; Lerondel, G.; Royer, P.; **"Optimization of SERS-active substrates for near-field Raman spectroscopy."**; Synthetic Metals (**2003**), 139(3), 621-624.
14. Kroo, N.; Krieger, W.; Lenkefi, Z.; Szentirmay, Z.; Thost, J. P.; Walther, H.; **"A new optical method for investigation of thin metal films."**; Surface Science (**1995**), 331-333(B), 1305-1309.

15. Faulds, K.; Smith W. E.; Grahama D.; Laceyb, R. J.; **"Assessment of silver and gold substrates for the detection of amphetamine sulfate by surface enhanced Raman scattering (SERS)"**; Analyst (**2002**), 127, 282–286.
16. Dou, X.; Yamaguchi, Y.; Yamamoto, H.; Doi, S.; Ozaki, Y.; **"NIR SERS detection of immune reaction on gold colloid particles without bound/free antigen separation."**; Journal of Raman Spectroscopy (**1998**), 29(8), 739-742.
17. Bermejo, J. S.; Reinecke, H.; Ugarte, C. M.; **"Confocal Raman microscopy applied to characterization of materials."**; Revista de Plásticos Modernos (**2001**), 81(539), 592-599.
18. Chase, D. B.; Rabolt, J. F.; **FT-Raman Spectroscopy, from concept to experiment** (**1994**), pp.26.
19. Bowie, B. T.; Chase, D. B.; Griffiths, P. R.; **"Factors affecting the performance of bench-top Raman spectrometers. Part I: instrumental effects."**; Applied Spectroscopy (**2000**), 54(5), 164A-173A.
20. Baldwin, K. J.; Batchelder, D, N.; Webster, S.; **"Raman microscopy: confocal and scanning near-field."**; Practical Spectroscopy (**2001**), 28(Handbook of Raman Spectroscopy), 145-190.
21. Mc Creery R. L.; **"Raman spectroscopy for chemical analysis"** (**2000**), Chapter 1.
22. Jeanmaire, D. L.; Van Duyne, R. P.; **"Surface Raman spectroelectrochemistry. Part I. Heterocyclic, aromatic, and aliphatic amines adsorbed on the anodized silver electrode."**; Journal of Electroanalytical Chemistry and Interfacial Electrochemistry (**1977**), 84(1), 1-20.
23. Albrecht, M. G.; Creighton, J. A.; **"Anomalously intense Raman spectra of pyridine at a silver electrode."**; Journal of the American Chemical Society (**1977**), 99(15), 5215-17.
24. Hidalgo, M.; Montes, R.; Laserna, J. J.; Ruperez, A.; **"Surface-enhanced resonance Raman spectroscopy of 2-pyridylhydrazone and 1,10-phenanthroline chelate complexes with metal ions on colloidal silver."**; Analytica Chimica Acta (**1996**), 318(2), 229-37.
25. Hu, J.; Zhao B.; Xu, W.; Li, B.; Fan Y.; **"Surface-enhanced Raman spectroscopy study on the structure changes of 4-mercaptopyridine adsorbed on silver substrates and silver colloids"**; Spectrochimica Acta Part A (**2002**); 58, 2827-2834
26. Carrasco F., E. A.; Campos-Vallette, M.; Leyton, P.; Diaz F., G.; Clavijo, R. E.; García-Ramos, J. V.; Inostroza, N.; Domingo, C.; Sánchez-Cortés, S.; Koch, R.; **"Study of the Interaction of Pollutant Nitro Polycyclic Aromatic Hydrocarbons with Different Metallic Surfaces by Surface-Enhanced Vibrational Spectroscopy (SERS and SEIR)."**; Journal of Physical Chemistry A (**2003**), 107(45), 9611-9619.
27. Kneipp, K.; Wang, J.; Kneipp, H.; Itzkan, I.; Dasari, R. R.; Feld, M. S.; **"Population pumping of excited vibrational states by spontaneous**

surface-enhanced Raman scattering."; Physical Review Letters (**1996**), 76(14), 2444-7.
28. Pettinger, B.; Krischer, K.; **"Comparison of cross-sections for absorption and surface-enhanced resonance Raman scattering for Rhodamine 6G at coagulated silver colloids."**; Journal of Electron Spectroscopy and Related Phenomena (**1987**), 45 133-42.
29. Kruszewski, S.; **"Enhancement mechanisms in the SERS phenomenon."**; Proceedings of SPIE-The International Society for Optical Engineering (**1998**), 3320 (Wave and Quantum Aspects of Contemporary Optics), 281-293.
30. García-Vidal, F. J.; Pendry, J. B.; **"Collective theory for surface enhanced Raman scattering. Physical Review Letters"**; (**1996**), 77(6), 1163-1166.
31. Campion, A.; Kambhampati, P.; **"Surface-enhanced Raman scattering."**; Chemical Society Reviews (**1998**), 27(4), 241-250.
32. Corset, J.; Aubard, J.; **"Foreword to the special issue on surface-enhanced raman scattering: new trends and applications."**; Journal of Raman Spectroscopy (**1998**), 29(8), 649-650.
33. Baletto, F.; Mottet, C.; Ferrando, R.; **"Molecular dynamics simulations of surface diffusion and growth on silver and gold clusters."**; Surface Science (**2000**), 446(1-2), 31-45.
34. Shalaev, V. M.; "**Electromagnetic properties of small-particle composites."**; Physics Reports (**1996**), 272(2 & 3), 61-137
35. Safonov, V. P.; Shalaev, V. M.; Markel, V. A.; Danilova, Yu. E.; Lepeshkin, N. N.; Kim, W.; Rautian, S. G.; Armstrong, R. L.; **"Spectral dependence of selective photomodification in fractal aggregates of colloidal particles."**; Physical Review Letters (**1998**), 80(5), 1102-1105.
36. Otto, A.; **"Theory of first layer and single molecule surface enhanced Raman scattering (SERS)."**; Physica Status Solidi A: Applied Research (**2001**), 188(4), 1455-1470.
37. Sanchez-Cortes, S.; Garcia-Ramos, J. V.; **"Influence of coverage in the surface-enhanced Raman scattering of cytosine and its methyl derivatives on metal colloids: chloride and pH effects."**; Surface Science (**2001**), 473(1-2), 133-142.
38. Weitz, D. A.; Oliveria, M.; **"Fractal structures formed by kinetic aggregation of aqueous gold colloids.";** Physical Review Letters (**1984**), 52(16), 1433-1436.
39. Yamaguchi, Y.; Weldon, M. K.; Morris, M. D.; **"Fractal characterization of SERS-active electrodes using extended focus reflectance microscopy."**; Applied Spectroscopy (**1999**), 53(2), 127-132.
40. McQuillan, A. J.; Hendra, P. J.; Fleischmann, M.; **"Raman spectroscopic investigation of silver electrodes."**; Journal of Electroanalytical Chemistry and Interfacial Electrochemistry (**1975**), 65(2), 933-44.
41. lbrecht, M. G.; Creighton, J. A.; **"Intense Raman spectra at a roughened silver electrode."**; Electrochimica Acta (**1978**), 23(10), 1103-5.

42. Norrod, K. L.; Sudnik, L. M.; Rousell, D. ; Rowlen, K. L.; **"Quantitative comparison of five SERS substrates: sensitivity and limit of detection."**; Applied Spectroscopy (**1997**), 51(7), 994-1001.
43. Vo-Dinh, T.; **"Surface-enhanced Raman spectroscopy using metallic nanostructures."**; TrAC, Trends in Analytical Chemistry (**1998**), 17(8+9), 557-582.
44. Keir, R.; Sadler, D.; Smith, W. E.; **"Preparation of stable, reproducible silver colloids for use as surface-enhanced resonance Raman scattering substrates."**; Applied Spectroscopy (**2002**), 56(5), 551-559.
45. Tran, C. D.; **"Subnanogram detection of dyes on filter paper by surface-enhanced Raman scattering spectrometry."**; Analytical Chemistry (**1984**), 56(4), 824-6.
46. Nie, S.; Emory, S.R.; **"Probing single molecules and single nanoparticles by surface-enhanced Raman scattering."**; Science (Washington, D. C.) (**1997**), 275(5303), 1102-1106.
47. Kneipp, K.; Wang, Y.; Kneipp, H.; Perelman, L. T.; Itzkan, I.; Dasari, R. R.; Feld, M. S.; **"Single molecule detection using surface-enhanced Raman scattering (SERS)."**; Physical Review Letters (**1997**), 78(9), 1667-1670.
48. Bello, J. M.; Stokes, D. L.; Vo-Dinh, T.; **"Titanium dioxide based substrate for optical monitors in surface-enhanced Raman scattering analysis."**; Analytical Chemistry (1989), 61(15), 1779-83.
49. Alak, A. M.; Vo-Dinh T.; **"Silver-coated fumed silica as a substrate material for surface-enhanced Raman scattering."**; Analytical Chemistry (**1989**), 61(7), 656-60.
50. Meier, M.; Wokaun, A.; Vo-Dinh, T.; **"Silver particles on stochastic quartz substrates providing tenfold increase in Raman enhancement."**; Journal of Physical Chemistry (**1985**), 89(10), 1843-6.
51. Vo-Dinh, T.; Meier, M.; Wokaun, A. **"Surface-enhanced Raman spectrometry with silver particles on stochastic-post substrates.";** Analytica Chimica Acta (**1986**), 181 139-48.
52. Giesfeldt, K. S.; Connatser, R. M.; De Jesus, M. A.; Lavrik, N. V.; Dutta, Pampa; Sepaniak, M. J.; **"Studies of the optical properties of metal-pliable polymer composite materials."**; Applied Spectroscopy (**2003**), 57(11), 1346-1352.
53. Moody, R. L.; Vo-Dinh, T. ; Fletcher, W. H.; **"Investigation of experimental parameters for surface-enhanced Raman scattering (SERS) using silver-coated microsphere substrates."**; Applied Spectroscopy (**1987**), 41(6), 966-70.
54. Bello, J. M.; Stokes, D. L.; Vo-Dinh, T.; **"Silver-coated alumina as a new medium for surfaced-enhanced Raman scattering analysis."**; Applied Spectroscopy (**1989**), 43(8), 1325-30.
55. Bello, J. M.; Stokes, D. L.; Vo-Dinh T.; **"Titanium dioxide based substrate for optical monitors in surface-enhanced Raman scattering analysis."**; Analytical Chemistry (**1989**), 61(15), 1779-83.

56. Gessner R; Rosch P; Kiefer W; Popp J.; **"Raman spectroscopy investigation of biological materials by use of etched and silver coated glass fiber tips."**; BIOPOLYMERS (**2002**), 67(4-5), 327-30.
57. Volkan, M.; Stokes, D. L.; Vo-Dinh, T.; **"A new surface-enhanced Raman scattering substrate based on silver nanoparticles in sol-gel."**; Journal of Raman Spectroscopy (1999), 30(12), 1057-1065.
58. Lee, Yuan-Hsiang; Dai, S. ; Young, Jack P.; **"Silver-doped sol-gel films as the substrate for surface-enhanced Raman scattering."**; Journal of Raman Spectroscopy (**1997**), 28(8), 635-639.
59. Lucht, S.; Murphy, T.; Schmidt, H.; Kronfeldt, H.-D.; **"Optimized recipe for sol-gel-based SERS substrates."**; Journal of Raman Spectroscopy (**2000**), 31(11), 1017-1022.
60. Volkan, M.; Stokes, D. L.; Vo-Dinh, T.; **"A new surface-enhanced Raman scattering substrate based on silver nanoparticles in sol-gel."**; Journal of Raman Spectroscopy (**1999**), 30(12), 1057-1065.
61. Yang, L.; Saavedra, S. S. (**1995**) **"Chemical Sensing Using Sol-Gel Derived Planar Waveguides and Indicator Phases"**; Analytical Chemistry, 67(8), 1307-1314.
62. Tadanaga, K.; Iwashita, K.; Minami, T.; Tohge, N.; **"Coating and water permeation properties of SiO2 thin films prepared by the sol-gel method on nylon-6 substrates."**; Journal of Sol-Gel Science and Technology (**1996**), 6(1), 107-11
63. Murphy, T.; Schmidt, H.; Kronfeldt, H.-D.; **"Use of sol-gel techniques in the development of surface-enhanced Raman scattering (SERS) substrates suitable for in situ detection of chemicals in seawater."**; Applied Physics B: Lasers and Optics (**1999**), 69(2), 147-150.
64. Shahriari, M. R.; Murtagh, M. T.; Kwon, H. C.; **"Ormosil thin films for chemical sensing platforms."**; Proceedings of SPIE-The International Society for Optical Engineering (**1997**), 3105(Chemical, Biochemical, and Environmental Fiber Sensors IX), 40-51.
65. Alvarez-Ros, M. C.; Sanchez-Cortes, S.; Francioso, O.; Garcia-Ramos, J. V.; **"Catalytic modification of gallic acid on a silver surface studied by surface-enhanced Raman spectroscopy."**; Journal of Raman Spectroscopy (**2001**), 32(2), 143-145.
66. Jang, N. H.; Suh, J. S.; Moskovits, M.; **"Effect of Surface Geometry on the Photochemical Reaction of 1,10-Phenanthroline Adsorbed on Silver Colloid Surfaces."**; Journal of Physical Chemistry B (**1997**), 101(41), 8279-8285.
67. Jeong, D. H.; Jang, N. H.; Suh, J. S.; Moskovits, M.; **"Photodecomposition of Diazanaphthalenes Adsorbed on Silver Colloid Surfaces."**; Journal of Physical Chemistry B (**2000**), 104(15), 3594-3600.
68. Tocón, I. L.; Centeno, S. P.; Otero, J. C.; Marcos, J. I.; **"Characterization of electronic properties of charge-transfer states of biological molecules by surface-enhanced Raman scattering.";** Spectroscopy of

Biological Molecules: New Directions, European Conference on the Spectroscopy of Biological Molecules, 8th, Enschede, Netherlands, Aug. 29-Sept. 2, 1999 (**1999**), 679-680.

69. Farquharson, S.; Smith, W. W.; Elliott, S.; Sperry, J. F.; **"Rapid biological agent identification by surface-enhanced Raman spectroscopy."**; Proceedings of SPIE-The International Society for Optical Engineering (**1999**), 110-116.
70. Dou, X.; Ozaki, Y.; **"Surface-enhanced Raman scattering of biological molecules on metal colloids: basic studies and applications to quantitative assay."**; Reviews in Analytical Chemistry (**1999**), 18(4), 285-321.
71. Corio, P.; Rubim, J. C.; **"Surface-enhanced Raman spectroscopy on electrode surfaces as a tool to characterize LUMOs of inorganic complexes with two different ligands. The case of the ion complex [Ru(bipy)2viol]+."**; Journal of Raman Spectroscopy (**1997**), 28(4), 235-241.
72. Zhang, J.; Liang, Y.; **"Surface-enhanced Raman scattering of malachite green on silver film obtained from chemical method (II)."; ** Gaodeng Xuexiao Huaxue Xuebao (**1991**), 12(9), 1225-8.
73. Doering, W. E.; Nie, S.; **"Single-Molecule and Single-Nanoparticle SERS: Examining the Roles of Surface Active Sites and Chemical Enhancement."**; Journal of Physical Chemistry B (**2002**), 106(2), 311-317.
74. Arenas, J. F.; Lopez-Tocon, I.; Centeno, S. P.; Soto, J.; Otero, J. C. **"How a resonant charge transfer mechanism determines the relative intensities in the SERS spectra of 4-methylpyridine.";** Vibrational Spectroscopy (**2002**), 29(1-2), 147-154.
75. Xu, X.; Yeung, E. S.; **"Direct measurement of single-molecule diffusion and photodecomposition in free solution."**; Science (Washington, D. C.) (**1997**), 275(5303), 1106-1109.
76. Vo-Dinh, T.; **"Advanced approaches in luminescence and Raman spectroscopy."**; Proceedings of SPIE-The International Society for Optical Engineering (**1991**), 1435, 197-202.
77. Lee, Y-H.; Farquharson, S.; Rainey, P. M. **"Surface-enhanced Raman sensor for trace chemical detection in water. ";** Proceedings of SPIE-The International Society for Optical Engineering (**1999**), 3857, 76-84.
78. Odziemkowski, M.; Koziel ,J. A.; Irish, D E; Pawliszyn, J. **"Sampling and Raman confocal microspectroscopic analysis of airborne particulate matter using poly(dimethylsiloxane) solid-phase microextraction fibers.";** ANALYTICAL CHEMISTRY (**2001**), 73(13), 3131-9.
79. Sheng, R.; Zhou, G.; Xiong, J.; Xu, Z.; Morris, M. D.; Zeng, Y.; **"The effect of laser irradiation on surface enhanced Raman scattering for silver film.";** Wuhan University Journal of Natural Sciences (**1997**), 2(1), 101-104.

80. Suh, J. S.; Jeong, D. H.; Lee, M. S.; **"Effect of inhomogeneous broadening on the surface photochemistry of phthalazine. ";** Journal of Raman Spectroscopy (**1999**), 30(7), 595-598.
81. Kiefer, W.; Bernstein, H. J.; "**Cell for resonance Raman excitation with lasers in liquids.";** Applied Spectroscopy (**1971**), 25(4), 500-1.
82. Sloane, H. J.; Cook, R. B.; **"Applications of the rotating solid sample technique in Raman spectroscopy."**; Applied Spectroscopy (**1972**), 589-93.
83. Zimmerer, N.; Kiefer, W.; **"Rotating surface scanning technique for Raman spectroscopy.";** Applied Spectroscopy (**1974**), 28(3), 279-81.
84. Ran, Y.; Yalkowsky, S. H.; **"Prediction of Drug Solubility by the General Solubility Equation (GSE)."**; Journal of Chemical Information and Computer Sciences (**2001**), 41(2), 354-357.
85. Ollers, S.; Singer, H. P.; Fassler, P.; Muller, S. R.; **" Simultaneous quantification of neutral and acidic pharmaceuticals and pesticides at the low-ng/L level in surface and waste water.";** Journal of Chromatography, A (**2001**), 911(2), 225-234.
86. Farre, M.; Ferrer, I. ; Ginebreda, A. ; Figueras, M.; Olivella, L. ; Tirapu, L. ; Vilanova, M. ; Barcelo, D.; **"Determination of drugs in surface water and wastewater samples by liquid chromatography-mass spectrometry: methods and preliminary results including toxicity studies with Vibrio fischeri.";** Journal of Chromatography, A (**2001**), 938(1-2), 187-197.
87. Roy, D.; Barber, Z. H.; Clyne, T. W**.; "Ag nanoparticle induced surface enhanced Raman spectroscopy of chemical vapor deposition diamond thin films prepared by hot filament chemical vapor deposition.";** Journal of Applied Physics (**2002**), 91(9), 6085-6088.
88. Dumont, M.; Chollon, G.; Dourges, M. A.; Pailler, R.; Bourrat, X.; Naslain, R.; Bruneel, J. L.; Couzi, M.; **"Chemical, microstructural and thermal analyses of a naphthalene-derived mesophase pitch.";** Carbon (**2002**), 40(9), 1475-1486.
89. Garcia-Rodriguez, F. J.; Perez-Robles, J. F.; Gonzalez-Hernandez, J.; Vorobiev, Y.; Jimenez-Sandoval, S.; Manzano-Ramirez, A.; **"Surface enhanced Raman scattering of graphite on metals.";** Solid State Communications (**1997**), Volume Date 1998, 105(2), 85-87.
90. Dodson, C. L.; Graham, J. F**.; "Vibrational spectrum of naphthalene anion.";** Journal of Physical Chemistry (**1973**), 77(24), 2903-6.
91. Osawa, M.; Matsuda, N.; Yoshii, K.; Uchida, I**.; "Charge transfer resonance Raman process in surface-enhanced Raman scattering from p-aminothiophenol adsorbed on silver: Herzberg-Teller contribution.";** Journal of Physical Chemistry (**1994**), 98(48), 12702-7.
92. Lin-Vien, D. ; Colthup, N. B.; Fateley, W. G.; Grasselli, J. G.; **"The Handbook of Infrared and Raman Characteristic Frequencies of Organic Molecules"**; Academic Press, San Diego (**1991**), Chap. 10, p. 155; 14, p. 225; 15, p. 251; 17, p. 277.

93. Dollish, F. R. ; Fateley, W. G. ; Bentley, F. F.; **"Characteristic Raman Frequencies of Organic Compounds";** John Wiley & Sons, New York, (**1974**), Chap. 3-5,p. 27; 8, p. 105; 13, p. 162.
94. Mc Murry, J.; **"Organic Chemistry";** Wadsworth Inc*,* Belmont, Ca, (**1982**). 3rd ed., p. 781.
95. Panicker, C. Y.; Varghese, H. T.; John, A.; Philip, D.; Istvan, K.; Keresztury, G.; **"FT-IR, FT-Raman and FT-SERS spectra of 4-aminosalicylic acid sodium salt dihydrate.";** Spectrochimica Acta, Part A: Molecular and Biomolecular Spectroscopy (**2002**), 58A(2), 281-287.
96. Ali, S.; Ahmad, F.; Mazhar, M.; Munir, A.; Masood, M. T**.; "Synthesis and spectral studies of di- and triorganotin(IV) complexes with 2-(6-methoxynaphthyl)propionic acid (Naproxen).";** Synthesis and Reactivity in Inorganic and Metal-Organic Chemistry (**2002**), 32(2), 357-372.
97. Emory, S. R.; Ambrose, W. P.; Goodwin, P. M.; Keller, R. A.; **"Observing single-molecule chemical reactions on metal nanoparticles."**; Proceedings of SPIE-The International Society for Optical Engineering (**2001**), 4258, 63-72.
98. Han, S. W.; Lee, S. J.; Kim, K.; **"Self-Assembled Monolayers of Aromatic Thiol and Selenol on Silver: Comparative Study of Adsorptivity and Stability."**; Langmuir (**2001**), 17(22), 6981-6987.
99. Hill, W.; Wehling, B.; **"Potential- and pH-dependent surface-enhanced Raman scattering of p-mercapto aniline on silver and gold substrates."**; Journal of Physical Chemistry (**1993**), 97(37), 9451-9455.
100. Zheng, J.; Li, X.; Gu, R.; Lu, T.; **"Comparison of the Surface Properties of the Assembled Silver Nanoparticle Electrode and Roughened Silver Electrode."**; Journal of Physical Chemistry B (**2002**), 106(5), 1019-1023.
101. Kneipp, K.; Roth, E.; Engert, C.; Kiefer, W.; **"Near-infrared excited surface-enhanced Raman spectroscopy of rhodamine 6G on colloidal silver."**; Chemical Physics Letters (**1993**), 207(4-6), 450-454.
102. EPA; **"Method 604, Phenols, Fed. Regist."**; Environmental Protection Agency, Part VIII, 40 CFR Part 136, (**1984**), October 26, 58.
103. EPA; **"Method 625, Base/ neutrals and acids"**; Environmental Protection Agency, Part VIII, 40 CFR Part 136, , (**1984**), October 26, 153.
104. Lu, G; Wang, C.; Yuan, X.; Zhao, Y.; **"QSBR study of substituted phenols and benzoic acids.";** Journal of Environmental Sciences (China) (**2003**), 15(1), 88-91.
105. Penalver, A.; Pocurull, E.; Borrull, F.; Marce, R. M.; **"Solid-phase microextraction coupled to high-performance liquid chromatography to determine phenolic compounds in water samples.";** Journal of Chromatography, A (**2002**), 953(1-2), 79-87.
106. Vandecasteele, K.; Gaus, I.; Debreuck, W.; Walraevens, K.; **"Identification and quantification of 77 pesticides in groundwater using solid phase coupled to liquid-liquid microextraction and**

reversed-phase liquid chromatography."; Analytical Chemistry (**2000**), 72(14), 3093-3101.
107. Wu, Y.; Huang, S.: **"Solid-Phase Microextraction Coupled with High-Performance Liquid Chromatography for the Determination of Aromatic Amines.";** Analytical Chemistry (**1999**), 71(2), 310-318.
108. Gonzalez-Toledo, E.; Prat, M. D.; Alpendurada, M. F. ; **"Solid-phase microextraction coupled to liquid chromatography for the analysis of phenolic compounds in water. ";** Journal of Chromatography, A (**2001**), 923(1-2), 45-52.
109. Llompart, M.; Lourido, M.; Landin, P.; Garcia-Jares, C.; Cela, R.; **"Optimization of a derivatization-solid-phase microextraction method for the analysis of thirty phenolic pollutants in water samples.";** Journal of Chromatography, A (**2002**), 963(1-2), 137-148.
110. Krutz, L. J.; Senseman, S. A.; Sciumbato, A. S.; **"Solid-phase microextraction for herbicide determination in environmental samples.";** Journal of Chromatography, A (**2003**), 999(1-2), 103-121.
111. Preiss, A.; Godejohann, M.; **"LC-NMR in environmental analysis.";** On-Line LC-NMR and Related Techniques (**2002**), 141-178.
112. Visser, T.; **"FT-IR detection in gas chromatography.";** TrAC, Trends in Analytical Chemistry (**2002**), 21(9/10), 627-636.
113. Ni F.; Thomas L.; Cotton T. M.; **"Surface-enhanced resonance Raman spectroscopy as an ancillary high-performance liquid chromatography detector for nitrophenol compounds.";** ANALYTICAL CHEMISTRY (**1989**)Apr 15, 61(8), 888-94.
114. Vo-Dinh T**.; "Advanced approaches in luminescence and Raman spectroscopy. ";** Proceedings of SPIE-The International Society for Optical Engineering (**1991**), 1435(Opt. Methods Ultrasensitive Detect. Anal.: Tech. Appl.), 197-202.
115. Odziemkowski, M.; Koziel, J. A.; Irish, D. E.; Pawliszyn, J.; **" Sampling and Raman Confocal Microspectroscopic Analysis of Airborne Particulate Matter Using Poly(dimethylsiloxane) Solid-Phase Microextraction Fibers.";** Analytical Chemistry (**2001**), 73(13), 3131-3139.
116. Kneipp, K.; **"Raman spectroscopy of single molecules.";** Single Molecules (**2001**), 2(4), 291-292..
117. Moskovits, M.; Tay, L.; Yang, J.; Haslett, T.; **"SERS and the single molecule.";** Topics in Applied Physics (**2002**), 82(Optical Properties of Nanostructured Random Media), 215-226.
118. Rivas, L.; Sanchez-Cortes, S.; Garcia-Ramos, J. V.; Morcillo, G.; **"Growth of silver colloidal particles obtained by citrate reduction to increase the Raman enhancement factor.";** Langmuir (**2001**), 17(3), 574-577.
119. Jensen, T. R.; Malinsky, M. D.; Haynes, C. L.; van-Duyne, R. P. **"Nanosphere Lithography: Tunable Localized Surface Plasmon Resonance Spectra of Silver Nanoparticles.";** Journal of Physical Chemistry B (**2000**), 104(45), 10549-10556.

120. De Jesús, M. A.; Giesfeldt, K. S.; Sepaniak, M. J.; **"Use of a sample translation technique to minimize adverse effects of laser irradiation in surface-enhanced Raman spectrometry."**; Applied Spectroscopy (**2003**), 57(4), 428-438.
121. Kuban, P.; Flowers, H.; **"On-line preconcentration for the ion chromatographic determination of chlorophenolic and phenolic compounds in environmental samples using electrochemical detection.";** Analytica Chimica Acta (**2001**), 437(1), 115-122.
122. Wegman, R. C. C.; Hofstee, A. W. M**.; "Chlorophenols in surface waters of the Netherlands (1976-1977).";** Water Research (**1979**), 13(7), 651-7.
123. EPA; **"National Oil and Hazardous Substance Pollution Contingency Plan; National Priorities List."**; Federal Registry EPA (**2003**), March 17, 2247-2252.
124. Kaschl, A.; Romheld, V.; Chen, Y.; "**Trace metal distribution in soluble organic matter from municipal solid waste compost determined by size-exclusion chromatography.";** Environmental Toxicology and Chemistry (**2002**), 21(9), 1775-1782.
125. Shaw, A. A.; Wainschel, L. A.; Shetlar, M. D.; **"The photochemistry of p-aminobenzoic acid.";** Photochemistry and Photobiology (**1992**), 55(5), 647-56.
126. Roy, D.; Barber, Z. H.; Clyne, T. W. "**Ag nanoparticle induced surface enhanced Raman spectroscopy of chemical vapor deposition diamond thin films prepared by hot filament chemical vapor deposition."** Journal of Applied Physics (**2002**), 91(9), 6085-6088.
127. Barteau, M. A.; Madix, R. J.; **"The Chemical Physics of Solid Surfaces and Heterogeneous Catalysis";** King, D.A.; Woodruff, D.B, Eds. Elsevier Scientific: New York, (**1982**); chpt. 4.
128. Bruzzoniti, M. C.; Sarzanini, C.; Mentasti, E.; **"Preconcentration of contaminants in water analysis.";** Journal of Chromatography, A (**2000**), 902(1), 289-309.
129. Sánchez-Cortés, S.; García-Ramos, J. V.; **"Adsorption and Chemical Modification of Phenols on a Silver Surface."**; Journal of Colloid and Interface Science (**2000**), 231(1), 98-106.
130. Yamamoto, H.; Liljestrand, H. M.; Shimizu, Y.; Morita, M.; "**Effects of Physical-Chemical Characteristics on the Sorption of Selected Endocrine Disruptors by Dissolved Organic Matter Surrogates.";** Environmental Science and Technology (**2003**), 37(12), 2646-2657.
131. Sanchez-Cortes, S.; Domingo, C.; Garcia-Ramos, J. V.; Aznarez, J. A.; **"Surface-enhanced vibrational study (SEIR and SERS) of dithiocarbamate pesticides on gold films.";** Langmuir (**2001**), 17(4), 1157-1162.
132. Rivas, L.; Sanchez-Cortes, S.; Garcia-Ramos, J. V.; Morcillo, G.; **"Growth of silver colloidal particles obtained by citrate reduction to increase the Raman enhancement factor."** Langmuir (**2001**), 17(3), 574-577.

133. Gu, X. J.; Akers, K. L.; Moskovits, M.; **"Reaction of dichloroethane and oxygen on a rough silver surface.";** Journal of Physical Chemistry (**1991**), 95(9), 3696-700.
134. Suh, J. S.; Michaelian, K. H.; **"Surface-enhanced Raman spectroscopy of acrylamide and polyacrylamide adsorbed on silver colloid surfaces: polymerization of acrylamide on silver.";** Journal of Raman Spectroscopy (**1987**), 18(6), 409-14.
135. Venkatachalam, R. S.; Boerio, F. J.; Roth, P. G.; **"Formation of p,p'-azodibenzoate from p-aminobenzoic acid on silver island films during surface-enhanced Raman scattering."**; Journal of Raman Spectroscopy (**1988**), 19(4), 281-7.
136. Tsai, W. H.; Boerio, F. J.; Clarson, S. J.; Montaudo, G.; **"Polymerization of nitro compounds on silver surfaces during surface-enhanced Raman scattering.";** Journal of Raman Spectroscopy (**1990**), 21(5), 311-20.
137. De Jesús, M. A.; Giesfeldt, K. S.; Sepaniak, M. J.; **"Improving the Analytical Figures of Merit of SERS for the Analysis of Model Environmental Pollutants."**; Journal of Raman Spectroscopy (in press).
138. Moskovits, M.; Suh, J. S.; **"The geometry of several molecular ions adsorbed on the surface of colloidal silver.";** Journal of Physical Chemistry (**1984**), 88(7), 1293-8.
139. Chowdhury, J.; Mukherjee, K. M.; Misra, T. N.; **"A pH dependent surface-enhanced Raman scattering study of hypoxanthine.";** Journal of Raman Spectroscopy (**2000**), 31(5), 427-431.
140. Pavel, I.; Szeghalmi, A.; Moigno, D.; Cinta, S.; Kiefer, W.; **"Theoretical and pH dependent surface enhanced Raman spectroscopy study on caffeine.";** Biopolymers (**2002**), Volume Date 2003, 72(1), 25-37.
141. Muniz-Miranda, M.; **"Adsorption mechanism of 2-amino-5-nitropyrimidine on silver substrates, as detected by surface-enhanced Raman scattering.";** Vibrational Spectroscopy (**2002**), 29(1-2), 229-233.
142. Chen, T.; Liang, F.; Zheng, L.; Chen, W.; **"Surface-enhanced resonance Raman scattering spectra of sodium fluorescein with different tautomers."**; Wuli Huaxue Xuebao (**1991**), 7(3), 300-4.
143. Chowdhury, Joydeep; Pal, Prabir; Ghosh, Manash; Misra, T. N.; **"Surface-enhanced Raman scattering of rhodamine 123 in silver hydrosols and in Langmuir-Blodgett films on silver islands."**; Journal of Colloid and Interface Science (2001), 235(2), 317-324.
144. EPA; **"Summary review of health effects associated with naphthalene: Health issue assessment.";** Report (**1987**), (EPA/600/8-87/055F; Order No. PB88-172374/GAR), 59 pp.
145. DellaGreca, M.; Monaco, P.; Pinto, G.; Pollio, A.; Previtera, L.; Temussi, F.; **"Phytotoxicity of low-molecular-weight phenols from olive mill waste waters.";** Bulletin of Environmental Contamination and Toxicology (**2001**), 67(3), 352-359.

146. Waterhouse, G. I. N.; Bowmaker, G.A.; Metson, J. B.; **"The thermal decomposition of silver (I, III) oxide: A combined XRD, FT-IR and Raman spectroscopic study.";** Physical Chemistry Chemical Physics (**2001**), 3(17), 3838-3845.
147. Zhang, W.; Xiao, X.; An, T.; Song, Z.; Fu, J.; Sheng, G.; Cui, M.; **"Kinetics, degradation pathway and reaction mechanism of advanced oxidation of 4-nitrophenol in water by a UV/H2O2 process."** Journal of Chemical Technology and Biotechnology (**2003**), 78(7), 788-794.
148. Aubard, J.; Bagnasco, E.; Pantigny, J.; Ruasse, M. F.; Levi, G.; Wentrup-Byrne, E.; **"An Ion-Exchange Reaction as Measured by Surface-Enhanced Raman Spectroscopy on Silver Colloids.";** Journal of Physical Chemistry (**1995**), 99(18), 7075-81.
149. Andryushechkin, B. V.; Eltsov, K. N.; Shevlyuga, V. M.; Yurov, Y. Yu.; **"Direct STM observation of surface modification and growth of AgCl islands on Ag(111) upon chlorination at room temperature.";** Surface Science (**1999**), 431(1-3), 96-108.
150. Andryushechkin, B. V.; Eltsov, K. N.; Shevlyuga, V. M.; **"Atomic structure of silver chloride formed on Ag(111) surface upon low temperature chlorination.";** Surface Science (**1999**), 433-435 109-113.
151. Suh, J. S.; Kim, J.; **"Three distinct geometries of surface-adsorbed carboxylate groups."**; Journal of Raman Spectroscopy (**1998**), 29(2), 143-148.
152. Ni, F.; Thomas, L.; Cotton, T. M.; **"Surface-enhanced resonance Raman spectroscopy as an ancillary high-performance liquid chromatography dectector for nitrophenol compounds."**; Analytical Chemistry (**1989**), 61(8), 888-94.
153. Saegmueller, B.; Brehm, G.; Schneider, S.; **"In situ generated photolytic silver in a gelatin matrix: an approach for high-throughput SERS spectroscopy applying microtiter plates."**; Applied Spectroscopy (**2000**), 54(12), 1849-1856.

VITA

Marco Antonio De Jesús was born on June 29, 1970 in Mayagüez, Puerto Rico. Marco graduated from the University of Puerto Rico at Mayagüez (UPRM) where he earned both his BS and MS degrees in Chemistry. He became an analytical chemistry instructor in the UPRM in 1997. He entered the doctoral program in Chemistry at the University of Tennessee, Knoxville in August of 2000 and pursued research in Analytical Chemistry. Marco is happily married to his wife Ideliz with whom he has two lovely girls Cindy and Kiara. He earned his Ph. D. in May 2004 and will be pursuing post-doctoral Research at the University of Tennessee, Knoxville, and Oak-Ridge National Labs. His research will involve the development of novel analytical techniques for the analysis of environmentally relevant compounds in a wide variety of matrices.